DEPARTMENT OF ELECTRONIC & ELECTRICAL ENGINEERING

University of Strathclyde Engineering

Control Design and Energy Optimisation of a Buoyant Airborne Wind Turbine

JONATHAN SAMSON

A thesis submitted for Degree of Philosophy

Supervisor: Reza Katebi

WIND ENERGY CDT

UNIVERSITY OF STRATHCLYDE

September 2018

This thesis is the result of the author's original research. It has been composed by the author and has not previously been submitted for examination which has led to the award of a degree.

Acknowledgements

This work has only been made possible through the kind love and support of many people in my life. Firstly, I would like to thank my supervisor Dr Reza Katebi and Dr Chris Vermillion for their support in the creation of this project and Altaeros Energies for collaborating with me on this work.

To all the members of the CDT, who have helped make this PhD so enjoyable. It is a thoroughly unique experience and would not be the same without the many students/staff members who support it. In particular, Drew Smith, William Leithead, Hong Yue and Alasdair McDonald are always there to offer advice and guidance. The CDT are lucky to have them! Massive thanks is also needed to every CDT student who are always keen to offer support with one, maybe two (or more) drinks after work.

To everyone who has supported me outside of Strathclyde, it has been a long hard slog and without them I may not have been quite as sane. Ross, Katie, Neil, Alan, Adam, Jenny, Mcdubb, Chris, Shona and everyone else (because this paragraph would never end) whose friendship over the years is so greatly appreciated. Also, a major shout out to the Archie Appreciation club, who help take my mind off PhD stress on a Saturday by replacing it with a totally different kind of stress. My PhD year 12/13 will forever be remembered for both interesting conferences and travelling to fife.

To both my parents, Margaret and George and my Aunt, Bernadette, who have always been there for me. Their support has been unwavering and they have given me the confidence to believe that whatever I put my mind to is achievable. I could not have done this without them.

Finally, the greatest thanks of all goes to my wife Jenny, who without her love and support the final part of this work simply would not have been possible. When I met Jenny 10 years ago it was hard to grasp the impact she would have on my life. We have grown up together and shared many amazing experiences including getting a new house(s), learning to fix a house (for me badly), getting married! and travelling, all of which have helped de-stress when times have been tough. Jenny was also the driving force in introducing two cats into our life during my first year at the CDT. To be clear, these cats have contributed very little to this work other than offering quiet judgement and silent assurance that at some-point this process will all be over.

Jenny is always there for me and is my best pal in life. This work is dedicated to her.

Contents

List of Figures

List of Tables

Nomenclature

Acronyms

HAWT	Horizontal Axis Wind Turbine
AWES	Airborne Wind Energy Systems
BAWT	Buoyant Airborne Wind Turbine
LCOE	Levelised Cost of Energy
VAWT	Vertical Axis Wind Turbines
O&M	Operation and Maintencance
PID	Proportional Integral Derivative control
LQR	Linear Quadratic Regulator
AWE	Airborne Wind Energy
MPC	Model Predictive Control
ESC	Extremum Seeking Control
GLG	Ground Level Generation
OBG	On Board Generation
GPS	Global Positioning System
HMPE	HIgh Modulus Polyethylene
IMU	Inertial Measurement Unit
RH	Receding Horizon
MHE	Moving Horizon Estimation

Symbols

δ	Wind Power Density
P_{ideal}	Ideal Power
ρ_{air}	Air density
v_w	Freestream Wind Speed
F_L	Aerodynamic Lift
C_L	Coefficient of Lift
A_{wing}	Area of rigid wing
v_a	Relative kite velocity
P_{AWES}	Kite Power
C_D	Coefficient of Drag
ξ	Zeta factor
A_{turb}	Area of Wind Turbine Rotor
$P_{turbine}$	Power of Turbine
M	Mass
D	Rotor Diameter
C_P	Coefficient of Power
R	Power Ratio
V_{shroud}	Shroud Volume
v_{ref}	Reference Wind Speed at z_r
z_{alt}	Operating Altitude
z_{min}	Minimum altitude
z_{max}	Maximum Altitude
z_r	Reference Altitude
z_0	Surface roughness
G_u	Turbulence Transfer function in x direction
σ_u	Turbulence intensity in x direction
L_u	Length scale in x direction

G_v	Turbulence transfer function in y direction
σ_v	Turbulence intensity in y direction
L_v	Length scale in y direction
G_w	Transfer function in z direction
σ_w	Turbulence intensity in z direction
L_w	Length scale in z direction
ϕ	Shroud roll
θ	Shroud pitch
ψ	Shroud yaw
p, q, r	Shroud rotational velocities around x, y and z axis
u, v, w	Shroud translational velocities in x, y and z direction
x_b, y_b, z_b	Shroud body fixed coordinates
x_g, y_g, z_g	Base station ground fixed cooridnates
m	Shroud mass
F_x^{aero}	Aerodynamic force in x direction
F_y^{aero}	Aerodynamic force in y direction
F_z^{aero}	Aerodynamic force in z direction
F_x^{net}	Net buoyancy force in x direction
F_y^{net}	Net buoyancy force in y direction
F_z^{net}	Net buoyancy force in z direction
F_x^{tether}	Tether force in x direction
F_y^{tether}	Tether force in y direction
F_z^{tether}	Tether force in z direction
M_x^{aero}	Aerodynamic moment in x direction
M_y^{aero}	Aerodynamic moment in y direction
M_z^{aero}	Aerodynamic moment in z direction
M_x^{net}	Net buoyancy moment in x direction
M_y^{net}	Net buoyancy moment in y direction

M_z^{net}	Net buoyancy moment in z direction
M_x^{tether}	Tether moment in x direction
M_y^{tether}	Tether moment in y direction
M_z^{tether}	Tether moment in z direction
d_{ref}	Reference distance
I_x	Shroud inertia in x direction
I_y	Shroud inertia in y direction
I_z	Shroud inertia in z direction
$v_{x_{app}}$, $v_{y_{app}}$, $v_{z_{app}}$	Apparent wind speed of shroud in x, y and z direction
v_{app}	Apparent wind speed
W_x, W_y, W_z	Wind speed components x, y and z direction
α	Angle of attack of shroud
β	Sideslip angle
C_S	Sideslip coefficient
α_0,α_1,α_2, b_0, b_1, c_0, c_1	Shroud aerodynamic coefficients
$C_{Mx,}$	Aerodynamic moment coefficient
$C_{My,}$	Aerodynamic moment coefficient
C_{Mz}	Aerodynamic moment coefficient
d_0, d_1, e_0, e_1, e_2, f_0 f_1	Aerodynamic coefficients
V_{shroud}	Volume of shroud
A_{throat}	Shroud aerodynamic throat area
A_{shroud}	Shroud area
F_B	Buoyancy force
A_{tether}	Tether area
E	Youngs modulus
l^i	Tether length
l_u^i	Unstretched tether length
$r_{\dot{x}}^{shroud}$	Acceleration of shroud in x direction

r_y^{shroud}	Acceleration of shroud in y direction
r_x^{bs}	Acceleration of base station in x direction
r_y^{bs}	Acceleration of base station in y direction
r_z^{bs}	Acceleration of base station in z direction
P_q^i	Tether Damping
C_V	Coefficient of Damping
I_{bs}	Inertia of base station
r_{bs}	Acceleration of base station
ψ_{bs}	Yaw angle of base station
M_z^{tether}	Friction moment of base station
u_{bs}	Base station velocity
v_{turb}	Wind speed at rotor plane
v_{exit}	Wind speed at exit area of shroud
A_{exit}	Area at exit of the shroud
γ	Buoyancy reduction factor
F_{net}	Net buoyancy force
F_g	Gravity force
l	Length of shroud
F_{hel}	Buoyant force from helium
F_{hyd}	Buoyant force from hydrogen
ρ_{helium}	Density of helium
$\rho_{hydrogen}$	Density of hydrogen
ρ_{gas}	Density of gas
δ	Blowdown angle
a	Distance from fore tether attachements to centre of buoyancy
b	Distance from fore tether attachements to centre of gravity
c	Distance from fore tether attachements to centre of gravity
Δx	Distance from centre of gravity and centre of buoyancy

v_{range}	Range of wind speeds
v_{rated}	Rated wind speed
θ_{min}	Minimum pitch
θ_{max}	Maximum pitch
$u(t)$	Control input vector
θ_{ss}	Steady state pitch set-point
z_{sp}	Steady state altitude set-point
$Y_{roll}(s)$	Roll output
$Y_{pitch}(s)$	Pitch output
$Y_{alt}(s)$	Altitude output
$U_1(s)$	Winch speed input fore tether
$U_2(s)$	Winch speed input from aft-starboard tether
$U_3(s)$	Winch speed input from aft-port tether
K_1	LQR state feedback gain
K_2	LQR integral gain
A_e	Augmented LQR state matrix
B_e	Augmented LQR input matrix
C_e	Augmented LQR output matrix
Q_e	LQR scaling matrix
R_e	LQR scaling matrix
K_m	MPID gain matrix
σ_{min}	Minimum singular value
σ_{max}	Maximum singular value
K_p	MPID proportional gain
K_I	MPID integral gain
K_D	MPID derivative gain

$p(U)$	Weibull probability distribution at wind speed U
A_p	Plant state matrix
B_p	Pant input matrix
C_p	Plant output matrix
$\dot{x}_p(t)$	Plant state
$y_p(t)$	Plant output
A_c	MPID Controller state matrix
B_c	MPID Controller input matrix
C_c	MPID Controller output matrix
$\dot{x}_c(t)$	MPID Controller state
$y_c(t)$	MPID Controller output
$u_c(t)$	Controller input
e_z	Error on altitude
e_ϕ	Error in roll
e_θ	Error in pitch
r_z	Reference altitude
r_ϕ	Reference roll
r_θ	Reference pitch
A_{tot}	Combined (Plant and controller) state matrix
B_{tot}	Combined (Plant and controller) input matrix
C_{tot}	Combined (Plant and controller) output matrix
$\dot{x}_{tot}(t)$	Combined (Plant and controller) state vector
$y_c(t)$	Combined state output matrix
x_{k+1}	Combined (Plant and controller) state vector in discrete time
y_k	Combined (Plant and controller) state vector in discrete time

A	Combined (Plant and controller) state matrix in discrete time
B	Combined (Plant and controller) input matrix in discrete time
C	Combined (Plant and controller) output matrix in discrete time
r_k	Reference vector for altitude, roll and pitch in discrete time
Δu_k	Rate of change of reference inputs in discrete time
n_y	Prediction horizon
n_u	Control horizon
W	Weighting matrix on altitude, roll and pitch set-points
R	Weighting matrix on input references in altitude, roll and pitch
R_s	Reference vector for altitude, roll and pitch in discrete time
${y_{alt}}^{min}$	Minimum allowable altitude (z_{min})
${y_{alt}}^{max}$	Maximum allowable altitude (z_{max})
${y_{pitch}}^{min}$	Minimum allowable pitch (θ_{min})
${y_{pitch}}^{max}$	Maximum allowable pitch (θ_{max})
${y_{roll}}^{max}$	Maximum allowable roll (ϕ_{max})
${y_{roll}}^{min}$	Minimum allowable roll (ϕ_{min})
P_{loss}	Power loss (kW)
P_{net}	Net power (kW)
${v_w}^*$	Optimal wind speed
${z_{alt}}^*$	Optimal altitude
ω_p	Perturbation frequency
ω_H	High pass filter constant
ω_L	Low pass filter constant
a	Perturbation amplitude
k	ESC integral gain

Abstract

Airborne Wind Energy Systems (AWES) aim to capture the wind energy potential at high altitudes by using a combination of tethers and bespoke aerofoils. In contrast to conventional horizontal axis wind turbines (HAWT), the tower is replaced with lightweight tethers resulting in a reduction in both the overall mass, and more importantly cost of the system. Currently, there is significant interest from a number of key stakeholders, both academic and industrial, aiming to optimise an airborne wind energy design that captures the wind energy resource found at high altitudes. Two key issues will drive the development of these systems, flight stability and power maximisation. Therefore, the control strategy for these systems will be imperative for reducing costs and optimising system performance. Through collaboration with Altaeros Energies, this thesis addresses the outstanding stability and performance optimisation for a specific AWES known as the Buoyant Airborne Wind Turbine (BAWT).

There are three key contributions within this work. Firstly, a comprehensive literature review of different airborne systems is provided with specific consideration given to power optimisation and dynamic stability. This results in a detailed understanding of the BAWT plant model through the introduction of two force ratio's relating the buoyancy contribution to the aerodynamic contribution on system loads across the operating envelope.

The model development is then expanded on to discuss the question of system stability and power optimisation. This is addressed via the development of a hierarchical control structure for the BAWT, which is broken into three distinct regions, low level control, medium level control and high level control. At the lowest level, flight stability, which is vital to providing optimum conditions for energy generation, is guaranteed using a multivariable controller.

This is carried out through the development of a PID controller using two methods, a frequency domain method known as MPID and an optimal control scheme, LQR. The results of this chapter inform the interaction of the controller with the underlying plant dynamics.

Finally, the broader issue of BAWT optimisation is addressed by implementing a hierarchical control architecture which builds upon the multivariable flight stability controller developed in Chapter 5. Medium level control is implemented using a hierarchical model predictive control scheme (MPC) which provides set-points to the low level controller in roll, pitch and altitude. These set-points are provided such that they are bounded within the defined envelope of operation to ensure that loads on the shroud are not increased beyond acceptable levels i.e. extreme tether loads due to high altitudes. The question of power optimisation is then addressed through the formulation of an Extremum seeking control (ESC) scheme which derives an optimal altitude for the system. This altitude is determined by trading off generated power from the rotor against power losses incurred by reeling the tether in/out at high wind speeds. Implementing a hierarchical control scheme of this type provides an example of how different control techniques can be combined to provide a degree of self-regulation whilst simultaneously providing system stability and power optimisation. Ultimately, this will increase autonomous operation of the BAWT which will help to reduce system costs and make this technology more viable in a competitive marketplace.

1 Introduction

Worldwide dependence on fossil fuels has driven society to seek sources of electricity that are low-carbon and renewable, in order to arrest the increase in global warming and carbon emissions. The UK alone has a binding target of 20% renewable power generation by 2020. However, to achieve these ambitious targets, large-scale investment is required in both onshore and offshore renewable energy technologies. Of all the current renewable technologies, the wind industry is the clear market leader with over 13,602.5MW of installed capacity in the UK to date [1].

1.1 Wind Energy Technology

Recent studies of the 2015 European wind energy market, including both onshore and offshore developments, demonstrate that wind energy represents a total of 15.6% of the EU power mix, compared to 2.4% in the year 2000 [2]. Specifically, the offshore market now represents 24% of the annual EU wind energy market up from 13% in 2014 [2].

In terms of wind technology, the Horizontal Axis Wind Turbine (HAWT) is the current industry standard for use in onshore and offshore wind farms. The most common HAWT design is the 3-bladed single rotor due to its superior power coefficients and loading performance [3]. These turbines have increased in size year on year and have now reached a capacity of 7MW [4]. However, the continuous drive for a reduction in levelised cost of energy (LCOE) has led some companies to consider alternatives forms of wind technology as a potential solution to the power generation problem. This is motivated primarily by the fact that there are maintenance and transportation issues with large wind energy

developments, especially offshore. One solution to this issue would be to design a system that is both flexible in terms of transportation and easily maintainable in order to ensure that the design requirements are less onerous. This will help drive down the overall LCOE as a result.

1.2 Alternative Technologies

Advancement in wind turbine design has given rise to a number of alternative systems to rival the conventional HAWT. Ducted rotors, multi-rotors and vertical axis turbines (VAWTS) are all designed to alleviate issues with availability and operations and maintenance (O&M) that affect conventional wind turbines [5].

However, an alternative design which has garnered much interest in the last few years is the Airborne Wind Energy System (AWES). This system removes the dependence on the heavy and expensive tower, replacing it with lightweight tethers. The concept of using airborne systems, such as a kite, for the generation of electricity dates back centuries. However, it was only in the 1980's when Miles Loyd published "Crosswind Kite Power" that the mathematical theory began to offer a qualitative analysis into the potential benefits these types of systems have [6]. This, coupled with technological advances in engineering, has resulted in a resurgence of interest within this area. To illustrate this more clearly, Figure 1-1 shows the different institutions currently working in airborne wind energy systems (AWES):

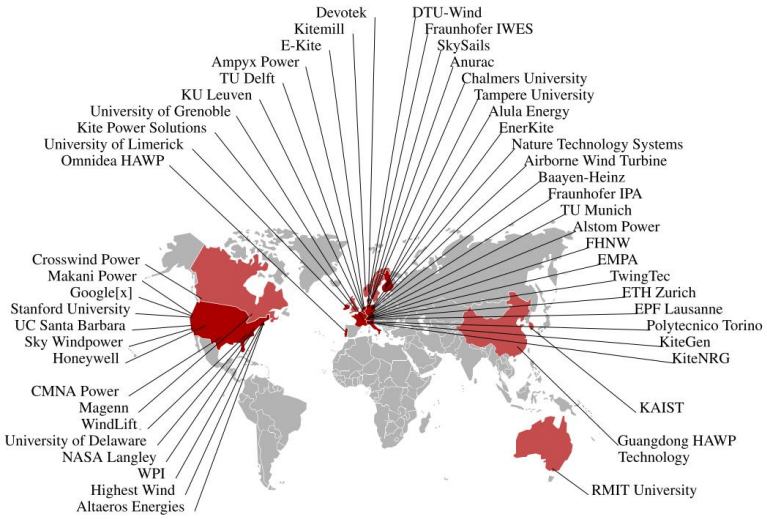

Figure 1-1 - Institutions currently working in or researching AWES [7]

It is clear from Figure 1-1 that there are a number of institutions are working in this area. This has grown substantially in the last ten years. As AWE research is still very much in its infancy, there are many contrasting systems and designs offering different solutions to the AWE problem. In the future, these systems may well be suited to offshore applications, with less dependence on foundations and excellent scaling arguments moving to higher rated power outputs. However, they are also ideally suited to off-grid applications.

One particular design stands out within the AWE field and that is the Buoyant Airborne Wind Turbine (BAWT). This technology is developed by Altaeros Energies and a key collaborator in the development of this work. This system benefits from buoyant stability gained at low wind speeds and aerodynamic stability at high wind speeds. It does not require complicated trajectory control (compared with a kite system) and is very portable so could operate well in disaster relief areas, in addition to farms in an offshore environment.

1.3 Motivation of Research

The over-arching motivation of this research is to investigate the challenges and barriers associated with the development of AWES, with a key focus on the BAWT developed by Altaeros Energies. There has been a significant amount of research into AWES, but there is still no consensus as to which type of technology is superior. Independently assessing each technology in terms of its advantages and disadvantages will inform the potential for this technology as it moves towards market acceptance.

Notwithstanding the mechanical design of the system, the primary challenge for successful operation of all AWES will be that of control design. In the long term, this will be fundamental in reducing costs, i.e. reducing the reliance on manned crews and optimising system performance. However, in order to do this an implicit understanding of system behaviour is required. The BAWT developed by Altaeros Energies is investigated to understand the dynamics of the system, informing the development of novel control strategies designed to enhance the performance of the system.

Furthermore, within the control community, the problem of multivariable control is becoming increasingly important due to the coupled of nature of most modern plants. In the case of Altaeros Energies, multivariable control plays a pivotal role in flight stability of the BAWT. An effort is made in this work to address this problem by employing multivariable techniques designed to suit the requirements of the system. Although, further effort is still required to fully understand the dual control problem of flight control and power optimisation.

The first control challenge is one of stability regardless of which type of AWES is being discussed. The second is that of electricity generation, as the primary goal of these systems is

to operate on a given trajectory to maximise the power capture across the operating envelope. Clearly, these issues are inherently linked but may also conflict with one another, at a given point in time. For instance, system stability could be guaranteed in low wind speed conditions, however, this may not be optimal conditions for maximising power capture. This work is motivated by gaining an increased understanding how these conflicting issues can be solved through modelling and control design.

1.4 Aims and Objectives

The motivation of this research rests in better understanding the underlying system behaviour of the BAWT and implementing control solutions to offer an increase in power performance whilst being aware of the various loading constraints presented across the operating envelope. This thesis is broken up into three main strands in order to achieve this goal:

1. Investigate the modelling and system behaviour of the Altaeros BAWT
2. Achieve flight stability under nominal operating conditions
3. Optimise the BAWT for maximum energy capture within the flight envelope. This will consist of deriving appropriate set-points for the system in roll, pitch and altitude which maximise the performance of the system and are constrained within the operating envelope. Note that, any gain in optimal performance in terms of energy capture will be traded off against the cost on system performance i.e. in terms of extreme loading on the system.

Ultimately, the balance between operating within these system constraints and generating maximum power will define the operation of the system.

In order to achieve these aims the following research topics are studied:

- *Modelling and Stability:* The issues of modelling and system stability are studied within a MATLAB/Simulink environment. To determine shroud behaviour at low and high wind speeds, a novel set of force ratios are introduced that demonstrate transition points for a given BAWT design. These allow for a full determination on the importance of aerodynamics to system stability. The use of two different buoyant gases are assessed namely, helium and hydrogen, to illustrate the potential performance benefit gained from higher buoyancy. Furthermore, the inherent stability of the system in relation to the system's attachment points is shown. This is intended to clearly illustrate the physical coupling of a chosen centre of buoyancy location in relation to the centre of mass, and its subsequent effect on system stability.
- *Multivariable Control Design for a BAWT:* A low-level multivariable PID controller is designed to provide flight stability over the operating envelope. The controller is designed to control the roll, pitch and altitude of the shroud. Two methods are proposed and investigated to deliver the required closed loop performance, including an assessment of performance under turbulent wind conditions. The first method, widely used in flight control, is the well-known linear quadratic regulator (LQR). This is then compared with, what is termed the Multiloop PID (MPID) method, which assesses the flight dynamics at a given frequency resulting in decoupled loops tuned using appropriate parameters.
- *Optimisation control for a BAWT:* The wind varies as a function of altitude. As such, it is important to optimise the altitude over the operating envelope to maximise the wind speed and thus maximise the power within tether loading constraints. The optimal altitude is computed based on the trade-off between the generated power

from the rotor against the power losses coming from the winch when reeling the tether in and out. In order to find the optimum altitude and achieve this altitude within the given system constraints the following control strategy is taken:

- A hierarchical control structure is implemented such that the altitude set-point of the system is modified to satisfy both the power and loading constraints on the system.
- This hierarchical control strategy consists of a medium level MPC controller that provides the low level PID controller set-points in roll, pitch and altitude. These set-points are derived such as to constrain system performance within a given envelope i.e. achievable roll, pitch and altitude set-points.
- Finally, an autonomous altitude set-point is provided through an ESC control scheme, which seeks to find the altitude that maximises the net power produced from the system.

Note that a key assumption in this work is that the shroud control and rotor control are completely decoupled i.e. moving to a particular altitude will result in the instantaneous power corresponding to that wind speed.

1.5 Outline of Thesis

The primary motivation behind this research is to investigate control techniques to provide a controller that stabilises the system during flight whilst also maximising power across the operating envelope. An additional contribution of this work provides a qualitative assessment of different airborne wind energy systems with a discussion focussed on dynamic stability and the control challenges that will be faced in the coming years. Through the development of three key control design techniques; proportional and integral control (PI),

MPC and ESC, the issues of flight stability and power optimisation are addressed. The following sections highlights the major contribution in each Chapter.

Chapter 2 - A Critical Review of Airborne Wind Energy Systems

This chapter extends the current knowledge in the literature by highlighting the main motivations behind AWE and discussing the technical, economic and social issues that will impact the wider success of these systems. The control architecture for each system is discussed and importantly sets out the necessary control challenges that need to be overcome for the future development of AWE. Then having critically assessed the sector in general, it is proposed that the buoyant system has several advantages that the others do not with Altaeros Energies being in an ideal market position for future development.

Chapter 3 – Modelling, Dynamics and Design of a BAWT

This chapter discusses the modelling of the wind profile and a six degree of freedom rigid-body model of the BAWT developed by Altaeros Energies. The mathematical modelling of the primary driving forces over the shroud in addition to the tether dynamics is presented. This chapter develops two novel force ratio's that implicitly relates the shrouds parameters to and their effect on system stability. Furthermore, the importance of aerodynamic drag, on both the tether and the shroud, is highlighted and illustrates the requirement to design a bespoke circular wing capable of generating aerodynamic lift. Finally, a comparison is made between a hydrogen and helium filled shroud, in order to inform the design choices behind a system of this type. The advantages and disadvantages associated with each are assessed along with other main design parameters such as tether width, tether length, and location of tether attachment points. The issue of model stability and future challenges are also addressed.

Chapter 4 – Control Design Review for BAWT Systems

This chapter motivates the requirement for the control algorithms used in the later chapters. A comprehensive literature review of the design and implementation challenges associated with the development of a multivariable PID control approach is provided. Furthermore, a further literature survey is then given on the use of optimal control algorithms within the AWES environment namely; MPC and ESC. Within Chapter 6, the implementation of these algorithms are discussed in the context of the BAWT and the control design challenges are presented, including a discussion on the trade-offs between power performance and loads. This motivates the requirement for investigation into why optimal algorithms such as these can be beneficial in the BAWT context.

Chapter 5– Multivariable Control Design for a BAWT

This chapter presents a multivariable control design methodology for the BAWT. Two tuning methods are introduced in order to derive multiloop controllers to stabilise the BAWT in roll, pitch and altitude. The discussion is centred on the augmented LQR method (guaranteeing zero tracking error) and the MPID method based off of work done by Maciejowski [8] a classical multivariable technique that has previously had success on ship positioning systems and chemical processing plants.

The main contribution of this chapter rests in the multivariable analysis of the Altaeros system with results demonstrating that suitable control over the BAWT can be achieved by using very few tuning parameters. Indeed, simulations show that a stable controller can be designed and implemented without any direct knowledge of the exact state of plant dynamics, confirming that plant inversion techniques such as the MPID method can be used to match the desired design specification.

Chapter 6 – Optimisation of a BAWT
This chapter combines the multivariable controller derived in the previous chapter with a MPC controller defined from the linearised state space model derived in Chapter 5. This is defined as a hierarchical scheme because the intention is to provide set-point regulation for the roll, pitch and altitude of the BAWT under certain constraints. This provides a method by through which the envelope of operation can be enforced i.e. bounding limits that define operation on the minimum and maximum roll, pitch and altitude.

Furthermore, the issues of how to determine the optimum altitude of the system are presented through an ESC scheme. This controller is motivated by the trade-off in power generation of the shroud, where power losses dominate at high wind speeds making it beneficial to operate the system around rated wind speed. This ESC seeks to find an altitude that maximises the net power from the rotor, defined as the power generated from rotor minus any losses associated with reeling in/out the tether.

1.6 Contribution

Chapter 2 discusses AWES holistically in terms of system design, comparing the advantages and disadvantages of each type of system. This places AWES in context within the current wind energy technologies. This extends the existing knowledge, to fully show the state of each system and the development that is still required in order for this industry to become competitive in the wind energy market.

Within Chapter 3 two novel force ratios are presented that show the relationship between buoyancy and the aerodynamic behaviour of the shroud. This is related parametrically to the dimensions of the shroud, and shows the changing effect that different dimensions will have on system behaviour. Through this analysis, a shroud filled with either helium or hydrogen is compared to determine any potential benefit in performance that could be had. Furthermore,

the stability of the system is highlighted, with the specific dependence on attachment point locations in reference to the centre of buoyancy and centre of mass.

Chapter 4 provides a comprehensive literature review on the types of control algorithm considered for design and implementation on a AWES. More specifically, the literature review motivates the control challenges associated with the BAWT, which are inherently multivariable in nature. The trade-offs in power maximisation and excessive loading that exist are also introduced which motivates the need to discuss different types of control optimisation this system.

In Chapter 5, flight stability is assessed. The system is multivariable so two low-level multivariable PID controllers are designed and compared to provide flight stability in roll, pitch and altitude over the operating envelope. What is shown is that a model-free tuning technique, termed the Multiloop PID, offers no significant loss in performance to the LQR case. Furthermore, to accurately control the BAWT over its full operating envelop, the performance is assessed at different points on the operating envelope, and controller assessment provided to inform whether there is a requirement for gain scheduling across the design envelope. This work augments existing controllers in the literature and discusses the merits of optimising the gains at particular operating points in terms of the BAWT's operating envelope.

Chapter 6 introduces the idea of power optimisation and system set-point satisfaction within the multivariable control framework previously laid out. This work extends Chapter 5, which is primarily focussed on system stability. To do this a hierarchical structure is proposed with a supervisory control loop consisting of MPC, for constraint satisfaction, and ESC for altitude set-point regulation. Firstly the motivation for designing a MPC controller to provide set-points is introduced and discussed. Then, optimising the altitude set-point to match the

rated wind speed of the turbine will result in rated power output and prevent high aerodynamic loading on the turbine. The primary contribution of this chapter rests in the discussion of the benefits of this applying this supervisory control architecture to the BAWT. It is made clear that to provide certainty and increase autonomy in operation, a supervisory control strategy will be required in order to trade-off system stability with load regulation. The control architecture proposed provides insight in how to achieve this.

1.7 Publications arisen from this Research

The work of this thesis has been presented in the following contributions:

Conferences

1. J. Samson, R. Katebi and C. Vermillion, "A critical assessment of Airborne Wind Energy Systems," 2nd IET Renewable Power Generation Conference (RPG 2013), Beijing, 2013, pp. 1-4.
2. J Samson, R Katebi, "Shroud Design Criteria for a Lighter than Air Wind Energy System", The Science of Making Torque from Wind, 17 - 20 June 2014, *J. Phys.: Conf. Ser.* **524** 012079
3. J. Samson and R. Katebi, "Multivariable control of a lighter than air system," *2014 UKACC International Conference on Control (CONTROL)*, Loughborough, 2014, pp. 256-261. – **Awarded UKACC Best Poster Prize 2014**
4. J. Samson and R. Katebi, "Adaptive envelope control design for a Buoyant Airborne wind energy system," *2015 American Control Conference (ACC)*, Chicago, IL, 2015, pp. 2395-2400.

Invited Presentations

1. J Samson "An Assessment of Airborne Wind Energy Systems and Design Considerations for Lighter than Air Technologies", *RSE-NNSFC joint project between Strathclyde and Southeast University, 23 September 2013, Nanjing China*
1. J Samson “An Overview of Airborne Wind Energy Technologies”, *Introductory Day lectures, 10th EAWE PhD Seminar on Wind Energy in Europe, 28-31 October 2014, Orleans,France*

2 A Critical Review of Airborne Wind Energy Systems

This Chapter extends the current knowledge in literature by highlighting the key drivers behind AWE and discussing the technical, economic and social issues that will impact the wider success of these systems. For these systems, autonomous control is imperative as it is vital to energy production and also cost reduction. As such, a critical assessment of each technology in terms of control, modelling and performance leads to a better understanding of the effectiveness of different types of AWE system. It is discussed that the system developed by Altaeros Energies, known as the BAWT, provides an ideal benchmark for further investigation.

2.1 High Altitude Wind Resource

There are a number of different types of AWES currently in development. However, irrespective of design, each system shares the common goal of trying to extract as much energy as possible from the wind at high altitudes [7]. To achieve this, the AWE system will use tethers attached to a bespoke aerofoil to generate electricity. These tethers replace the heavy tower on a conventional horizontal axis wind turbine and allow the system to reach higher altitudes where there is, as of yet, a large untapped wind resource. The type of aerofoil and how the electricity is produced is then a matter open to debate. To illustrate the potential of the wind resource at higher altitudes, the wind power density, shown in Equation (2-1) is commonly used:

$$\delta = \frac{P_{ideal}}{A_{turb}} = \frac{1}{2}\rho_{air} v_w^3 \tag{2-1}$$

where P_{ideal} is the ideal power extracted from the wind, A_{turb} is the unit Area of the turbine, ρ_{air} is the density of air $\left(\frac{kg}{m^3}\right)$ and v_w is the operating wind speed. The wind power density (δ), Equation (2-1), assesses power potential at higher altitudes because it relates two important quantities; air density and wind-speed. This gives the power potential per m^2 for a given site, which is independent of turbine size or rating [9]. Full scale AWE systems will operate in a greater range of altitudes, typically between 200-800m, compared to HAWT's which operate at 10-300m. Therefore, comparing wind power density at a given altitude provides a good indicator as to the amount of potential energy that exists. To illustrate this more clearly, Figure 2-1 compares the wind power density that was exceeded 50%, 68% and 95% of the time at an altitude of 80m (Left) and 500m (Right). These resource maps were created using wind speed, temperature, pressure and specific humidity data [9].

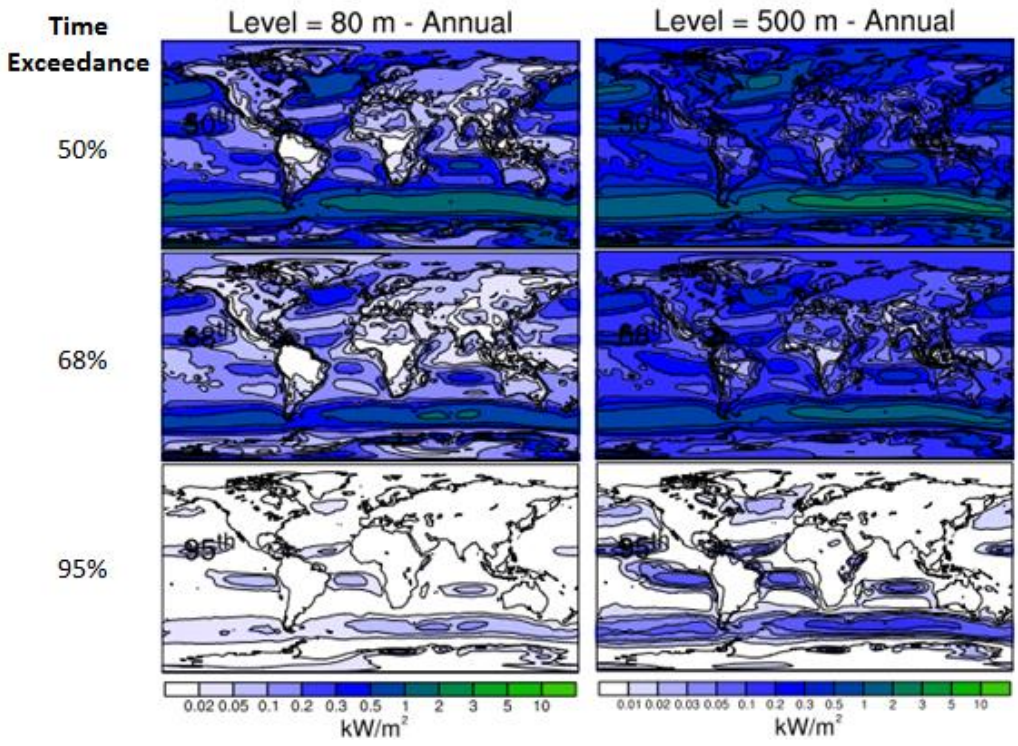

Figure 2-1 – Global wind power density (kW/m^2) at 80m (left) and 500m (right) that is exceeded 50%, 68% and 95% of the times during the year [9]

Figure 2-1 is presented by Archer in [10] who characterises the wind resource in order to assess the potential benefit for AWE applications. As can be seen from Figure 2-1, there is, on average, a greater wind power density at $500m$ compared with $80m$ for all time exceedances considered. Most notably it is clear that there is a more consistent resource in the 95th percentile at 500m compared to 80m. At $80m$, few locations, other than the most southerly ones, can guarantee an average wind power density of 0.1kW/m^2 over 95% of the time. This is in comparison to an average of 0.3kW/m^2 at $500m$, over a wider range of geographical locations.

The reason why this difference occurs is driven primarily by the relationship between altitude and wind speed, known as wind shear. Wind shear is the relationship between wind speed and altitude which implies a logarithmic increase in wind speed with altitude. Since there is a cubic dependence of power density on wind speed, seen in Equation (2-1), a modest increase in wind speed will result in a substantial increase in wind power density. It is also noted that because of this cubic relationship, any difference in air density at higher altitudes can be neglected [11]. Therefore, because there are higher wind speeds at higher altitudes the power density is greater and subsequently, the power potential is greater.

2.2 Airborne Wind Energy Systems (AWES)

Having established that a greater wind resource exists at higher altitudes, it is then necessary to evaluate each technology seeking to harness this potential energy. There are three main AWE designs available in the current marketplace; a kite, a rigid-body and a lighter than air design. The aerofoil and actuators are unique to each system. However, although each system is tethered to the ground there are fundamental differences in how each system is controlled and how electricity is generated.

In the case of rigid or flexible kite systems, the aerofoil is designed to fly crosswind replacing the outermost part of a conventional wind turbine blade. This is the part of the wind turbine which is known to generate the most torque and therefore power. This point is illustrated in Figure 2-2 where the wind turbine on the left is replaced by a rigid or flexible aerofoil on the right, operating in a circular trajectory. Using this design ensures there will be a significant mass reduction compared to conventional turbines, in turn implying a much higher power to mass ratio. This has the potential to provide huge cost-savings compared to the conventional systems.

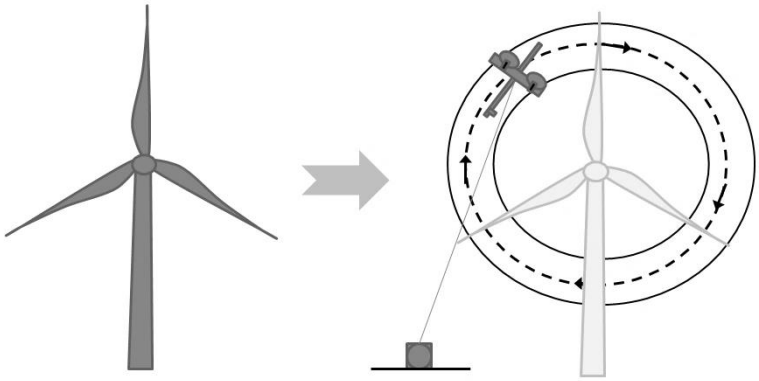

Figure 2-2 - AWE replaces the outer third of the turbine blade (Left) with a bespoke aerofoil (Right) [7]

The idea of tethered crosswind power generation was first argued by Miles Loyd who patented the principle in [6]. The goal was to fly an aerofoil crosswind and use the tension in the tether developed by the aerofoil to facilitate electricity generation through either mechanical or electrical means An intuitive understanding of why this works can be made by considering the flight of a simple kite. If the kite starts to fly in crosswind loops the tension in the lines increases significantly. This arises because the aerodynamic lift over the kite increases with the square of the apparent wind speed. This relationship is shown in Equation (2-2)

$$F_L = \frac{1}{2}\rho_{air} C_L(\alpha) A_{wing} v_a^2 \tag{2-2}$$

where v_a is the effective wind speed of the kite, A_{wing} is the area of the aerofoil wing and $C_L(\alpha)$ defines the lift coefficient of the kite's aerofoil relative to its angle of attack (α). If the kite is flown to a position where the flight is directly crosswind i.e. the aerofoil is parallel to the tether, then the speed through the air is increased above the oncoming wind speed [6]. Therefore, a kite flying with an effective wind speed v_a that is ten times the speed of the oncoming wind speed v_w, will result in an increase in line tension by a factor of one hundred compared to the static case. This potential power from either high crosswind speeds or high tensions can be harnessed to capture the potential energy in the wind field. However, there are certain limitations to how much power can be extracted. If drag losses are accounted for, the resulting power for a kite/rigid body system can be approximated using Equation (2-3). The proof of this equation is given in [7] and can also be found in Appendix A.

$$P_{AWES} = \frac{1}{2}\rho_{air} A C_L(\alpha) v_a^2 (v_w C_L(\alpha) - v_a C_D(\alpha)) \tag{2-3}$$

where, $C_D(\alpha)$ is the drag coefficient of the kite. In Equation (2-3), the power of the kite/rigid body system is seen as a function of both the area of the wing or aerofoil and the aerodynamic coefficients associated with it. Therefore, to maximise power, the drag $C_D(\alpha)$ of the system must be reduced as much as possible, a point that is discussed in greater detail in Section 2.6.

Loyd [6] denoted two types of aerofoils related to crosswind flight namely; a system operating in *Lift Mode* whereby the tension in the line is used to unwind a drum connected to an electrical generator on the ground or *Drag Mode* where the system drives a turbine located on the wing of the aerofoil and sends the electricity through one of these tethers back to ground. The addition of the turbine increases the overall drag of the system which is why these systems are deemed to operate in *Drag Mode*.

When operating in *Lift* mode the aerofoil is reeled out at an optimum speed, shown to be one third of the operating wind speed, and then flown at an optimum speed relative to the remaining two thirds of the wind speed [7]. As the optimum speed will involve crosswind flight, the most optimum control strategy takes the form of a figure of eight pattern as shown in Figure 2-3 below:

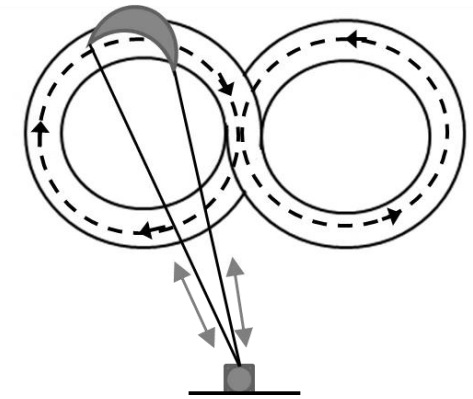

Figure 2-3 - Kite System Controlled in a figure of eight crosswind flight pattern [12]

Figure 2-3 shows the crosswind flight trajectory of kite system. This strategy is known as *lift mode* which is divided up into two phases of operation; the *Traction Phase* and the *Passive Phase*. The traction phase is where electricity is being generated. The winches reel out the tether as a consequence of the high tension force. Once the cycle is complete and the tether has been fully reeled out, the aerofoil is rolled by 90 degrees so that there is little or no lift. At this point the kite begins to stall. This is the beginning of the *Passive Phase*. Once the kite has lost all aerodynamic lift, power is sent to the motor winches to reel the kite back into the appropriate starting position. This process repeats over a number of cycles making power generation periodic [13]. The goal of the control system is to maximise the power during the *Traction Phase* and minimise it's consumption during the *Passive Phase*. These aerofoils can be used for ground based electricity generation, a carousel formation (an extension of ground based generation) or used for vehicle propulsion [14]–[16]. *Lift* mode devices typically use

flexible aerofoils such as flexible kites for power generation although some systems use rigid bodies.

Alternatively, when operating in *Drag Mode* the tether length is kept constant and the power is generated by an on-board turbine and sent back to ground through one of the tethers. Again, the system is flown crosswind but in this case a circular trajectory is employed rather than the figure of eight, as the tether length remains constant. This is illustrated in Figure 2-4 below:

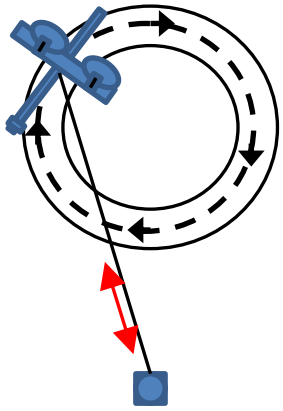

Figure 2-4 - Trajectory of Drag Based aerofoil [17]

Since the turbine is fixed onto the aerofoil, *Drag* based devices are rigid-aerofoils designed predominately from lightweight carbon fibre materials.

Thus far the discussion has centred on the division of tethered airborne systems into two distinct modes of crosswind operation; *Lift* and *Drag* mode. But this categorisation only covers systems that have kite or rigid-body designs as aerofoils. There is a third type of system which does not rely on crosswind flight for operation. This is based on lighter than air technology.

Lighter than air or buoyant airborne systems have an inherent stability in lower winds that kite/rigid aerofoils do not. The most notable designs is that of Altaeros Energies, which has a tethered helium filled shroud, holding an off the shelf wind turbine rotor within its core [18]. The operation does not rely on crosswind flight, instead power generation is achieved once the system is stabilised at a given altitude in the air. Active control over the tether lengths is employed to provide this stability. Importantly, the rotor is an off the shelve HAWT. This ensures that power conversion is more mature than other AWE technologies.

To account for the lighter than air design within an AWE context, it is beneficial to separate all AWE systems into two distinct classes; Ground Level Generation and On-board Generation. However, in doing so this reveals an important issue that it is not yet clear which design is most optimal for power generation. The proceeding section seeks to give a fuller appraisal of the major AWE companies in terms of system operation, modelling, control design, optimisation, scaling potential and economic considerations. This is in an attempt to determine what the current challenges are for AWES and which companies are in the best position commercially for future deployment.

2.2.1 Ground Level Generation (GLG)

Ground level generation (GLG) systems consist of, either one or two, tethers wound round a mechanical drum or a fixed station. The traction generated as a result of aerodynamic forces on the aerofoil unwinds the tethers causing the drum to rotate and subsequently turn an electrical AC generator. Each of these devices fall into the category of *Lift Mode* devices discussed earlier. Four companies, KiteGen, SkySails, Kitepower Systems, Ampyx Power, Omnidea and Windlift generate electricity at ground level [19]–[21].

In terms of AWE technology, SkySails was the first industrial application of an AWE system. It was first utilised to help propel a ship in order to preserve fuel [22] but can now be

bought independently as a stand-alone wind energy extraction device. The system is depicted in Figure 2-5 below:

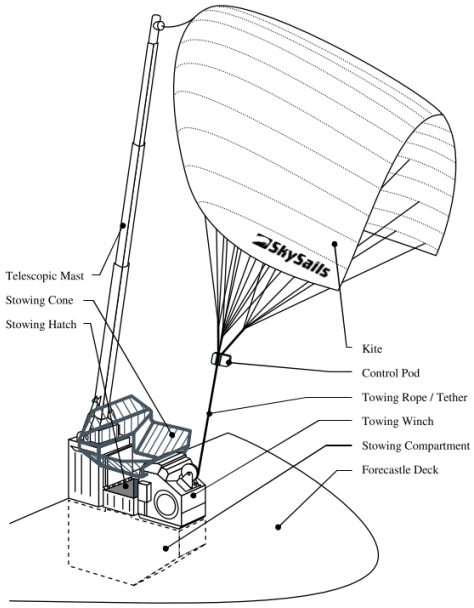

Figure 2-5 - CAD illustration of Skysails system [23]

In Figure 2-5, the kite itself is double skinned and made from polyamide with an aerodynamic profile created by ribs rigidly attached to two sides of the material. The control pod regulates the aerodynamic characteristics of the kite thus controlling the orientation. There are two methods of operation. If the kite is designed to pull a ship then the system operates in open-loop as the vector of aerodynamic force can be controlled relative to the ships position. However, if it is to generate electricity it must operate in closed loop therefore employing a crosswind flight trajectory, typically a figure of eight pattern. This is true for all kite systems [23]. More information on the control of these systems can be found in Section 2.4.2.

KiteGen also use a kite as their aerofoil. However, their design employs two tethers located at either end to facilitate differential control over the kite's aerodynamics. The base station

houses the drums, electric drives, sensors and control unit which communicate with the on-board sensors on the aerofoil during operation. This is shown clearly in Figure 2-6.

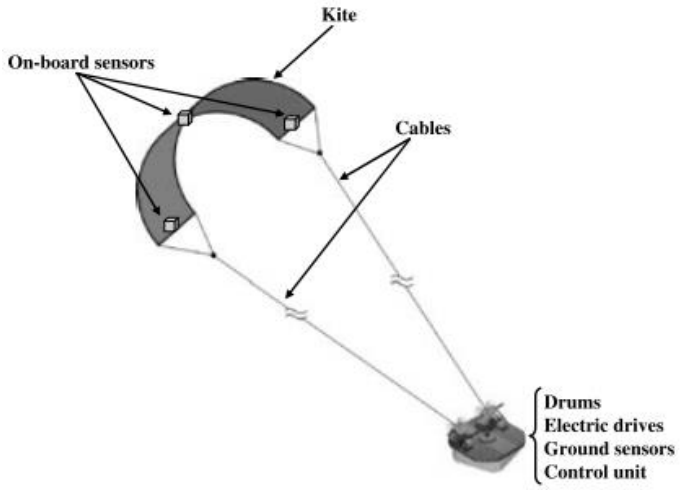

Figure 2-6 - KiteGen AWE system [13]

Although this has a kite as its aerofoil this design is fundamentally different from that of the Skysails design. Comparing Figure 2-5 with Figure 2-6 shows that the Skysails system has smaller individual tethers collocated at one main bridle point on the main tether compared to two main tethers fixed at either side of the aerofoil in the KiteGen design. The KiteGen design can produce a peak of 60kW with an average power production of around 5kW [24]. Similarly, the SkySails design is rated at 55kW, but again because of the pumping cycle the average power generated will be lower than this [20]. Furthermore, Kitegen have also experimented with using multiple aerofoils, in a carousel formation, to pull a load connected to one generator at ground level [16]. However, this concept may be more suited to offshore development.

Alternatively, Ampyx Power utilise a rigid body aerofoil instead of a flexible aerofoil to drive a ground based generator. The rigidity of the plane comes from two wings, one at the

front and one at the rear [25]. An inflatable tube forms the leading edge of the wing. The system is depicted in Figure 2-7 below:

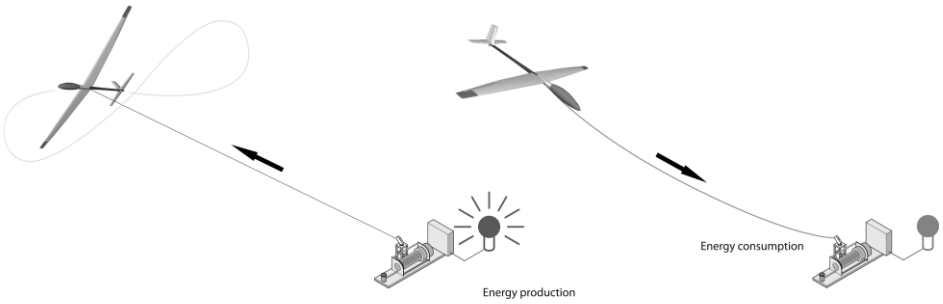

Figure 2-7 - Ampyx Power system [26]

In Figure 2-7, the rigid body offers a higher degree of stability during flight operation over the kite design. This is because actuators in the form of flaps, ailerons and rudders can be placed on the plane that alter the aerodynamics and provide increased control [27]. The wings are typically made out of carbon fibre, helping to achieve a very light but stable structure. Due to the preliminary success of these systems, a number of publications now assess the benefits of GLG devices in terms of modelling and control [18], [28]–[29].

Additionally, there is one ground based power generation design that uses pumping but not crosswind flight. Omnidea have developed a lighter than air design based on horizontal axis rotation employing the Magnus effect [7] to lift the system up causing different tether tensions [31]. However, this product is still in an early stage of development to other GLG based devices.

2.2.2 On-Board Generation (OBG)

On-Board Generation devices consist of a rotor that is fixed onto an aerofoil that is tethered to the ground. The aerofoil is flown either crosswind or is kept stationary depending on the

technology, and electricity is sent back to ground through a conductive tether. There are several AWE companies that have OBG and these are; Altaeros Energies, Makani Power, SkyWindPower, and Magenn [17], [18], [32], [33] Each of these systems generate power through an on-board rotor and send this power back to ground through a conductive tether, typically made of aluminium because of its lightness compared with copper.

SkyWindPower has proposed a multi-purpose rigid body structure consisting of two arrays comprising a number of rotors. Each rotor is able to convert mechanical energy into electrical energy at high altitude. For take-off, power is provided to each generator from the grid causing the rotor to act like a propeller. Once the system has reached a safe height the power supplying the array is turned off and the system is flown in a crosswind direction in order to maximise energy production on each of the rotors.

Conversely Makani power uses a power plane with rotors positioned upwind. Recently bought over by Google, one prototype has reached a power output of 30kW. It has now commissioned a 600kW prototype to fully demonstrate its potential. The system comprises a rigid plane made from carbon fibre composites and 8 brushless DC motors for energy generation [17]. The conductor used within the tether is aluminium and, the tether length is held constant and the system is flown in a circular path to generate electricity, making it a *Drag Mode* device. The flight path and the system in flight is shown in below:

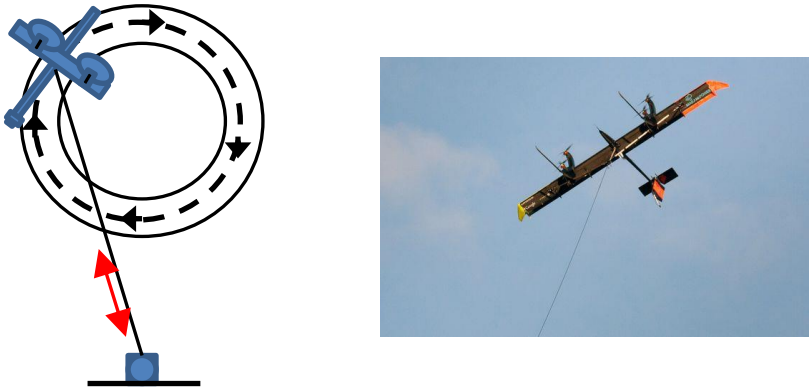

Figure 2-8 - Makani Power flight path (Left) and system in flight (Right) [17]

In addition to the rigid body designs there are two lighter than air systems currently in development. Magenn power has developed a Savonius turbine consisting of a helium filled cylinder that rotates horizontally about its axis [33]. Whereas, Altaeros Energies have taken a standard wind turbine rotor and fixed this within a buoyant shroud.

The Altaeros Energies design is known the BAWT and is still in the prototype stage, with testing currently underway on a 30kW machine. The system is comprised of the following; a base station that holds three independent motor drives, three tethers that attach the aerostat to ground, a buoyant shroud filled with helium, and a standard HAWT rotor mechanically fixed within the shroud. The power is transferred from the shroud back to ground through one of the tethers [34]. An illustration of the system is shown in Figure 2-9:

Figure 2-9 - Altaeros Energies BAWT System during testing [18]

Lighter than air systems, such as the one shown in Figure 2-9, will have a higher degree of stability borne out of their buoyant properties compared to other designs. This makes the system appealable as it does not rely on aerodynamic lift at low wind speeds, so will not need to be fully retracted in periods of no or little wind [35]. In the Altaeros case (Figure 2-9), the shroud can be designed to augment the incoming flow so as to increase the wind speed seen at the rotor. This has the potential to reduce the overall system, increase the rated wind speed and increase the power to volume ratio, a point discussed in greater detail in Section 2.6. However, the downside compared with other OBG and GLG devices is that the system will carry more weight. This is due to the large volume of gas required to ensure the system is buoyant in periods of low wind. This leads to questions about the validity of using a buoyant gas, typically Helium for a renewable energy system. However, although the gas is a finite resource, the natural reserves will not be in danger for hundreds of years thus meaning it is still applicable for use in lighter than air systems [36]. One significant benefit of the Altaeros design is that by using a HAWT rotor, the generated power is not periodic as is the case with all other OBG and GLG devices.

2.3 AWE System Design

2.3.1 Tethers

The tether is a key element of any airborne wind energy system. It performs two functions. Firstly, it ensures that the system is secured to the ground and secondly, it facilitates power generation through either electrical or mechanical means. A typical tether for GLG device is shown in Figure 2-10:

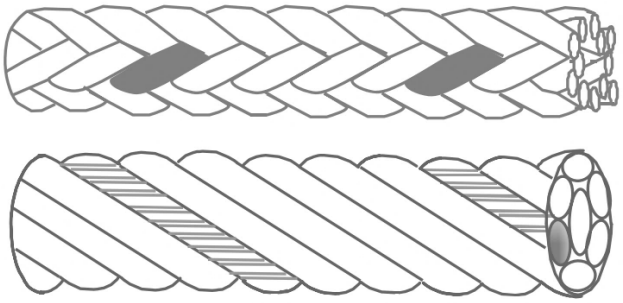

Figure 2-10 - Top: Braided tether, no untwisting when loaded. Bottom: Laid Tether: un-twisting when loaded [37]

The key for any airborne system will be to ensure adequate system performance whilst limiting the effect of lifetime fatigue of the tether. Therefore, a particular design of the tether will be required depending on whether the system generates electricity in the air or at ground level.

For GLG devices the design of the tether is quite generic, since it is adapting tethers already in use in similar applications i.e. kite-surfing. However, with OBG devices the design becomes more specific. This is because the tether needs to be electrically conducting to transfer the generated power back to ground. This will involve the addition of a conductor within the tether itself, therefore adding to the overall cost of the system, There is, as of yet, a design process that can be broadly applied to OBG devices because each system is entirely

unique. However, some criteria for tether design can be applied to all AWE systems. These can be broken into the following requirements:

1. *High strength to weight ratio*: Each tether must be as lightweight as possible to reduce the overall system weight. However, they must also have sufficient strength to withstand the high tensile forces and bending moments that will be induced by the aerofoil during nominal operation.
2. *Sufficient Resistance to Environment:* Each tether will have to be highly resistant to the effects of the operating environment on lifetime fatigue. It will also have to limit the impact of UV irradiation and rain during its lifetime.

Point one, is fundamental for any AWE systems. This is primarily because one of the key advantages of AWE systems is that they employ lightweight aerofoils. If the tethers were heavy, this advantage would become obsolete as the design would be driven by the gravity losses from the tether. Therefore, it is imperative that each AWE system use a tether that has the sufficient high strength to weight ratio. To decide which fibre is best suited for operation, a comparison is made between the different types of high performance materials in terms of strength to weight and strength to area ratios. This can be seen in Figure 2-11:

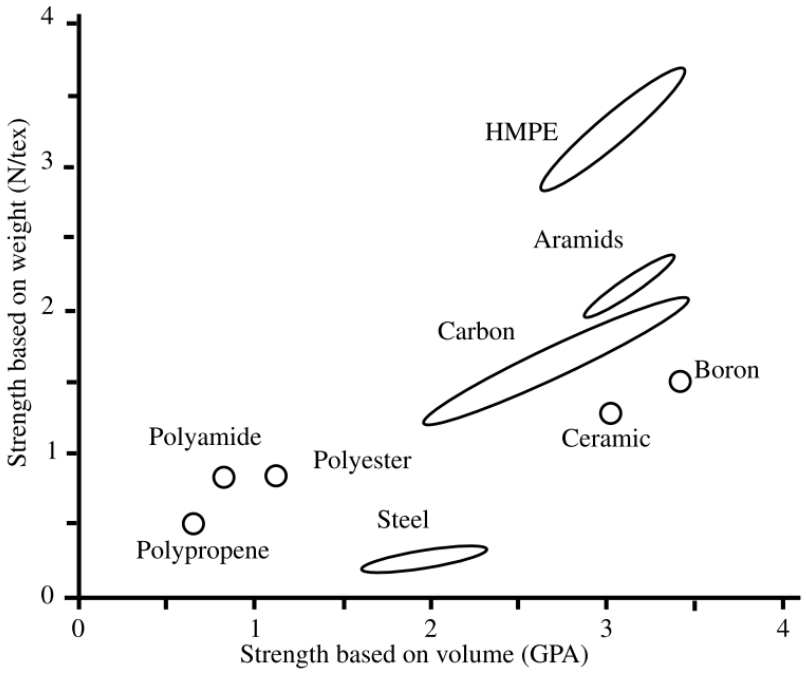

Figure 2-11 - Strength per Weight and Strength per Volume for Higher performance fibres [38]

In Figure 2-11 the strength to weight ratio is given in units of N/tex which defines the force (N) divided by the linear mass density of the material (tex). The strength based on volume is measured in Giga-Pascals and is equivalent to the Young's modulus of the material.. It can be seen that high modulus polyethylene (HMPE) fibres have a very high strength to weight ratio compared to the other materials, thus making it the best candidate for AWE systems [31]. Additionally, it is known that these fibres have high durability and resilience to weathering effects (Point 2) so compound the value to an AWE system.

In order to ensure the overall weight of the tether is kept low, the diameter of the tether must be constrained to a minimum value. However, the diameter of the tether, and the subsequent minimum breaking load of the tether, is driven by the aerodynamic loading on the aerofoil during operation. So for each aerofoil there will be a static load, driven at high wind speeds that will be dominant for a given AWE system. To decide what diameter of tether is required, the maximum load during operation is computed and then multiplied by a safety

factor. This safety factor will affect the number of cycles to failure of the tether. A high safety factor implies low stresses and long lifetimes but comes at the cost of a higher diameter, which is undesirable for AWE systems. The computed minimum breaking load for the AWE system is then compared to the datasheet of the tether fibre, to determine what diameter is required. A typical curve for the minimum breaking load of Dyneema SK78, a standard AWE tether material, as a function of diameter is seen in Figure 2-12 below:

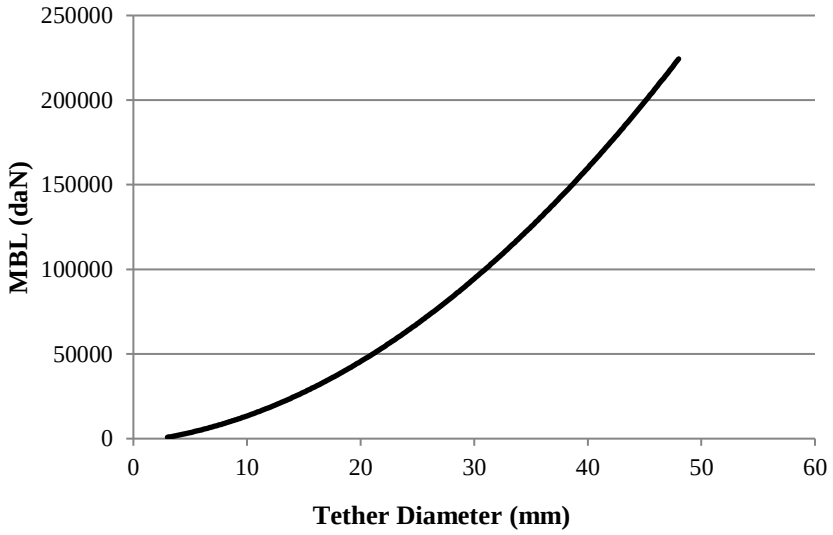

Figure 2-12 - Minimum Breaking Load (MBL) of Dyneema SK78 fibre [39]

Figure 2-12 shows the Minimum Breaking Load (MBL), presented in dekanewton's (daN) as a function of tether diameter. Most AWE's have an absolute maximum tether diameter, determined based on tether weight as a function of operating altitude. For instance, Kitepower Systems give a maximum diameter of 7mm at an operating load of 12kN.

Furthermore, the lifetime of a tether will vary depending on what type of system it is employed for. Depending on the AWE system, the tether will experience periodic stresses which may cause fatigue after a certain amount of time. This includes tether bending and load application. The temperature of the ambient air will also be an important consideration

in the stress levels of the tether. In addition to reverse bending, external abrasion, particle ingress and rope twisting that can also affect the lifetime and fatigue of the tether [37].

2.3.2 Sensors and Actuators

A number of sensors are required for the successful operation of an AWE system. These can be divided between position and velocity sensors and force transducers. The position and velocity are estimated using a global positioning system (GPS), which consists of three accelerometers, three gyroscopes and a magnetometer. This is typically referred to as the on-board Inertial Measurement Unit (IMU). The collected measurements from these sensors are then used to provide an estimate of the systems speed and position in an inertial reference frame. At ground level, attached to the base station, there are pressure sensors, GPS, wind speed and direction sensors. Force transducers are located at the base station to measure tether tension. Tether encoders then give information on the tether length and velocity which is used as feedback for the control of the system [7]. In the Makani system, surface encoders are employed to measure deflections from the rudders and flaps. In contrast, the Altaeros System has additional barometric pressure sensors to monitor the buoyancy of the shroud and ensure it remains within prescribed levels. Finally, in all systems pressure transducers are located on the base station to ensure safe landing and take offs.

As each AWE system is tethered, winch actuation plays a key role in the control over these systems. However, some systems depending on their design may have additional actuators on the aerofoil itself to facilitate control. For instance, the rigid body system will have flaps, rudders and ailerons to guide the angle of attack so that the desired trajectory is followed. For a full assessment of each system, a comparison in Table 2-1 and Table 2-2 is made between the key GLG's and OBG's in terms of actuators and sensors. The extent of the variation in design of each system becomes clear on inspection of Table 2-1 and Table 2-2. In terms of GLG the number of motor winches varies markedly compared with the number

of on-board rotors in the OBG case. To the authors best knowledge these are the designs in wide-spread deployment. Please note any information that could not be found was left blank.

Table 2-1 - Ground Level Generation (GLG) - AWE Comparison

Company	**Wing Type**	**Material Used**	**Ground Sensors**	**Airborne Sensors**	**Actuators on aerofoil**	**Tether Material**	**Number of Motor Winches**	**Current Status**
KiteGen	Power Kite	Ripstop polyester	Force Transducers, wind speed and direction	Triaxial accelerometer and a pair of triaxial magnetometers	Control Pod, IMU	Composite	2	60kW yo-yo system designed
SkySails	Power Kite	Ripstop polyester	Tow point sensors, angular sensors (wave motion compensation)	Accelerometers, magnetometers	Control pod, acting on steering lines (IMU)	Synthetic fiber	1	30kW system
WindLift	Power Kite	Ripstop polyester	Force Transducers, wind speed and direction	Accelerometers, magnetometers	None	Composite	2	12kW system
Ampyx Power	Powerplane	Carbon fiber	GPS, force transducer	3D Accelerometers at each wingtip	Rudders, ailerons, flaps	Polyethylene fiber 1Dyneema	1	10kW prototype

Table 2-2 - On Board Generation - AWE comparison

Company	**Wing Type**	**Material Used**	**Ground Sensors**	**Airborne Sensors**	**Actuators on aerofoil**	**Tether Material**	**Number of Rotors**	**Current Status**
Altaeros Energies	Helium Shroud, with rotor fixed inside	Aramid scrim fabric (outer), Polyurethane bladders (inner)	Ground level pressure sensors, GPS, wind/direction sensors, touch sensors, force transducers	Barometric pressure sensors, wind/direction sensors, accelerometers, magneotmeters, three pressure transducers	Valves (active for venting air), inflatable wings (passive) designed for stability, ducted shroud (enhance air flow)	-	1	Currently testing 30kW prototype
SkyWindPower	Structural array holding a number of rotors	Carbon fiber, composite	-	-	Differential pressure differences over rotors, pitching on rotor	-	4	Concept stage
Makani Power	Gliderplane with generators attached	Carbon fiber, e-glass coating	Force transducers, position sensors	-	Rudders for stability	Pultruded carbon fiber	6/8	Currently testing a 600kW protoytpe

2.3.3 Communication

Furthermore, communication between the aerofoil and the base station is paramount. The communication link must be secure to ensure the safety and successful operation of the system. For most AWES, this is performed via a wireless link between the aerofoil and ground. However, this may also occur via a low-power connection within the tethers. The disadvantage of this is that it may increase the cost, weight and diameter of the tether significantly. Thus, wireless links are preferred. However, reliable communication with the controller is imperative and can be compromised by transmission delays. Therefore there must be sufficient system redundancy built in to ensure smooth operation in the case of a communication failure.

2.4 Modelling and Control of AWE Systems

For these systems to become cost-competitive with conventional wind energy systems they will must demonstrate their ability to withstand long periods of operation without fault, be robust to the operating conditions imposed i.e. wind gusts and be optimised to generate power as efficiently as possible. In addition, the system will have to handle certain constraints such as ensuring a minimum amount of tether tension, constraining the tether length, keeping to actuator limits and deploying/retracting the system autonomously in a safe manner.

To facilitate this, a thorough understanding of the dynamics is assessed through high fidelity simulations augmented with experimental validation. The mathematical model will provide a basis upon which to derive appropriate control strategies whilst physical experiments will prove how effective these strategies are. For each AWE system, the control strategies employed will be different as there are a number of different designs using a variety of

actuators for control. However, the overriding control objective of maximising energy capture from the wind remains the same regardless of the system employed.

2.4.1 Modelling of AWES

Looking specifically at the model dynamics of an AWE system, the mathematical model should account for all the key driving forces on the system. Typically, the aerodynamics over the aerofoil will dominate in any AWE model; therefore an explicit formulation of these forces is paramount. In addition, as all AWE systems are tethered, modelling the tether tension as well as overall tether drag is another key consideration. The tether drag in particular is important as it is known to be a key issue in the efficiency of these systems. Accounting for winch actuation i.e. the reeling dynamics of the tether is another important consideration. In addition to any other actuators that provide control i.e. flaps, ailerons or rudders present on the rigid body.

The mathematical models aim to capture the kinematics of the system, usually deriving the systems position with respect to an inertial reference frame. Euler's equation of motion are used for the Ampyx and Altaeros system and can be expressed in a Spherical or Cartesian coordinate system [40]–[44]. Typically, at a given point in time, instantaneous flight is approximated through a steady state balance between the aerodynamic and tether forces. This gives rise to a force balance from which the power and tension forces can be calculated. Furthermore, as the aerodynamics will vary rapidly with time, in addition to a significant disturbance in the form of wind, the model will be highly non-linear. As for most plants, the nonlinear model, for any AWES, is placed in the form shown in Equation (2-4) for control design:

$$\dot{x} = f(x(t), u(t), w(t)) \tag{2-4}$$

where $x(t)$ represents the state vector of the system (positions, velocities), $u(t)$ is the control input and $w(t)$ is the disturbance profile. Equation (2-4) allows the system to be expressed as a function of all known states, inputs and disturbances, allowing application of optimization algorithms. The primary disturbance for all AWES is the wind due to its stochastic nature, so an appropriate wind model is also required to test with any AWE system.

Point mass models are most commonly used for the kite system whilst, systems more akin to conventional flight control such as the Makani, Ampyx and Altaeros Energies benefit from more widely known flight mechanic theory and aircraft dynamics. However, there are still open issues in need of more research. For instance, tether aerodynamics, HVDC cable modeling and rotor/aerofoil interaction are all avenues that have yet to be fully explored.

2.4.2 Control of Kite Systems

In the case of the kite system, common control inputs include the difference of length of the steering tethers, some form of the "tether roll angle" and the lift coefficient $C_L$which is controlled through changing the angle of attack [32], [34]. Optimisation techniques are employed to deliver appropriate trajectory control whilst ensuring sufficient constraints on a number of states. One such optimal control problem may be the maximisation of average power output over given period of time t. Constraints on maximum altitude, angle of attack, actuator limits and boundary conditions are then enforced to keep the system within realistic bounds [35].

Some other types of control methods, employed on kite/rigid-body systems, are based on Model Predictive Control, adaptive control and evolutionary robotic techniques [36]. Work has been done into the formulation of path planning using Non-Linear model predictive control techniques, which allow for robust tracking of the desired figure of eight path whilst

also ensuring sufficient constraints on parameters such as tether length, tether tension and angle of attack. This is typically an extension of LQR based techniques shown in [34]. This control action is computed through a receding horizon (RH) strategy that computes the solution to a constrained optimal control problem at a pre-defined sampling time. However, this method encounters problems due to the typically long sampling rates required to achieve the desired solution. For a kite system where the dynamics are fast, work has had to be done to extend these model predictive methods to allow for sufficient computation within the small sampling times required. This has been achieved using an offline approach whereby the desired control law is derived on the basis of the off-line computation of a finite number of exact control moves. There is always a trade-off between the amount of computational memory required and the closed loop performance of the system [37].

The problem of online state estimation is important for an AWE system and is looked at as a dynamic optimization problem. Moving Horizon Estimation (MHE) is common whereby a time window of fixed length in the past is considered, on which the difference between the predicted measurements and the actual measurements is minimized. This is similar to Kalman filter design for linear unconstrained systems with Gaussian white noise. Furthermore, optimisation algorithms are then employed to compute the desired path under given constraints. These techniques have been investigated for the kite system and applied in the literature [22].

For real time performance these methods may be less advantageous than using a more simplified hierarchical control structure. This may be required because optimization methods rely on fast computing power that may not always be available whilst a simplified control structure will offer the advantage of being relatively intuitive and simple to tune and debug in real time [26].

As an example, the control architecture developed for a kite system by Fagiano et al in [45], [46] is evaluated. The controller is aimed at regulating the wing's path through a steering deviation δ which influences the kite's roll angle and consequently the lateral component of the lift force relative to the centre of mass. It is shown in Figure 2-13 below:

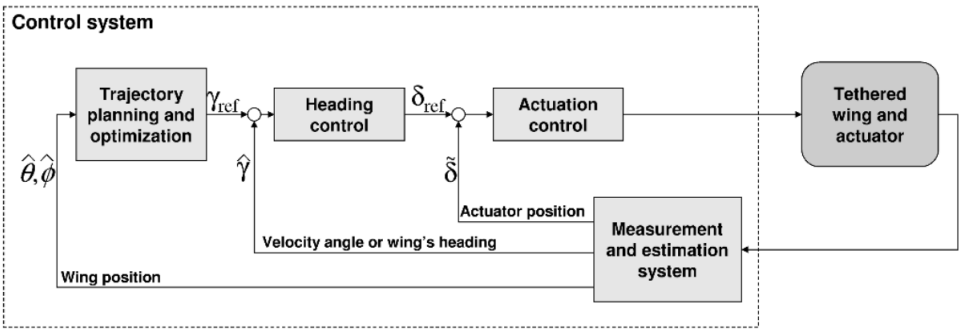

Figure 2-13 - Proposed Control System for Kite application [45]

There are three loops within the control system shown in Figure 2-13. A position loop, a velocity loop and an outer loop that defines the trajectory of the system as a function of both pitch and roll angle. Within the wing-line configuration there exists feedback of a "geometric input" that takes into account any offset that occurs when the wing's lines are not aligned precisely with the x-axis, causing a steering deviation. The inner position loop is determined using standard loop shaping techniques and through a derived gain that computes the desired tether difference required [47]. Outside this, lies a velocity loop which computes the desired velocity angle of the aerofoil, defining the heading of the system. This is given by a simple proportional control law. The outermost control loop then computes the desired velocity angle or heading, through a guidance strategy incorporating both the pitch and roll angle of the aerofoil.

2.4.3 Control of Rigid Body Systems

In the case of Ampyx power where crosswind flight is the main concern, the model is set-up based similarly to those of standard aircraft models to include the weight effects with typical aircraft actuators for control such as flaps, ailerons and rudders. Longitudinal control is achieved by tracking the angle of attack as well as tracking the rotational velocity of the winch. Lateral control is employed in the same way as that of a glider. The result giving a full tractable system that delivers figure of eight loops for electricity generation [48].

Makani Power, is the other main system that uses a rigid body system. Their control system is divided up into four distinct regions. The first is flight maintenance where constraints are imposed on tether tension, the second is power generation which is defined over a circular trajectory, the third is tension constrained generation where the limit on allowable tether tension has been reached and the fourth is maximum power generation where the system operates as efficiently as possible [49]. The control methods employed for kite and rigid-body systems are inherently the same and can be modified for a particular design.

2.4.4 Control of Buoyant Airborne Wind Turbines (BAWT)

For a BAWT the model and control strategy implemented is very similar to that of an aircraft or similar aerostat and satellite applications [50]. The model is derived using standard Euler equations of motion [51] and it treats the three winches located at the base station attached to the fore and aft-port and aft-starboard of the shroud respectively as control inputs. Previous work breaks the controller into a hierarchical structure comprising of high level and low level parts [52].

Low level control regulates the winch speed for each tether subsequently controlling the unstretched tether length [53]. The overall difference in fore, aft starboard and port starboard tether lengths regulate the orientation of the shroud in the rotational direction. The rate at

which the tethers are reeled in/out regulate the position of the shroud in the translational direction. The medium level controller determines the desired pitch and altitude set-points which is then mapped to an appropriate value using a known function of the system's operating envelope. The high level controller seeks to optimise these set-points.

A reference governor approach was investigated in [54]. This looked at computing a control input based on a constraint admissible set $y(t)$ for a given desired set-point $r(t)$. This work is essentially an add-on predictive control scheme that enforces pointwise-in-time constraints when a discrete linear model is available. In addition, MPC schemes have been investigated in [55] showing that appropriate constraints on altitude, pitch and tether tension can be achieved without affecting the overall performance of the system.

This control strategy contrasts with KiteGen or Ampyx Power where focus is placed on the regulation of the roll angle in order to follow a prescribed trajectory. Stationary power generation under normal flight conditions is unique to the Altaeros Energies system. In other systems, actuators are utilised to provide further aerodynamic control but the system is still reliant on constant crosswind motion of the aerofoil therefore increasing the likelihood of unstable behaviour.

2.5 Wider Issues with Control

2.5.1 Dynamic Control

There are clear control strategies in place for kite and rigid-body systems that employ crosswind flight. The control structure for these systems can be categorised into low-level control and high level control. Low level control produces a low-level command to the aerofoil based on a given flight trajectory. Typically, this output alters aerodynamic performance of the aerofoil by affecting the angle of attack. The High level Control adds

optimisation for maximising system efficiency, tracking the systems operating envelop and handling system constraints. However, because the system operates in crosswind flight, the system is never at rest and therefore constantly accelerating. This makes it difficult to attain equilibrium. As the system relies solely on aerodynamic lift, in periods of low wind the system has to be retracted or compensated by actuators on the aerofoil. In contrast, lighter than air systems remain in the air during periods of little or no wind. For example, the BAWT generates electricity when the shroud is stationary in the air. This makes the control design of the system less constrained by rapid reaction times compared with other AWES. However, in the BAWT case, this at comes at the cost of an increase in the overall weight of the system therefore making it more expensive.

2.5.2 Coordinated Control between aerofoil and rotor

There are a wide variety of control strategies presented in literature discussing control tracking for optimal power generation of AWES. For GLG devices, the crosswind strategies maximize the tension on the tether thus maximising power. However, the power is cyclical and so an average power is used to determine the rated power of the system under given wind conditions. Similarly, for OBG devices, crosswind flight results in a cyclical variation of power over the flight path. This arises due to changes in wing speed and wind speed. In both cases, much research has focussed on the optimisation of given flight paths with little discussion as to the efficiency of power capture from the generator. Therefore, more work is still required in terms of coordinating the operational flight path with maximum energy capture from the rotor.

2.6 Power Potential for AWES

Assuming the kite/rigid-body is directly downwind of the tether and flying at a crosswind speed directly parallel to the oncoming wind flow, the power potential can be derived under ideal operating conditions. This is shown in Equation (2-3). For a full proof please see

Appendix A [7]. Differentiating Equation (2-3) with respect to the kite velocity v_a yields the theoretical maximum kite speed that will maximise power:

$$v_a = \frac{2}{3}\frac{C_L(\alpha)}{C_D(\alpha)}v_w \tag{2-5}$$

This can be substituted back into Equation (2-3) to yield the maximum power for an AWE system:

$$P_{AWE} = \frac{2}{27}\rho_{air}A_{wing}{v_w}^3\frac{C_L(\alpha)^3}{C_D(\alpha)^2} \tag{2-6}$$

Equation (2-6) shows the absolute maximum power that can be captured from a crosswind system under completely idealised conditions (directly downwind and orthogonal flight to the oncoming wind). The dependence of power on the wing's aerodynamic profile is clearly seen through the lift-drag ratio $\left(\frac{C_L(\alpha)}{C_D(\alpha)}\right)$. As the drag $C_D(\alpha)$ scales quadratically, reducing the overall drag loss through aerodynamic design becomes a fundamental to the success of these systems.

The metric used to assess the power potential from an AWE system is known as the zeta factor. This relates the useful power that is harvested from an AWE system at a given area A_{wing} to the ideal wind power that passes through a cross-sectional area of the same size $P_{ideal} = \frac{1}{2}\rho A_{turb}{v_w}^3$. Dividing Equation (2-6) by P_{ideal} yields:

$$\xi = \frac{4}{27}\frac{C_L(\alpha)^3}{C_D(\alpha)^2} \tag{2-7}$$

The zeta factor is analogous to the maximum power coefficient achieved at the Betz limit [7]. Given the maximum $C_P = \frac{16}{27}$ the metric $\frac{27}{16}\,\xi$ will give an indication as to how much more power can be gained from a wing of area A_{wing} to that of a wind turbine swept area A_{turb}. The proposed theoretical limit is $\xi = 30$ at a $C_L(\alpha) = 1$ and $C_D(\alpha) = 0.07$ [7]. For example, assuming a zeta factor of $\xi = 8$ (achieved by the Makani system) at an overall lift

$C_L = 1.5$ and drag $C_D = 0.25$, and taking a realistic C_P value for a HAWT of $C_P = 0.5$ and substituting in to equation (2-6), the swept area of the AWE system and the HAWT can be compared for a given power output by using the following equations:

$$A_{wing} = \frac{27}{2}\frac{C_D(\alpha)^2}{C_L(\alpha)^3}\frac{P_{AWE}}{\rho_{air}{v_w}^3} \tag{2-8}$$

$$A_{turb} = 2\frac{P_{turb}}{\rho_{air}{v_w}^3 C_P} \tag{2-9}$$

where, P_{AWE} is the power from the airborne system and P_{turb} is the power from the wind turbine. The rated wind speed is defined when P_{AWE} and P_{turb} equal rated power and was assumed to be 10m/s in this case. The comparison for a given area is shown in Figure 2-14 as a function of rated power for both a HAWT and an airborne system:

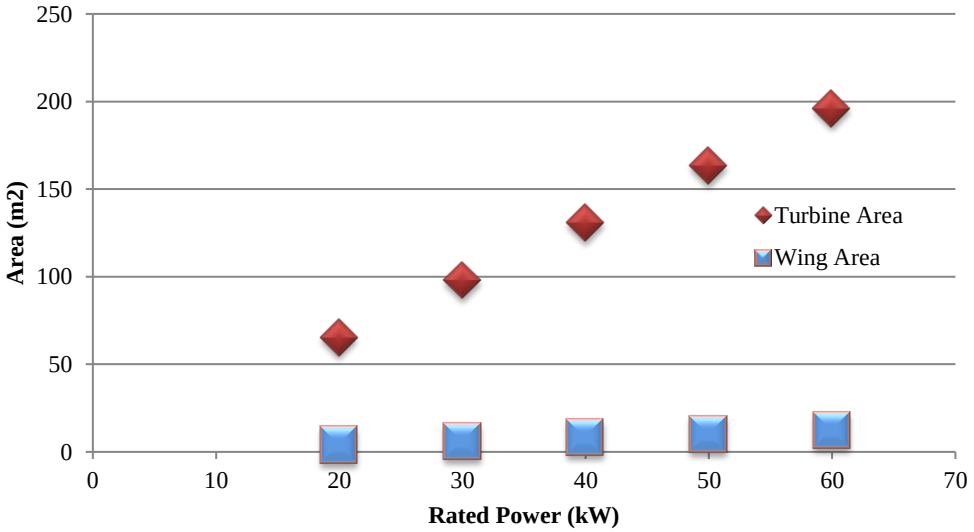

Figure 2-14 - Comparison of Wing Areas for given rated power output

From Figure 2-14 the marked difference in wing area A_{wing} can be seen compared to turbine area A_{turb} at a given rated power. What is clear from examining equations (2-8) and (2-9) is that for a given rated power the kite wing can be designed at 1/16 of the size i.e. the area required for a given rated power of a kite is 16 times that for a HAWT. This provides an

understanding into the scalability of airborne systems and thus the power potential that could be attained at a lower area and ultimately lower cost.

2.7 Optimisation and Scaling Potential

The tether drag and weight also play an important role in optimising system performance. Assuming the aerofoil drag is low, tether drag will dominate. However, as the glider scales in size and assuming a well-designed aerofoil, the lift to drag ratio will increase thus the impact of tether drag is reduced. Therefore, tether drag is more of an issue with smaller systems [48]. To address the issue of tether weight, the tether must be designed with the minimum diameter required to handle the full range of operational forces. This is important since as these systems move to higher altitudes, the weight will increase as a result. Therefore, choosing a small tether diameter not only reduces tether drag but weight as well.

Other studies for kite/rigid-body systems have looked at the normalized power capture with respect to a reeling factor (i.e. what speed the winches should be reeled out at) which gives an indication of how the power output varies with respect to it. This captures the influence of elevation angle and the effect this has on the apparent velocity and consequently power output. It was shown that the power increases with lower elevation angles and decrease with higher elevation angles [56].

Conversely, for lighter than air systems the issue of overall system mass is more pressing. The amount of buoyancy required is related to the overall weight of the system. Therefore, using the Altaeros System as an example, the relationship between system mass and rated power may become prohibitive at high rated powers (>1MW). However, because the Altaeros system has the potential to augment the upstream wind at the rotor plane, coupled with a higher average wind speed, the turbine rotor could be designed to operate at a higher rated wind speed. Operating at a higher rated wind speed will mean that the overall system

mass can be reduced. This can be seen more clearly in Figure 2-15 showing the relationship between system mass and rated power output for the Altaeros system at a rated speed of 10 and 15 m/s respectively. The mass is calculated as a function of rotor diameter, scaling as $M = 9.0674D^{1.8345}$ with an additional 10% of this term added to account for the intrinsic mass of the shroud. The rotor diameter for a rated power is calculated by finding the turbine area from equation (2-9), assuming $C_P = 0.5$, then solving for D i.e. $D = \sqrt{\frac{4A_{turb}}{\pi}}$

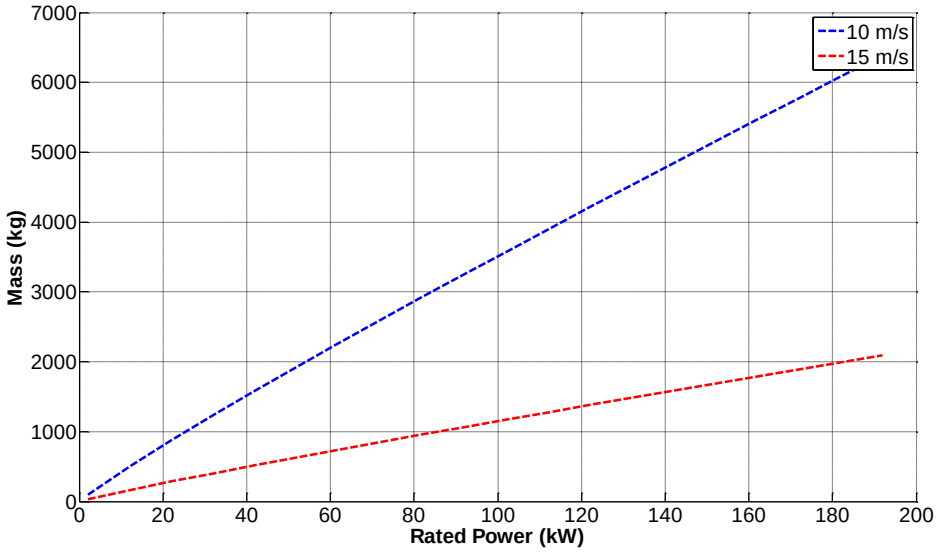

Figure 2-15 - Altaeros Shroud Mass scaling with rated power of the turbine

It can be seen from Figure 2-15 that at a rated wind speed of 15m/s, the overall mass of the shroud is substantially reduced compared to 10 m/s. This is driven by the fact an increase in rated wind speed will allow a higher rated generator speed, which will reduce the generator torque, translating into reduced loading on the BAWT.

The efficiency of a lighter than air design can be assessed in terms of its power to volume ratio. This is stated in Equation (2-10) below:

$$R = \frac{P_{turb}}{V_{shroud}} \tag{2-10}$$

where, P_{turb} is power at rated speed and V_{shroud} is the shroud's volume. The power to volume ratio will have an impact on the cost of energy. If the ratio is low then the cost of filling a given shroud volume V_{shroud} may not be worthwhile in relation to the amount of power that is captured. It is also directly related to the system mass, so if the mass is reduced the amount of buoyancy and therefore volume of gas is reduced meaning a higher power to volume ratio. The effect of this can be seen in Figure 2-16 which shows the power to volume ratio for an Altaeros system, again at a rated wind speed of 10 m/s and 15 m/s.

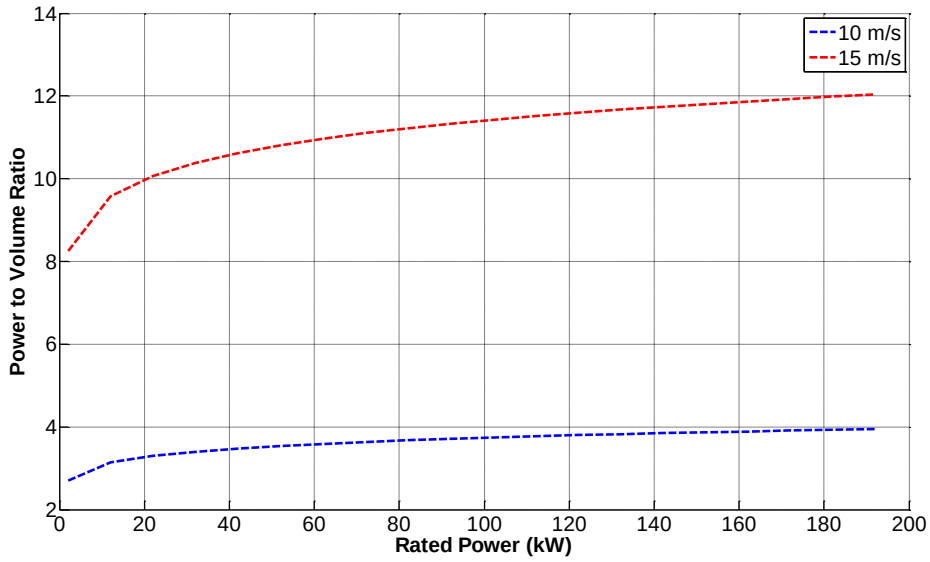

Figure 2-16 - Power to Volume ratio for Altaeros System at different rated wind speeds

In Figure 2-16 it is seen that as the rated power increases the power to volume ratio increases. Additionally, operating at a higher rated wind speed results in a higher power to volume ratio therefore confirming the importance of mass saving. A similar study was also conducted in [52] that demonstrated this effect. The cost of the system, predominately scales cubically with mass (which is proportional to volume), therefore at rated powers above 200kW the cost associated with filling the required volume will become prohibitive in relation to the generated power. This makes the Altaeros system appeal to lower power output ranges (30-200kW) compared to the kite/rigid-body designs.

2.8 Economic and Regulatory Considerations

2.8.1 Economic Viability

AWE provides the opportunity to couple a relatively low-cost generator alongside technology that has been proven in different fields of engineering. However, since this industry is still in its infancy there are still many challenges associated with proving the systems viability on a commercial scale. Clearly, a number of factors including safety and political agreements will need to be addressed but the main driving mechanism behind the viability of such an innovation will be the overall cost of energy of the system.

For any innovation it is important to reduce the cost of energy of the system. A typical life-cycle for start-up companies can be established showing the relationship between the perceived risk and capital requirements in 5 distinct development stages. In addition to this, the main funding sources for each developmental phase can also be included so that it is clear at which point in the technologies life-cycle the funding becomes largely independent of a particular funding body. An illustration of this is shown in Figure 2-17.

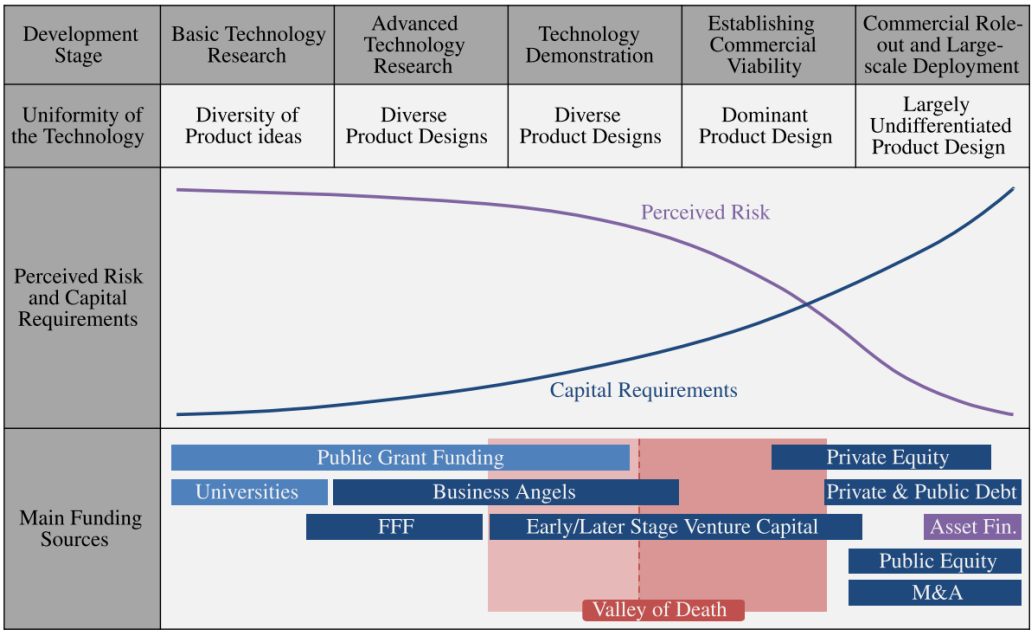

Figure 2-17 - Typical Technology Life Cycle for a Renewable Energy technology [57]

There are five main developmental phases; Basic Technology research, Advanced Technology Research, Technology Demonstration, Establishing Commercial Viability and Commercial Role-out and Large-Scale Deployment. Most work conducted so far in the AWE industry is limited up to the Technology Demonstration stage with the exception of Skysails. This is largely funded by public grants, angel investments or the founders themselves with help from family or friends (FFF). However, as the technology becomes more established, larger funding pools become accessible. For instance, Makani Power received an investment of 13 million dollars from Google in 2013 [58]. As well as Ampyx power which received funding from KLM, an aircraft company which realises the implications that high altitude systems may have on desired airspace.

However, it is clear for an AWE to prove commercial viability it will require a significant amount of capital investment in order for this technology to reach large scale roll out, where asset finance and mergers and acquisitions (M&A) will play a much more significant role in defining the success of these systems. A number of factors are behind this which at this stage are predominately technical and safety related in nature. Firstly as the system is inherently more dynamic than a conventional wind turbine the safety of the system for all possible operating conditions is paramount. If there is a fault with an actuator, the system cannot easily be switched off as it is flying on a specific trajectory, instead redundancy for this system must be treated as seriously as that for a commercial aircraft. Secondly the operating costs of the system cannot afford a manned crew which means that autonomous landing and take-off of the system will be imperative if this technology is to be successful. As it currently stands a lot more research is required in this area [57].

It is also important to attract investors especially during this phase of development. Although investors may be put off by the associated risk with this particular innovation. This comes from the fact that there are a number of different types of AWE system with no one system yet to become dominant in the market-place. This is analogous to the wind industry in the 1980's where the standard 3-bladed horizontal axis turbine became the leading design over others, such as the vertical axis turbine. This happened after extensive research indicated it was the most cost-effective and efficient way of generating electricity from the wind [59]. Therefore, on-going research is still required to reach a similar conclusion for AWES.

To reduce both the cost of energy and improve the efficiency, it is desirable that the system should be modularised. This will make building components for each airborne system much easier when scaling up to competitive power ratings [5]. It will also increase efficiency and availability of given components within the system. Fortunately, the airborne wind industry is based primarily on technology that already exists for other applications. For instance kite airfoils have been developed for kite sport, sensors and controls can be used from the aviation industry as well as strong and lightweight tethers from shipping and other industries. It is however the bespoke nature of each system and the fact that technology still needs to be proven that increases the price and risk associated in its investment. Although, driving down the cost of energy in addition to the potential increase in capacity factor should make these systems more appealing to the wind energy market-place today.

2.8.2 Safety and Regulatory Issues

There is a significant weight differential between an airborne generation system i.e. Altaeros Energies and a GLG i.e. KiteGen. However, both systems will have similar safety and regulatory concerns. There will be an effect on system performance if the communication between the ground station and the aerofoil is lost. To resolve this issue most AWE systems have a back-up link.

Lightning protection will also be a serious issue. For OBG devices, the protection of the conducting tethers will have to be greater for the airborne systems than those used for the ground level systems. How much protection is required will depend on what type of converter is used to transfer the electrical energy to ground.

There is more risk associated with OBGs and GLGs during a fault i.e. if a tether breaks free or the system loses lift because of the electrical conductivity of the tether. There is some degree of mitigation though. The system is designed under stringent operating conditions whereby there are limits on how much the aerofoil can be pitched and what the maximum tension the tether can withstand. These limits exist for all AWE systems however, lighter systems such as kites or rigid-planes will not require as much power or effort to reel it back in under a period of disturbance. Some companies put in additional fail-safes in case of tether breaks. For instance, Makani power have designed their system so that it can disconnect from the tether and land autonomously in an emergency situation [17].

One of the main regulatory issues with AWES is height restrictions. These are in place to ensure the system does not affect the operation of any other airborne systems such as aircrafts or helicopters. Current regulations prohibit air vehicles obtaining more than 600m in altitude. This will be problematic for airborne companies as they seek to scale designs to gain the benefit of higher wind speeds but is of no real concern at the moment. Whether or not new regulations should be written is a matter for debate, but there will be no development in this area until the new technology has proved that it is ready to compete in the current marketplace.

2.9 Discussion

As it stands, there is currently no consensus as to which type of AWE system offers the best alternative in terms of performance, efficiency, availability and reliability compared to a conventional HAWT. By replacing the tower with tethers, an inherently stable system has been exchanged for a highly dynamic one. However, depending on a particular design the degree to which it relies on a dynamic flight trajectory will vary thus making the attempt to quantify overall benefit between these systems more difficult. It was demonstrated in Section 2.6 and 2.7 that the power potential for AWE is huge. This is primarily down to the high zeta factors that can be reached with a rigid-wing compared to a similarly sized HAWT. Of all the companies with a kite or rigid wing design, Makani Power is the market leader with a high zeta factor of 8 and the highest rated power output of 600kW. This is due to the increased investment it has had in recent years. SkySails is another company which now operates in a commercial context, however the main use of this system is not concerned with direct energy generation instead it is mainly used to supplement the propulsion generated by the engine of a ship.

Fundamentally, all AWE systems are competing with established HAWT wind technology. There are many reasons why this technology is more advanced but the main advantages come down to efficiency, availability, reliability and performance over time. Guaranteeing high percentages in all these metrics result in a lower cost of energy. Therefore, to compete with this technology an AWE system must demonstrate its robustness to operating conditions and efficiency in power production. For instance, as all kite/rigid-body systems will be deployed on a particular flight path, demonstrating autonomous flight for significant amounts of time will be paramount. Similarly, the Altaeros system will be required to operate autonomously to ensure overall system costs are reduced. This shows AWE systems have a significant dependence on autonomous control and design in order to reduce the cost

of energy sufficiently to compete with HAWT technology. In terms of applying analysis of HAWT technology to AWE systems, there is only one system, the Altaeros Energies, which relies on the same HAWT technology for energy generation.. This means that energy capture will be more consistent compared to the variable power cycles that occur in all other AWES.

A summary of the advantages and disadvantages of each type of system is presented in Table 2-3 below:

Table 2-3 - Advantages and Disadvantages of Airborne systems [60]

Type of System	**Advantages**	**Disadvantages**
Kite	Light-weight Flexible Low airborne costs	Complex trajectory control High lift to drag ratios required leading to instability Cyclic power generation
Rigid Body	Light-weight More actuators available to provide aerodynamic control	Complex trajectory control Difficult to model High airborne costs Cyclic power generation
Buoyant	Stationary Better understanding of modelling and dynamics Excellent scalability Augmented Flow	Increased weight Increased safety risk High airborne costs Helium requirement

The kite/glider system bases its power output on the aerodynamic efficiency of the aerofoil whereas Altaeros Energies and Makani power use rotors that are located in the air. Power generation is cyclical on the kite/rigid body system as it is constantly switching between the traction and passive phase of control [13]. This is not the case with either the Altaeros

system or the Makani system, with an additional benefit of the Altaeros system being that there may be augmented flow if the shape of the shroud is designed appropriately.

However, it can also be seen from Table 2-3 that although the Altaeros system is disadvantaged is terms of cost and weight compared with other airborne systems it is offset by the fact that power generation in this case is stationary. Building upon established wind turbine technology may make this approach more practical compared with other systems.

Throughout this discussion, it should be evident that there is a case for lighter than air technology compared with other systems within the AWE market. Since this system is still at the prototype stage it makes sense to evaluate it more thoroughly in terms of modelling and control of the system. Over the course of this PhD, the author has worked with Altaeros Energies in order to refine their plant model and offer insight as to which control designs would be the best and most efficient to stabilise the system. Then, the broader issue of power optimisation is assessed and placed into context with the control developments and challenges required to facilitate this. This work will hopefully lead to a fuller discussion about the autonomous strategies required for power optimisation.

2.10 Conclusions

AWE systems are a new class of devices that seek to extract energy from the wind at high altitudes. These systems replace the heavy mass (tower, rotor) of a conventional HAWT with lightweight aerofoils and tethers, reaching higher altitudes where the wind resource is greater on average and less turbulent. Three main types of airborne wind energy system were discussed in detail namely; a kite, a rigid-body and a lighter than air system. Looking at the kite/rigid body system, there are a number of start-ups that have developed this system. The system is very lightweight which is promising when scaling to larger power ratings. However, each system must be operated on a defined trajectory, typically a figure of eight

pattern, or circular pattern in the case of Makani Power, which increases the apparent wind speed and therefore tension on the cables. Long term issues of robustness and power variability will disadvantage this system compared with HAWT technology.

In contrast, comparatively little research has been published on lighter than air technologies. Altaeros Energies combines state of the art technology with known aerodynamic theory to produce a system that has the potential rival a wind turbine through aerostatic technology. This system does not need to follow a prescribed trajectory to generate electricity and as a result is inherently more stable. In addition, the system uses standard HAWT technology as a starting point for power generation and combines this with novel airborne technology. This means that if the system is suitably controlled it will be stable and more importantly, optimised for electricity generation. An informed and coordinated approach to control design between flight stabilisation control and power capture control will increase the viability of this technology moving forward.

3 - Modelling and Design Challenges for a BAWT

This chapter discusses the modelling of both the wind profile and the six degree of freedom rigid-body model of the BAWT, developed by Altaeros Energies. The mathematical modelling of the driving forces over the shroud, in addition to the tether dynamics is presented. This chapter also derives two force ratios that implicitly relate the shrouds parameters to its effect on system stability. As a consequence, the issue of aerodynamic drag over the shroud is highlighted. Furthermore, system operation is discussed and control issues are raised in order to inform the remaining work in subsequent chapters.

3.1 Wind Modelling

Wind arises from the differential heating of the earth due to radiation from the sun. A typical wind profile has both deterministic, wind shear, and stochastic, turbulence, parts which can exhibit large scale variations both temporally and geographically [61]. Topographical features will also influence its behaviour as winds are known to be affected by local architecture such as mountain tops or buildings. As the power output of a wind turbine depends on the cube of the wind speed, characterising the wind profile both in the short term and long term, is fundamental in determining the quality of power output and in a broader sense the viability of a given wind farm site.

3.1.1 Wind Shear

Wind speeds are known to increase with altitude as surface effects are minimised. This is characterised by wind shear which describes the change of wind speed with height depending on location as shown in Figure 3-1. This is one of the driving reasons behind why AWE has received a lot of interest. Consider a standard wind turbine fixed to the ground. This system will be subject to extreme differential loading (depending on size of turbine) which affects performance and causes fatigue. However, a system that could reach higher altitudes will overcome some of these issues as a reduction of turbulent effects at higher altitudes will be observed.

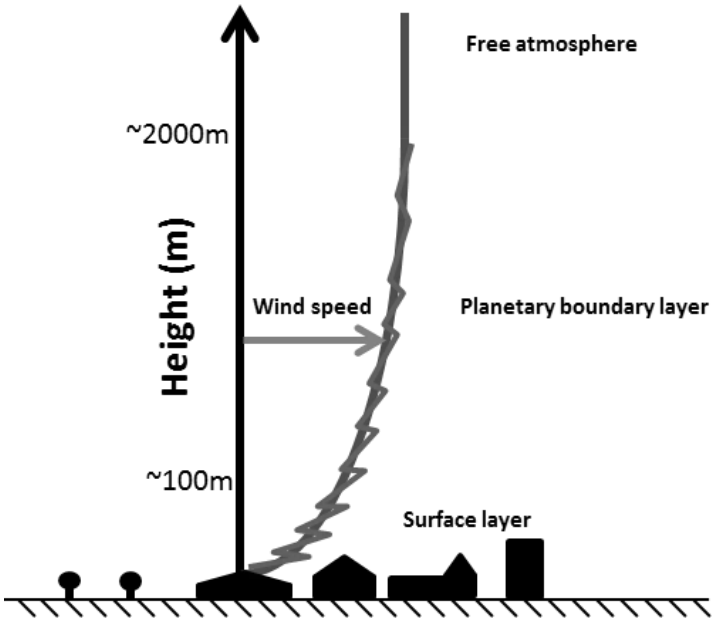

Figure 3-1 - Wind Shear Profile

The wind is affected at ground level by surface friction effects that steadily decrease as the altitude increases [3]. The 'roughness' of the ground will determine the gradient of the curve in Figure 3-1. This is demonstrated with a simple log law that defines the wind shear given a prescribed terrain and roughness factor z_0

$$v_w = v_{ref} \frac{\log(\frac{z_{alt}}{z_0})}{\log(\frac{z_r}{z_0})} \tag{3-1}$$

where v_w is the computed wind velocity at operational altitude z_{alt}, v_{ref} is the wind velocity at reference altitude z_r and z_0 is the surface roughness.. An example of different surface roughness values over different types of terrain is given in Table 3-1:

Table 3-1 - Typical Surface Roughness Lengths [61]

Types of terrain	**Roughness Length z_0 (m)**
Cities, Forests	0.7
Suburbs, wooded countryside	0.3
Villages, countryside with trees/hedges	0.1
Open farmland	0.03
Flat grassy plains	0.01
Flat desert, rough sea	0.001

3.1.2 Turbulence

In reality, the wind is not constant; it exhibits turbulent effects and seasonal variations over short and long timescales. To capture this turbulence, the wind is modelled using a Dryden Turbulence model [62]. The Dryden turbulence model adds turbulent variations in the x, y and z directions to a nominal base wind speed. This model has been predominately used by the United States for military and aerospace applications. The three main equations of the turbulence model for the three linear velocities considered (u, v and w) can be defined in transfer function for below:

$$G_u(s) = \sigma_u \sqrt{\frac{2L_u}{\pi v_w}} \frac{1}{1 + \frac{L_u}{v_w} s} \tag{3-2}$$

$$G_v(s) = \sigma_v \sqrt{\frac{2L_v}{\pi v_w}} \frac{1 + \frac{2\sqrt{3}L_v}{v_w} s}{\left(1 + \frac{L_u}{v_w} s\right)^2} \tag{3-3}$$

$$G_w(s) = \sigma_w \sqrt{\frac{2L_w}{\pi v_w}} \frac{1 + \frac{2\sqrt{3}L_w}{v_w} s}{\left(1 + \frac{L_w}{v_w} s\right)^2} \tag{3-4}$$

where, v_w is the the oncoming wind speed, σ_u, σ_v and σ_w are the turbulence intensities of the spectra in the x, y and z directions, L_u, L_v and L_w define appropriate length scales

For medium to high altitudes (greater than 600m) the turbulence length scales and intensities are based on the assumption that the turbulence is isotropic. In this work, a typical length scale, given in metres, would be $L_u = L_v = L_w = 530m$ and $\sigma_u = \sigma_v = \sigma_w = 0.855$.

3.2 The Buoyant Airborne Wind Turbine (BAWT) Model

In Chapter 2, the Altaeros system was discussed and compared with other AWE technologies. In many aspects, the Altaeros system compares favourably to other systems and as such warrants further investigation. The system is comprised of three main components. A shroud with a standard turbine rotor fixed within its shell, 3 tethers and a rotating base station that has three motor winches regulating the tether length and subsequent position of the shroud [52]. One tether is connected to the fore of the shroud whilst two are connected to the aft of the shroud, one on the aft-port side and the other on the aft-starboard side. An illustration of the system is shown in Figure 3-2. The left side shows the Cartesian frame of reference used to relate the shrouds position to the base stations which is done through Euler rotational matrices. Note that three Euler Angles help describe the shrouds

position in roll (ϕ), pitch (θ) and yaw (ψ). The right hand picture is a real life illustration of the system during testing.

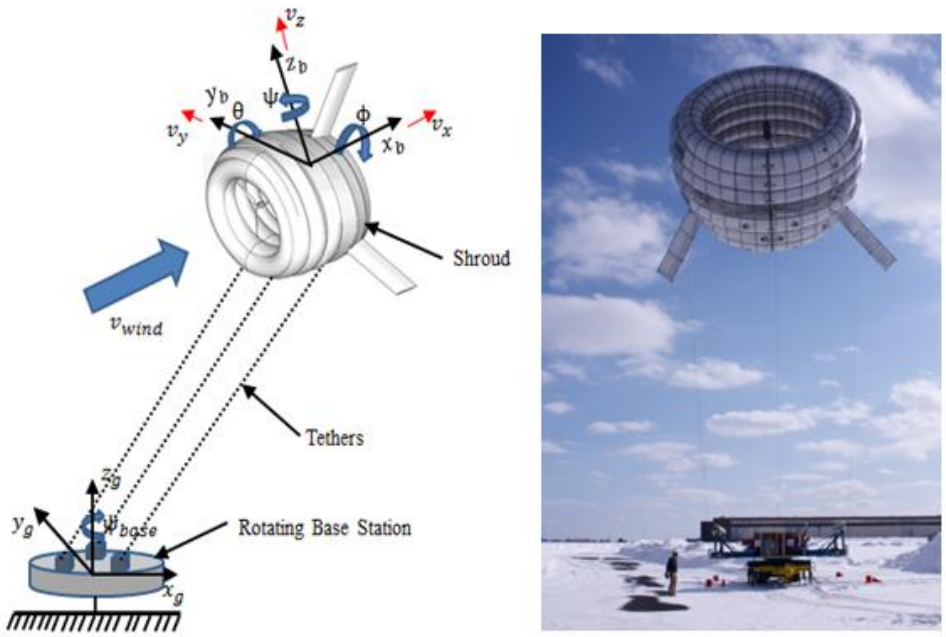

Figure 3-2- Altaeros Energies System - Cartesian Reference Frame (Left) and system during testing (Right) [54]

Figure 3-2 shows the Altaeros Energies System during testing (RIGHT) and the relationship between the systems body fixed axis on the shroud relative to the ground (LEFT). The shroud will move in 6 degrees of freedom. There are three translational velocities u, v and w and three rotational velocities p, q and r defined with respect to the body fixed axis (x_b, y_b, z_b) of the shroud. The angular rates can then be related to the attitude rates in roll (φ), pitch (θ) and yaw (ψ) of the shroud according to the following relationships [53]

$$\dot{\phi} = p + q \sin\phi \tan\theta + r \cos\phi \tan\theta \tag{3-5}$$

$$\dot{\theta} = q \cos\phi - r \sin\phi \tag{3-6}$$

$$\dot{\psi} = (q \sin\phi + r \cos\theta) \sec\theta \tag{3-7}$$

This result relates the body fixed axis to the inertial reference frame in terms of the three Euler angles. This is a well-known result and follows from standard aircraft theory. The

translational and rotational rates are combined with Euler's equations of motion to compute the accelerations in 6 degrees of freedom. These rates can then be related to the ground fixed axis (x_g, y_g, z_g) through standard Euler rotation matrices. Please see Appendix A2 for a full derivation of the equations of motion. These equations of motion can be seen in Equations (3-8) – (3-13):

$$\dot{u} = \frac{1}{m}\left(F_x^{aero} + F_x^{tether} + F_x^{net}\right) + (vr - wq) \tag{3-8}$$

$$\dot{v} = \frac{1}{m}\left(F_y^{aero} + F_y^{tether} + F_y^{net}\right) + (wp - ur) \tag{3-9}$$

$$\dot{w} = \frac{1}{m}\left(F_z^{aero} + F_z^{tether} + F_z^{net}\right) + (uq - vp) \tag{3-10}$$

$$\dot{p} = \frac{1}{I_x}\left(M_x^{aero} + M_x^{tether} + M_x^{net} - qr\left(I_z - I_y\right)\right) \tag{3-11}$$

$$\dot{q} = \frac{1}{I_y}\left(M_y^{aero} + M_y^{tether} + M_y^{net} - pr(I_x - I_z)\right) \tag{3-12}$$

$$\dot{r} = \frac{1}{I_z}\left(M_z^{aero} + M_z^{tether} + M_z^{net} - pq\left(I_y - I_x\right)\right) \tag{3-13}$$

where, m is the system mass, I_x, I_y and I_z are the system inertia's in the p, q and r direction. Together, equations (3-8) – (3-13) determine the motion in six degrees of freedom of the lighter than air system. The sum of axial forces in the x, y and z direction are denoted as F_x, F_y and F_z and the sum of the moments are given by M_x, M_y and M_z. Contributions from aerodynamics and tethers are denoted with superscripts $aero$ and $tether$ respectively in

each direction. The superscript net represents the total contribution from buoyancy minus any gravitational forces.

3.3 Shroud Aerodynamics

The shroud is designed to generate significant amounts of aerodynamic lift during operation throughout the whole operating envelope. In order to generate aerodynamic lift, the shroud is designed in a toroid shape with a streamlined aerofoil cross-section that produces lift in the same manner as an aircraft wing. This is necessary as it offsets drag effects at higher wind speeds. The translational and rotational aerodynamics, are then a function of the apparent wind speed of the shroud as well as a reference area and an estimate of an aerodynamic coefficient at a particular angle of attack.

The apparent wind speed is computed as a function of the oncoming freestream wind velocity and the translational velocity of the shroud in three degrees of freedom, developed in (3-14).

$$\begin{bmatrix} v_{x_{app}} \\ v_{y_{app}} \\ v_{z_{app}} \end{bmatrix} = \begin{bmatrix} W_x \\ W_y \\ W_z \end{bmatrix} - \begin{bmatrix} u \\ v \\ w \end{bmatrix} \tag{3-14}$$

where, W_x, W_y and W_z are the x, y and z components of the wind velocity vector v and u, v and w are the translational velocities of the shroud. The apparent wind speed is computed in body fixed coordinates and then converted to inertial coordinates through the use of rotation matrices described in Appendix A2. The resultant vector has three components in the x, y and z direction. Using the apparent wind speed in its component parts, the angle of attack and sideslip angles, denoted α and β, can be then be derived as follows:

$$\alpha = \tan^{-1}\left(\frac{v_{z_{app}}}{v_{x_{app}}}\right) \tag{3-15}$$

$$\beta = \tan^{-1}\left(\frac{v_{x_{app}}}{v_{y_{app}}}\right) \tag{3-16}$$

The angle of attack and sideslip angle are shown in Figure 3-3. The angle of attack is shown as the angle between the chord line and the oncoming wind speed. Similarly, the sideslip angle is described as the angle between the shroud and the oncoming velocity.

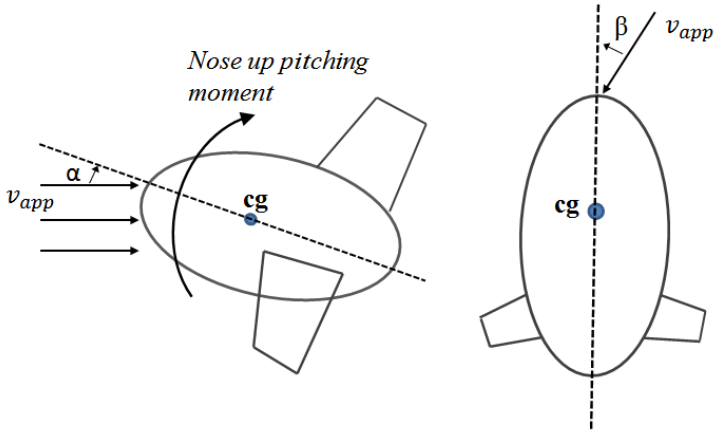

Figure 3-3 - Angle of Attack of Shroud (Left) and Sideslip Angle (Right)

From Figure 3-3 it is seen that if the angle of attack is zero, the apparent wind velocity will be in line with the chord. This will adversely affect the generated aerodynamic lift as the aerodynamic coefficients C_D, C_S and C_L, which denote the drag sideslip and lift coefficients, are directly related to the angle of attack. The aerodynamic forces in the x, y and z direction denoted by x, y and z are given below:

$$F_x^{aero} = \frac{1}{2}\rho_{air} {v_{app}}^2 A_{throat} C_D \tag{3-17}$$

$$F_y^{aero} = \frac{1}{2}\rho_{air}{v_{app}}^2 A_{throat} C_S \tag{3-18}$$

$$F_z^{aero} = \frac{1}{2}\rho_{air}{v_{app}}^2 A_{throat} C_L \tag{3-19}$$

where C_D defines the drag coefficient in the x direction, C_S defines the side-slip coefficient in the y direction and C_L defines the lift coefficient in the z direction, A_{throat} denotes a characteristic reference area of the shroud used for aerodynamic calculations, ρ_{air} the density of air whilst v_{app} is the total apparent wind speed incident on the shroud, defined in (3-14) as a function of the wind and shrouds translational velocity.

The aerodynamic coefficients C_D, C_S and C_L are then computed respectively as follows [34]

$$C_D = \alpha_0 + \alpha_1\alpha^2 + \alpha_2\beta^2 + \alpha_3{h_t}^2 \tag{3-20}$$

$$C_S = c_0 + c_1\beta \tag{3-21}$$

$$C_L = b_0 + b_1\alpha \tag{3-22}$$

where, , α_0, α_1, α_2, b_0, b_1, c_0 and c_1 are aerodynamic coefficients and h_t is the angular momentum contribution of the rotor.

Similarly, the aerodynamic moments in the rotational directions denoted as x, y and z are computed as

$$M_x^{aero} = \frac{1}{2}\rho{v_{app}}^2 A_{throat} d_{ref} C_{Mx} \tag{3-23}$$

$$M_y^{aero} = \frac{1}{2}\rho{v_{app}}^2 A_{throat} d_{ref} C_{My} \tag{3-24}$$

$$M_z^{aero} = \frac{1}{2}\rho {v_{app}}^2 A_{throat} d_{ref} C_{Mz} \tag{3-25}$$

where, C_{Mx} is the moment coefficient about the x axis, C_{My} is the moment coefficient about the y axis and C_{Mz} the moment coefficient about the z axis, and d_{ref} is a reference distance

The aerodynamic coefficients are then defined as $C_{Mx,}$, $C_{My,}$ and C_{Mz} and given respectively by [34]:

$$C_{Mx} = d_0\beta + d_1 h_t^2 \tag{3-26}$$

$$C_{My} = e_0 + e_1\alpha - e_2\frac{q d_{ref}}{v_{app}} \tag{3-27}$$

$$C_{Mz} = f_0\beta - f_1\frac{r d_{ref}}{v_{app}} \tag{3-28}$$

where, d_0, d_1, e_0, e_1, e_2, f_0 and f_1 are aerodynamic coefficients obtained from CFD simulation for the calculation of aerodynamic moments.

3.4 Buoyancy and Gravitational Forces

One of the primary driving forces in this system is the buoyancy force produced by the shroud. During periods of low wind speed the buoyancy force will ensure that the system remains stable in the air. This buoyancy force will offset the gravitational pull caused by the combined mass of the tethers, mechanical fixings and rotor. The gravitational and buoyancy forces are modelled respectively as follows [35]:

$$F_g = -mg \tag{3-29}$$

$$F_B = V_{shroud}(\rho_{air} - \rho_{gas}) \tag{3-30}$$

where, m is the total mass of the system, g is the gravitational constant, V_{shroud} is the shrouds volume and ρ_{air} and ρ_{gas} are the air and buoyant gas densities respectively.

Equations (3-29) and (3-30) are combined so as to give the total buoyancy force negating gravitational effects. This is done through a buoyancy reduction factor γ. This factor is defined in Equation (3-31) and results in F_{net} being defined as in equation (3-32).

$$\gamma = \frac{\left(V_{shroud}(\rho_{air} - \rho_{gas}) - m\right)g}{V_{shroud}(\rho_{air} - \rho_{gas})} \tag{3-31}$$

$$F^{net} = \gamma V_{shroud}(\rho_{air} - \rho_{gas}) \tag{3-32}$$

The reduction factor relates the total buoyancy force to the total mass of the system m including the mass of the shroud, rotor, mechanical fittings and tethers. This results in F^{net} being computed as the net buoyancy force acting on the system. Note that applying Euler rotations derived in Appendix A2 gives the buoyancy and gravity contributions in the x, y and z directions. These are denoted as F_x^{net}, F_y^{net} and F_z^{net} and M_x^{net}, M_y^{net} and M_z^{net} in Equations (3-8) - (3-13) respectively.

3.5 Tether Modelling

The tether model is derived primarily from [63], [64]. Each of the three tethers is modelled as a lumped-mass with the tether comprised of nodes connected by damping and stiffness coefficients denoted by K and C. The tension force dominates so the effects of bending stiffness can be ignored. There are two types of forces working on the cable namely; internal and external forces [63], [64]. The internal forces are characterized by the axial stiffness and the internal damping which are shown in Figure 3-4. There will also be external forces on the tether in the form of drag and gravitational loadings which are also included in the model.

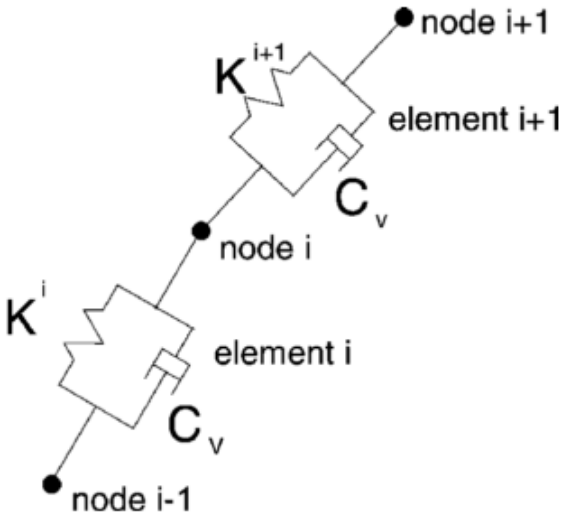

Figure 3-4 - Spring Damper model [64]

The tether tension can be defined as a function of the Young's modulus *E*, tether spring coefficient ε and cross-sectional area A_{tether}. It is defined as follows

$$F^{tether}{}_i = A_{tether} E \varepsilon \qquad \varepsilon = \frac{(l^i - l_u^i)}{l_u^i} \tag{3-33}$$

Equation (3-33) determines the tension in node i of the system. A_{tether} is the cross-sectional area of the tether and E is young's modulus of the material. ε denotes the difference in length between the stretched length of the tether l^i i.e. the stretched length of the tether and the unstretched length l_u^i which is regulated by the winch speed of independent motor *i* located on the base station [63]. Note that the tether tension is constrained to being positive at all times.

The stretched length is calculated as a function of the shroud's position relative to the base station:

$$l_i = \sqrt{\left[\left(r_x^{shroud} - r_x^{bs}\right)^2 + \left(r_y^{shroud} - r_y^{bs}\right)^2 + \left(r_z^{shroud} - r_z^{bs}\right)^2\right]} \tag{3-34}$$

where, r_x^{shroud}, r_y^{shroud} and r_z^{shroud} is the tether location on the shroud in the x, y and z direction respectively, and r_x^{bs}, r_y^{bs} and r_z^{bs} is the tether location at the base station in the x, y and z direction respectively

The damping effect on the tether is also considered through the following equation

$$P_q^i = C_v \dot{\varepsilon} l_u^i \tag{3-35}$$

where, C_v is the coefficient of damping. However, during the simulation P_q^i was observed to be small in relation to the strain F^{tether} therefore equation (3-35) dominates and P_q^i can be neglected. Equation (3-36) combines the contribution from each tether. Applying appropriate Euler rotation matrices the control inputs $F_x^{tether}, F_y^{tether}, F_z^{tether}, M_x^{tether} M_y^{tether}$ and M_z^{tether}, seen in Equations (3-20) - (3-22) in a body fixed frame of reference are determined as a function of the sum of total tether tension in all three tethers:

$$F^{tether} = \sum_{i=1}^{3} F_i^{tether} \tag{3-36}$$

3.6 Actuator Dynamics

The unstretched tether length l_u^i in Equation (3-33), is regulated by an DC motor winch speed input u_i. Three DC motors are located on a rotating base station, which has an active slew drive that allows control over the shroud heading. The motor is not modelled explicitly in this formulation. Instead, represented a first order transfer function defined with a time constant of τ is implemented to provide a suitable delay from the winch speed u_i . A pure integrator is then included to provide the desired change in unstretched length l_u^i from its initial condition. The modelled winch speed dynamics for a single tether along with the rotating base station is shown in Figure 3-5:

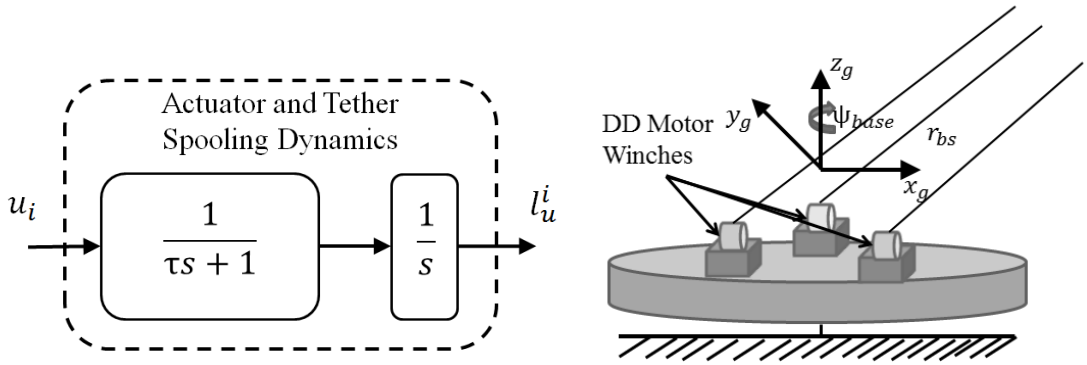

Figure 3-5 –Actuator and Tether Spooling Dynamics (Left) and Rotating Base Station (Right)

3.7 Base Station Dynamics

The base station dynamics are important to the overall operation of the system. The base station can either rotate passively or actively into the wind depending on the desired specification. The yaw of the base station is given by ψ_{bs} and is related to the angular acceleration r_{bs}, through the rotational inertia I_{bs} and the tether z axis moment $M_z^{tethers}$. Additionally, there is a moment generated at the base station by the friction between the rotating and non-rotating elements of the base station, this is represented by $M_z^{friction}$. The overall dynamics are given by:

$$\dot{\psi}_{bs} = r_{bs} \tag{3-37}$$

$$\dot{r}_{bs} = \frac{1}{I_{bs}}(M_z^{tethers} - M_z^{friction} + u_{bs}) \tag{3-38}$$

3.8 Combined Plant Dynamics

The speed of the three motor winches located on the base station form the control inputs to the system. The difference in reel in/out speed of each tether the shroud allows the system to be controllable in 6 degrees of freedom. The plant dynamics based on the derived equations can be broken up as shown in Figure 3-6:

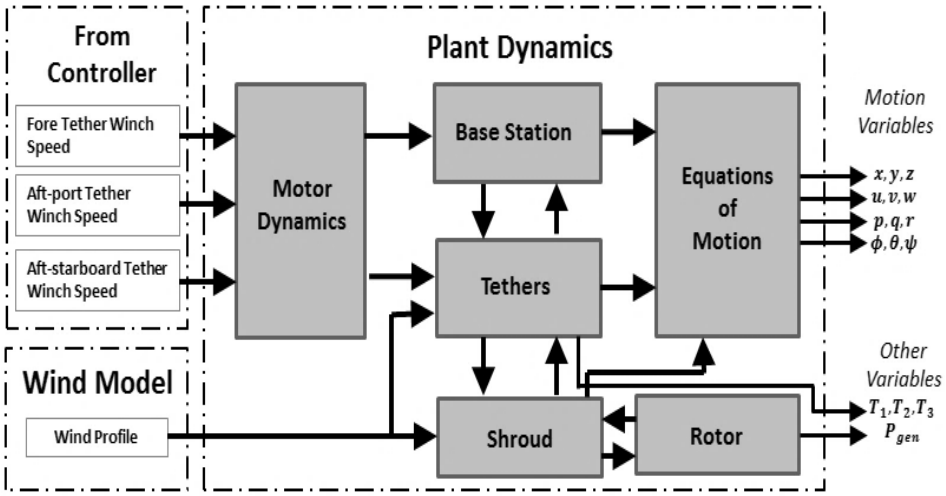

Figure 3-6 - Plant Dynamics of Altaeros Energies System [51]

Figure 3-6 introduces the plant dynamics of the system with each block corresponding to individual sub-systems created within a model in MATLAB/SIMULINK. The main inputs to the model include the three motor winch speeds to the three tethers and the wind model. The three tethers are attached at different points to the shroud to facilitate 6DOF control. One tether is located at the fore of the shroud and the other two tethers are located at the aft, one on the port side and the other on the starboard. The arrows indicate interactions between each of the subsystems.

3.9 Flow Augmentation

One of the main benefits of the BAWT is that the shroud can be designed to augment the freestream wind velocity at the rotor plane, resulting in an increase in power for a given freestream velocity. Power augmentation is achieved through designing the shroud akin to that of a diffuser or ducted wind turbine. The primary result from diffuser/ducted wind turbine theory states that there should be an accelerated mass flow at the rotor plane in the presence of a duct, if appropriately designed [65]. As the area at the rotor plane is reduced, due to conservation of mass flow, the speed at the rotor plane is increased. The reader is

referred to [62], [65] for a more complete description. Both the stream tube in the presence of a duct (left) as well as the definition of how A_{shroud} relates to A_{throat} (right) is shown in Figure 3-7 below:

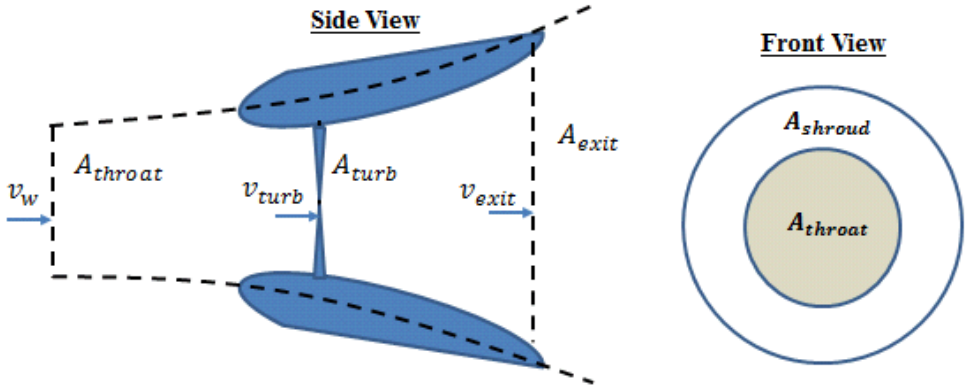

Figure 3-7 – Side view of shroud with reference throat area, turbine swept area and exit area (Left), Front view of shroud showing reference throat area and shroud area (Right) [66]

Figure 3-7, shows from the side view (left), of a streamtube around a ducted turbine and the velocity at which the flow enters (v_{turb}) and exits (v_{exit}) the duct. Due to the pressure being below atmospheric at the duct, it is inferred that $v_{turb} > v_w$ whilst the negative pressure gradient upon leaving the duct implies that $v_{exit} < v_{turb}$. There are also three areas visible in this side view namely; the turbine throat area, A_{throat}, the area of the turbine A_{turb} and the exit shroud area A_{exit}. Therefore, to satisfy the implied change in velocity it can be inferred that $A_{throat} > A_{turb}$ and $A_{exit} > A_{turb}$. The right-hand side of Figure 3-7 shows the front on view of the shroud. This defines the relationship between A_{throat} and A_{shroud}. The primary benefit of designing the shroud as a duct is that the increase in velocity at the rotor plane means the rotor can be designed to have a higher rated wind speed, which offers the potential to reduce the overall mass and ultimately cost of the system.

3.10 Pressure Management and Choice of Buoyant Gas

The Altaeros system requires a mechanism to maintain adequate envelope pressure within acceptable bounds over a range of operating conditions. This can be passive, through the use of elastic materials or active, whereby valves actively regulate the pressure based in response to the environment. However, in each case it is clear the choice of buoyant gas will be important. There are two types of gas that can be used to provide the required buoyant force namely; Helium and Hydrogen. Helium is inert and therefore provides a good degree of safety during normal operation. However, it is also a finite resource, one that may not be readily available in large quantities if and when these systems are scaled up. Conversely, Hydrogen is readily available and cheaper as it does not need to be farmed. The downside in using this is that it is highly combustible and thus means there is an increased safety risk. It is expected that as the Helium price increases, more lighter than air systems will rely on Hydrogen for buoyancy [50].

Section 3.11 and 3.12 describes the challenges associated with shroud design in terms of two force ratios. These ratios provide a method of assessing the aerodynamic performance for a given shroud design against the total net buoyancy force created from the buoyant gas. This methodology allows for a direct inspection of where the transition from buoyancy to aerodynamic behaviour is on the operating envelope. It also provides a method for comparing two designs of a BAWT system; one with helium and one with hydrogen in order to determine if there is any obvious benefit of using a particular buoyant gas.

3.11 Shroud Design through Force Ratios

In order to inform the design choices behind the system, it is important to discuss the interaction of the aerodynamics and the buoyancy forces developed previously. The primary goal of this section is to demonstrate that there is a clear argument as to why the shroud

needs to be designed aerodynamically (i.e. being able to generate aerodynamic lift). Furthermore, a side benefit in this analysis, allows the comparison of using either Helium or Hydrogen, determining if there is any quantifiable benefit in performance with a particular type of gas.

As the wind turbine rotor is fixed within the shrouds structure, the shroud must be stable during the standard wind speed range for electricity generation, typically in the range of 3.5 – 25 m/s. What is analysed here is how the design of the shroud will directly impact the captured energy in a positive or adverse manner depending on the aerodynamic design. This analysis will determine where in the shrouds operating envelope the buoyancy to aerodynamic transitions take place. This is important from a control perspective, as it will help to quantify where in the operational envelope the physical dynamics are likely to change. This is advantageous as the controller could then be designed to mitigate any negative effects this could have and ensure a smooth transition between different regions.

To do this, let us introduce the concept of two force ratios, one that relates buoyancy to lift and the other that relates buoyancy to drag. The ratio is calculated as a function of either C_L or C_D which are calculated at a particular angle of attack. The angle of attack has been defined in equation 3-19 as α and is equal to the pitch angle denoted θ. The shroud is assumed to be cylindrical so that the volume is calculated as a function of the shrouds area and length. Although, this will not exactly match the physical design, it is considered to be a good approximation. Two force ratios are derived based on the combination of equation (3-32) with equations

(3-17) and (3-19) with the assumption that the shroud's volume is computed as $V_{shroud} \approx A_{shroud} l$, where A_{shroud} is the shroud area and l is the length of the shroud. The force ratios are derived below. Note that for ease of notation F_L denotes the shrouds aerodynamic lift and

is equal to F_z^{aero} from Equation (3-19), F_{net} denotes the net buoyancy force in the z direction which is equal to F_z^{net}, and the shroud aerodynamic drag denoted F_D is equal to F_x^{aero} in Equation (3-17). The two force ratios are defined as:

$$\frac{F_{net}}{F_L} = \frac{2l\gamma}{{v_{app}}^2 C_L}\left(1 - \frac{\rho_{gas}}{\rho_{air}}\right)\left(\frac{A_{shroud}}{A_{throat}}\right) \tag{3-39}$$

$$\frac{F_{net}}{F_D} = \frac{2l\gamma}{{v_{app}}^2 C_D}\left(1 - \frac{\rho_{gas}}{\rho_{air}}\right)\left(\frac{A_{shroud}}{A_{throat}}\right) \tag{3-40}$$

It can be seen from equations (3-39) and (3-40) the ratio of buoyancy to drag/lift will vary inversely with the square of the apparent wind speed squared. It can also be deduced that the amount of buoyancy force produced will be directly proportional to the relative difference between the density of gas used and the density of air, in addition to the length of the cylinder l. There is also a dependency on total system mass shown through the buoyancy reduction factor γ. If the mass of the tethers, rotor and mechanical fittings is large then the net buoyancy force will suffer as a consequence. This indicates why the system mass must be kept to an absolute minimum. Therefore, these force ratios can be used to assess the following in relation to shroud design:

- If the volume of the shroud $A_{shroud}l$ is large in comparison to A_{throat} then the buoyancy force will dominate. Therefore, understanding the balance of how $\frac{A_{shroud}}{A_{throat}}$ impacts this relationship will inform where the aerodynamic to buoyancy transition points are in the operating envelope.
- If the overall system mass is high then in turn, the buoyancy reduction factor γ will be low. This will ultimately lead to poor buoyancy performance which will impact the stability in low wind speeds. This motivates the requirement of keeping total system mass to a minimum.
- The aerodynamic behavior will be dictated by C_L and C_D, thus keeping a high $\frac{C_L}{C_D}$ ratio will be paramount in terms of stability at higher wind speeds.

These force ratios provide an opportunity to assess the impact of a particular shroud geometry on the driving forces in relation to a fixed system mass. This is quantified in the area ratio $\frac{A_{shroud}}{A_{throat}}$ which relates the shrouds outer area A_{shroud} to its characteristic area A_{throat}. The definition of A_{shroud} and A_{throat} can be seen clearly in Figure 3-7. If A_{shroud} is large in relation to A_{throat} i.e. $A_{shroud} \gg A_{throat}$ then F_{net} will dominate the aerodynamic force ratio in relation to F_L and F_D. This is an important observation as if the system is buoyancy driven then the stability of the system is affected at high wind speeds. This is discussed in more detail in Section 3.12.

Understanding how the physical design of the shroud affects the aerodynamic and buoyant forces and the coupling between them will ultimately determine the stability of the system. In this section the impact of a given shroud design is investigated with an assessment of two buoyant gases namely; helium, with the corresponding buoyant force denoted F_{hel}, and hydrogen with the corresponding force denoted F_{hyd}.

The parameters that were used for this simulation study are shown in Table 3-2:

Table 3-2 - Shroud Parameters

Parameters	**Value**
ρ_{helium} – density (kg/m^3)	0.1664
$\rho_{hydrogen}$ – density (kg/m^3)	0.0899
l – shroud length (m)	10
m – System Mass (kg)	400
θ – Angle of Attack (degrees)	10

The angle of attack (or pitch) of the shroud was fixed at 10 degrees, considered to be optimum for the shroud [52] and the lift and drag coefficients were calculated as a function of this angle [34]. In addition, the type of gas used to fill the shroud was varied to investigate the difference in increased buoyancy. This will give an indication as to what improvement, if any, can be made with a particular gas and what the main factors behind the choice of a particular gas are. The two gases compared in this case are Hydrogen and Helium. The gas density ρ_{gas} in Equations (3-39) and (3-40) were then varied to investigate the impact.

The simulation was conducted for 3 different area ratios to illustrate how the geometry of the shroud will affect performance. Figure 3-8 shows the force ratios for both hydrogen and helium taken at different values of area ratio namely 1.2, 2 and 20. When the force ratio is equal to 1, the buoyancy and aerodynamic force are balanced. This is indicated by the constant black line and the following relationships hold when interoperating the results in Figure 3-8

$$\frac{F_{net}}{F_L} < 1 \; - \; Aerodynamic\ lift\ dominates \tag{3-41}$$

$$\frac{F_{net}}{F_L} > 1 - \; Buoyancy\ dominates \tag{3-42}$$

$$\frac{F_{net}}{F_D} < 1 \; - \; Aerodynamic\ drag\ dominates \tag{3-43}$$

$$\frac{F_{net}}{F_D} > 1 - \; Buoyancy\ dominates \tag{3-44}$$

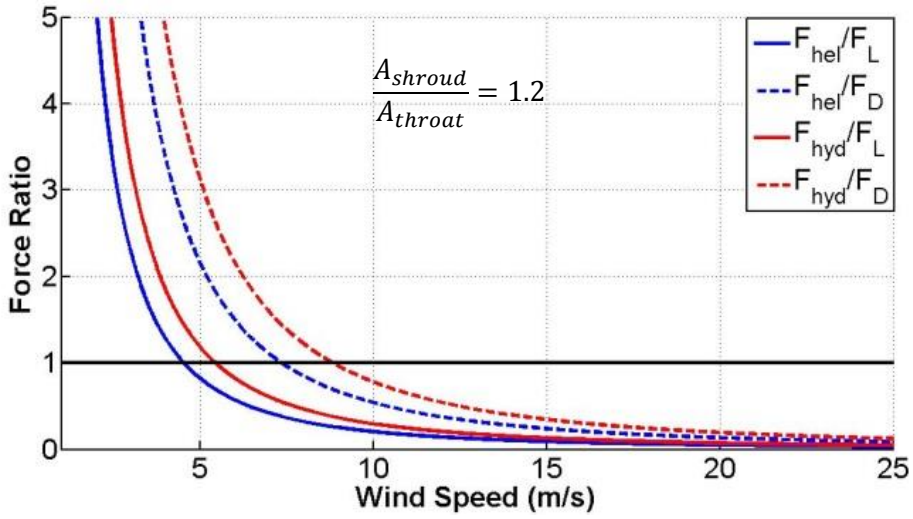

(a)

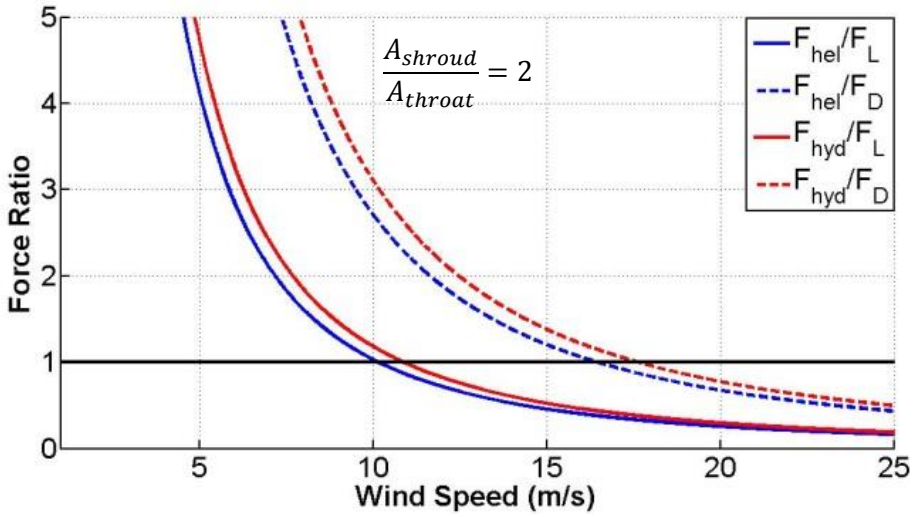

(b)

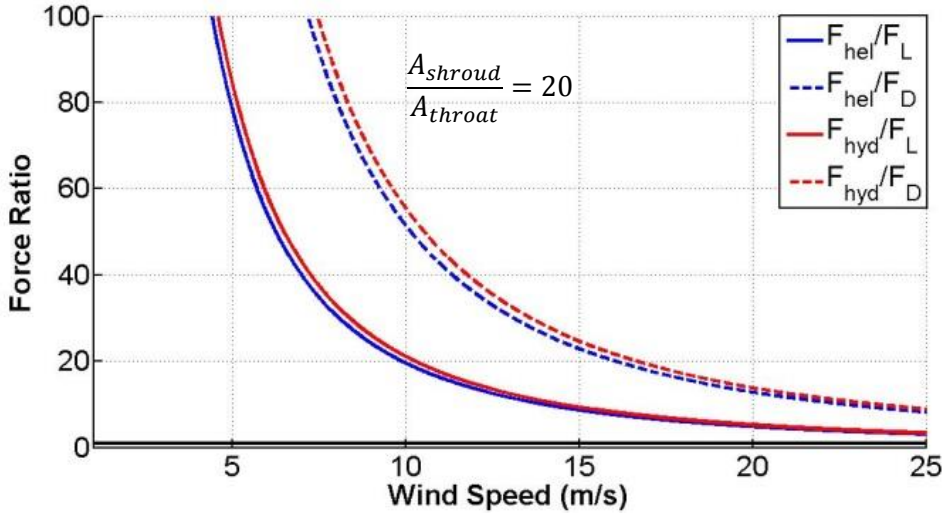

(c)

Figure 3-8 - Force Ratio vs Wind Speed (m/s) with varying Area Ratio's ($\frac{A_{shroud}}{A_{throat}}$)

Figure 3-8 (a), (b) and (c) shows three separate scenarios showing the impact that a particular type of gas will have on the system along with a varying area ratio $\frac{A_{shroud}}{A_{throat}}$. The shroud should be designed in such a way that the buoyancy is not driving across the full operating envelope i.e. at some point on the operating envelope the ratio should drop below zero. Therefore from Figure 3-8 we can infer the following results:

- As hydrogen is a lighter gas than helium, the buoyancy force dominates for longer periods in low wind speeds
- For high area ratio's, above 20, the buoyancy force always dominates. This would represent a poor design choice as the system would be susceptible to blowdown at higher wind speeds (More information provided in Section 3.12)
- A high ratio would also negate some of the impact from the winch actuation as the primary response of winch actuation is to regulate the tether tension that by extension causes a change in the aerodynamic behaviour of the shroud. This change in behaviour would be comparatively small if the system were to be dominated by buoyancy i.e. a high area ratio.

The optimal design performance of the system should therefore be set such that stability is guaranteed in low winds from buoyancy, but at medium to high winds, typically in the region of 8-30 m/s, the aerodynamic behaviour of the shroud should dominate.

3.12 Operational Stability

If the physical design of the shroud is considered without the influence of an aerodynamic design i.e. $F_L = 0$, then the impact on system stability could be severe. From the analysis above, the shroud would become susceptible to drag within a wind speed range of 8-30 m/s

if the area ratio was fixed at any point between 1.2 and 2. These winds speeds are within the operational range of the wind turbine rotor fixed within the shroud. Therefore, if the system is dominated by aerodynamic drag then it will adversely affect energy capture and move the system to an inefficient and unstable position. To emphasise this, a blowdown angle is shown in Figure 3-9, which relates the total drag force to lift force from the zenith position. This angle can be calculated using Equation (3-43).

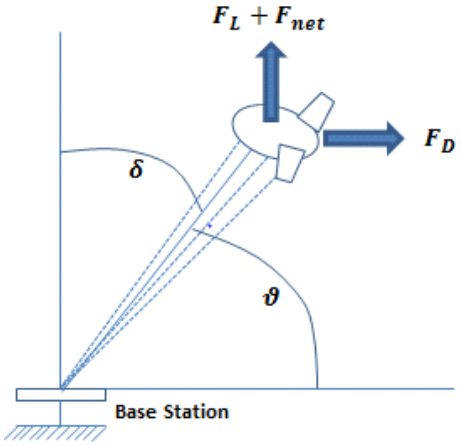

Figure 3-9 - Blowdown Angle as a result of net lift and drag [50]

$$\delta = \tan^{-1}\left(\frac{F_D}{F_{net} + F_L}\right) \tag{3-45}$$

If the shroud does not generate aerodynamic lift then $F_L = 0$ and the shrouds angle will only be related to the buoyancy and drag force (still present) on the shroud. However, if the shroud is designed to produce aerodynamic lift then $F_L \gg 0$, which will subsequently reduce the blowdown angle relative to the origin. A ratio of 1 will imply a force balance and this equates to an angle of 45 degrees from the zenith. Above 45 degrees, drag will dominate and the angle from the zenith will increase as a function of wind speed. Therefore, the system is considered to be unstable above 45 degrees and stable below 45 degrees. This is shown in Figure 3-10 and Figure 3-11 where the effect of adding aerodynamic lift is investigated. The

simulation has again been conducted for a shroud filled with helium and hydrogen and results are shown for an area ratio of 1.2.

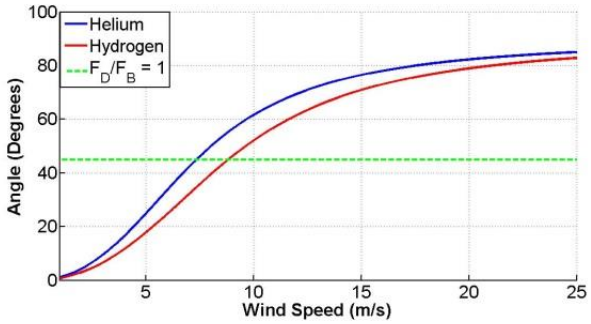

Figure 3-10 - Blowdown angle with no Aerodynamic Lift relative to wind speed

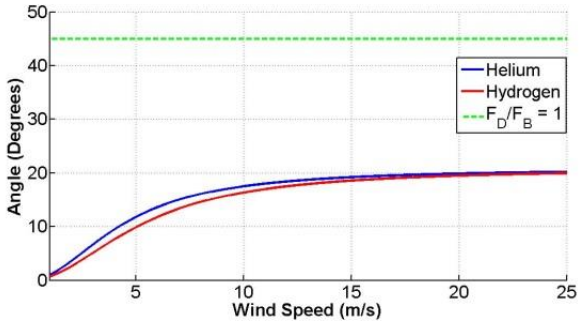

Figure 3-11 - Blowdown angle with aerodynamic lift relative to wind speed

From Figure 3-10 and Figure 3-11 the effect of including aerodynamic lift can be seen for systems filled with helium and hydrogen. Figure 3-10 shows the lighter than air system relying purely on buoyancy force as support relative to drag. In the case of helium, at a wind speed of 7.36 m/s, the angle is equal to 45 degrees. Similarly, the transition point for hydrogen occurs at 8.8 m/s. Therefore, although hydrogen is less dense than helium, the transition point has not moved significantly which demonstrates two points. Firstly, the impact of filling the shroud with helium will offer increased stability from buoyancy for a slightly longer period of time. Secondly, the importance of the aerodynamic design of the shroud becomes clear as the angle relative to zenith continues to rise beyond 45 degrees as a function of wind speed from approximately 9m/s onwards. Thus, without any aerodynamic lift the shroud will be susceptible to blowdown at the rated wind speed of the rotor i.e. where

peak power is being captured. To investigate this further, Figure 3-11 shows that with the addition of aerodynamic lift the stability angle of 45 degrees is never reached in the case of either helium or hydrogen. The maximum angle that each system reaches is 20 degrees. This means that the system remains stable and gives a good stability margin in the operating region of the rotor.

In this section a comparison was made between Helium and Hydrogen for the use on the BAWT. This was done in order to quantify the impact on system performance that a particular gas can provide. As the system will succumb to drag within the operating envelop of the rotor, the shroud will have to have an aerodynamic design. One benefit of using hydrogen is that its lighter properties provide an increase in buoyancy per m^3 in comparison to helium. However, there are significant safety issues associated with the use of hydrogen as it is highly combustible compared to the inert nature of helium. Unless absolute safety could be guaranteed using anti-static materials, helium would still be the appropriate choice for a lighter than air application of this type [35]. Furthermore, a wider benefit of relating the shroud's dynamic properties in a parametric way allows for appropriate scaling ratio's to be determined based on a particular shroud geometry. For instance, work is being conducted by Vermillion [66] into the scaled modelling of these systems utilising a similar force ratio approach.

3.13 Shroud Stability

An understanding of the overall impact of the driving forces on the shroud has been given in Section's 3.11 and 3.12. This section extends this by looking specifically at the key dynamics of the system which reside at shroud level. The position and the stability of the shroud will be imperative for the successful operation of the system. Figure 3-12 shows a free body diagram of the shroud with distances a, b and c marked from the center of gravity

to the tether attachment points. In turn, the offsets Δx and Δz describe the position of the centre of buoyancy in relation to the centre of gravity.

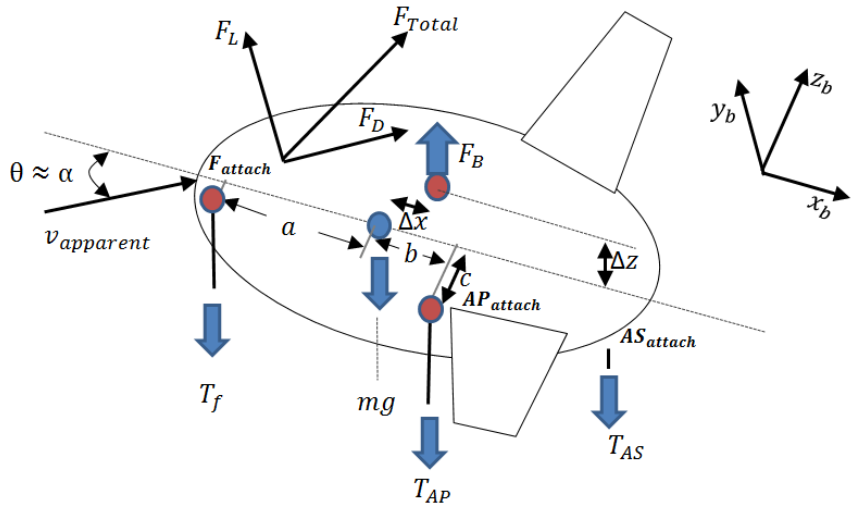

Figure 3-12 – Shroud Free-Body Diagram

The passive design requirements of the shroud based on Figure 3-12 were described in detail by Vermillion in [52]. In this paper the key design requirements for lateral and longitudinal stability were discussed. It was shown that system disturbances can be characterized in the longitudinal and lateral directions. Typically, abrupt changes in wind speed will cause a longitudinal disturbance which will dominates any associated lateral movement, assuming the torque from the turbine is low. The primary cause of instability in the longitudinal direction was the relationship between the centre of buoyancy and centre of gravity. If the centre of buoyancy is located behind the centre of mass, the system will become unstable. However, if the centre of buoyancy is located at the centre of mass the system will be stable in open-loop. This was shown clearly in [52] and [67]. Namely the system was assessed when $\Delta x = 0$, known as Configuration 1 and when $\Delta x = 0.5$ known as Configuration 2. The two systems are compared in Figure 3-13:

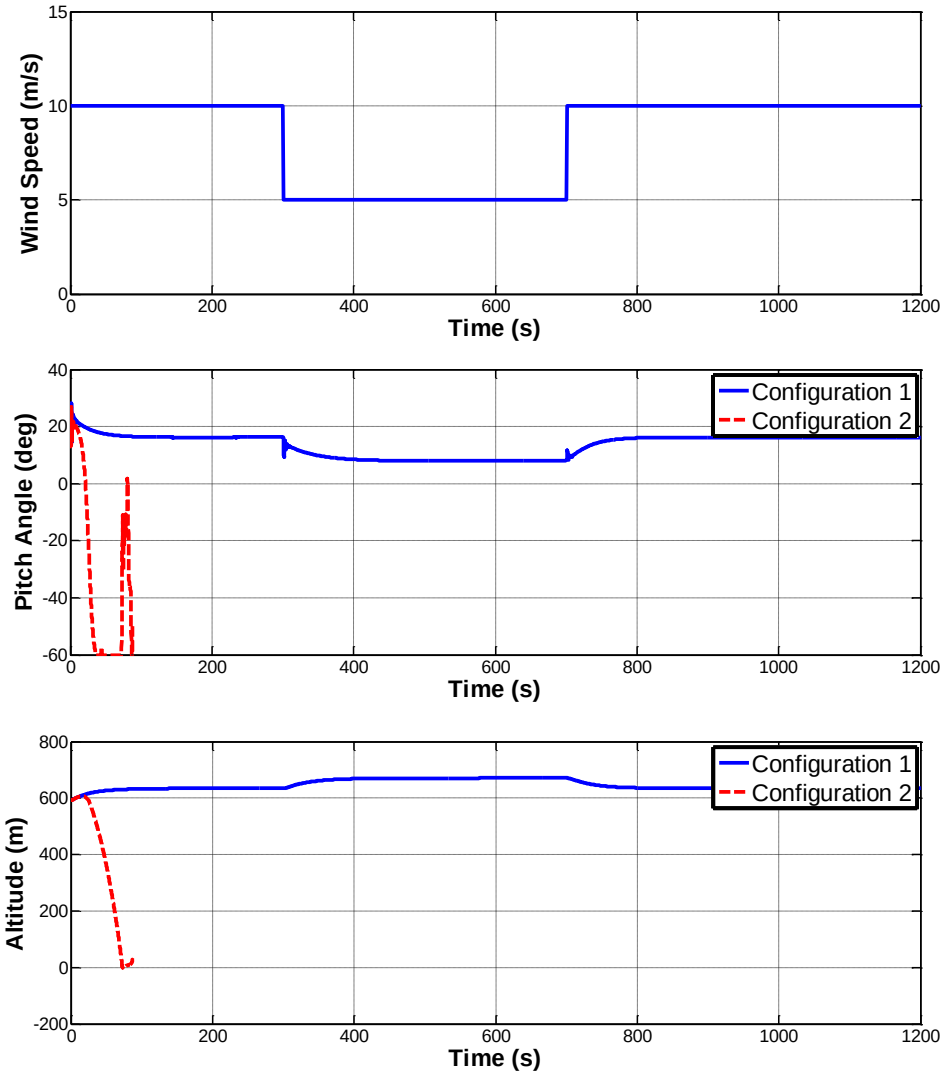

Figure 3-13 - Open Loop simulation under different centre of buoyancy locations

From Figure 3-13 it can be seen that if there is an offset in buoyancy (Configuration 2) then the system becomes unstable at the beginning of the simulation. The primary reason behind this is the buoyancy moment caused by the offset. This results in a decreased pitch angle, resulting in negative lift and ultimately a complete reduction in altitude. In contrast, Configuration 1 remains stable even in the presence of a step change in wind.

A similar analysis has been done for lateral motion. Any change in wind direction will cause a lateral disturbance that dominates system behaviour having a knock-on consequence for

longitudinal states. It was shown in [52] that a lateral disturbance can be stabilised using three key mechanisms. The first being that immediately following a perturbation there will be a restoring force from buoyancy. In addition, if a roll moment is induced through the tethers this can cause sideslip and stabilise translational motion. However, stabilisation about the z axis is only addressed through the incorporation of vertical and horizontal stabiliser as well as spatially distributed tether release points. One design consideration may be the spacing of the tether attachment points in addition to the offset that may or may not exist between the centre of buoyancy and the centre of gravity. Studies have been conducted in [52] that demonstrate that the stability of the shroud is directly related to the distances at which the tether attachment points are placed. If all tether attachment points are collocated, the mass distribution will be concentrated at one point, thus making the shroud behave like that of an inverted pendulum, which is inherently unstable. However, if the attachment points are equally distributed the response becomes good damping and the system is more stable as a result.

3.14 Open Loop Behaviour

To validate that the model is open-loop stable for the configuration shown in Table 3-3 some further model responses are assessed. Firstly, the roll and yaw of the shroud is shown in Figure 3-14.

Table 3-3 - Tether attachment parameters

Shroud Parameters	**(m)**
a	2.5
b	4.5
c	5
$\Delta \boldsymbol{x}$	0
$\Delta \boldsymbol{z}$	2.5

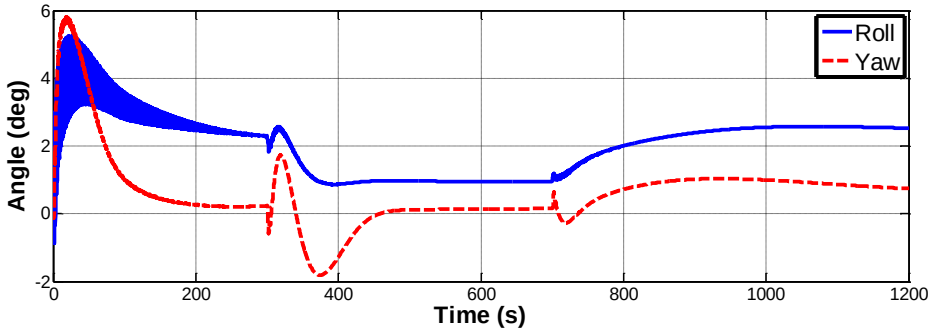

Figure 3-14 - Roll and Yaw response - Open Loop

From Figure 3-14 the open-loop roll and yaw response can be seen. It is shown there is a certain amount of roll and yaw as the wind speed changes. However, over the course of the simulation the response is stable. Next, the pitch angle is assessed along with the aerodynamic and tether moments. The plots are shown in Figure 3-15 below:

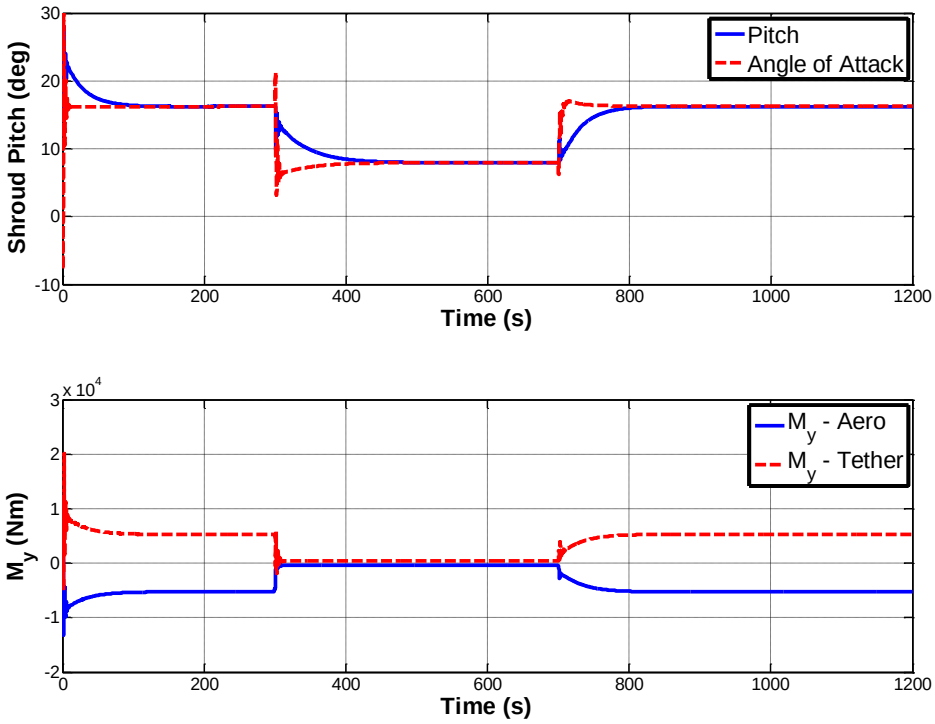

Figure 3-15 - Pitch angle and Angle of Attack and body-fixed moments

From Figure 3-15 the angle of attack is shown to be approximately equal to the pitch angle as a function of time. Furthermore, it is shown that there exists a body-fixed aerodynamic moment which is cancelled out equally by the moment from the tethers.

Finally, the shroud position in terms of the fixed tether attachment points are assessed as a function of time. This is shown in Figure 3-16 below**:**

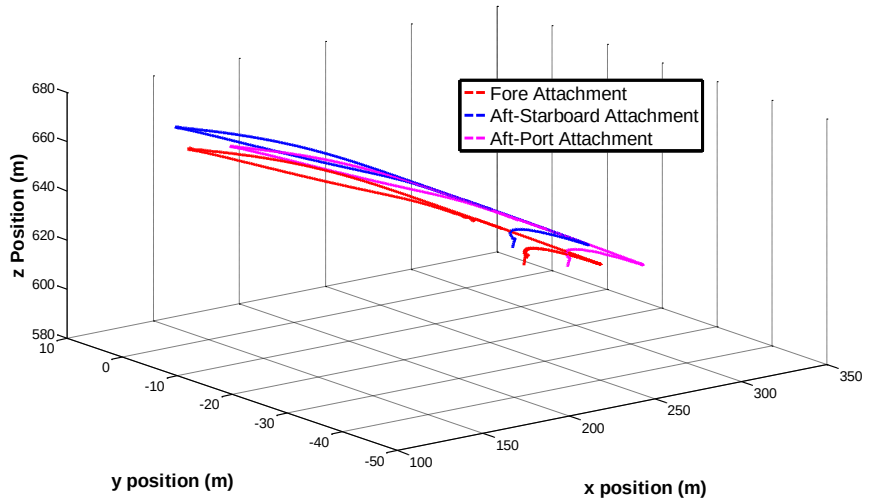

Figure 3-16 - Tether Attachment Positions - Fore (red), Aft-Starboard (blue), Aft-Port (pink)

The tether attachment points can be seen clearly in Figure 3-16. It is shown that there is a clear difference in attachment points between the three main points, the fore, aft-starboard and aft-port. Distributed spacing like this allows for good damping and sufficient rotational and translational control which is required to stabilise the system for electricity generation.

3.15 Model Summary and Future Challenges

Throughout this chapter the model of the 6DOF model of the Altaeros system has been assessed. The implicit dependence on attachment points on the shroud in relation to stability has been discussed. It was shown if the centre of buoyancy is collocated with the centre of gravity and if the attachment points are evenly distributed about the shroud then the shroud will be stable in open loop. Each part of the model, tethers, shroud and base station have

been modelled in sufficient detail as to allow a comprehensive analysis of system performance to be undertaken. However, in the future some additional amendments could be added to better understand the forces at play on the shroud. For instance, more detailed aerodynamic modelling could lead to a better understanding of the relationship between shroud and turbine aerodynamics. Furthermore, a more accurate tether model will soon be required that explicitly models the power transfer from shroud to ground. Currently, the power capture is modelled only with a power transfer loss associated with it. In reality, a more detailed description will be needed.

Fundamentally, all of the dynamics considered in this chapter can be combined to produce a viable operational envelope for the Altaeros system. The driving parameters to consider for adequate operation of the system include the pitch, wind speed and altitude at which the system is stable and optimally generating power. Assuming a valid set of operational points for a particular location a hierarchical control strategy can be developed to ensure stability and maximise the overall performance. The proceeding chapters seek to answer this question through control design that first stabilises the shroud, and then optimises it for maximum power capture.

3.16 Conclusions

This Chapter introduced the BAWT developed by Altaeros Energies. The six-degree model was derived along with a wind model to supplement control development. A new set of force ratios were introduced that implicitly related design parameters of the shroud in relation to the aerodynamic and buoyant behavior of the shroud. Analyzing the system in this way will lead to a better understanding of how the system should scale as the design changes. Furthermore, the model was validated and shown to be open loop stable considering the

distributed location of tether attachment points and the relevant location of the center of buoyancy to the center of mass.

4 Control Design Review with application to a BAWT

This chapter reviews three specific control design techniques namely; PID, MPC and ESC and discusses their application to the BAWT. A short literature review is provided on each technique and the motivation for using each controller within a BAWT context is provided.

4.1 Multivariable Control

The primary aim of this section is to discuss the types of control methodology that can be applied to aid multivariable control over complex plants. The three techniques that are focussed on here are Multivariable PID regulation, MPC and ESC design. The chapter is organised to provide the reader a background into each control technique. Then, the remaining part of this chapter discusses how each technique is relevant for BAWT design.

4.1.1 PID Regulation

Modern day plants are increasingly complex, with most exhibiting dynamically coupled interactions between a number of inputs and outputs, required for maintaining the desired response of the system. As such, single loop feedback control is becoming a rarity and multiloop design is becoming more and more relevant. Compared with single input single output (SISO) systems, multi-input multi-output (MIMO) plant control can be more challenging and difficulties can arise when translating known SISO tuning techniques into a multivariable form [68]. Therefore, to design a suitable controller, a true multivariable

strategy is required. This feedback is derived so the closed loop system can have both good performance and robustness properties i.e. good reference tracking response for multiple outputs with resilience to model disturbances and uncertainties. To reduce the complexity of the problem, techniques are employed to decouple the system to minimise loop interactions and make the system diagonally dominant. This allows multiloop regulators to be designed to control the system. Due to their simplicity, PID multiloop controllers are by far the most common control method employed. This simple strategy can be implemented to take account of important practical issues such as actuator saturation and integral wind-up, in addition to responding to specifications on performance such as load disturbance and set point response [69]. Astrom argued this point in [70], discussing the perceived merits of this design over more advanced and complicated architectures.

The standard multivariable feedback for a typical plant $G(s)$ will take the form shown in Figure 4-1:

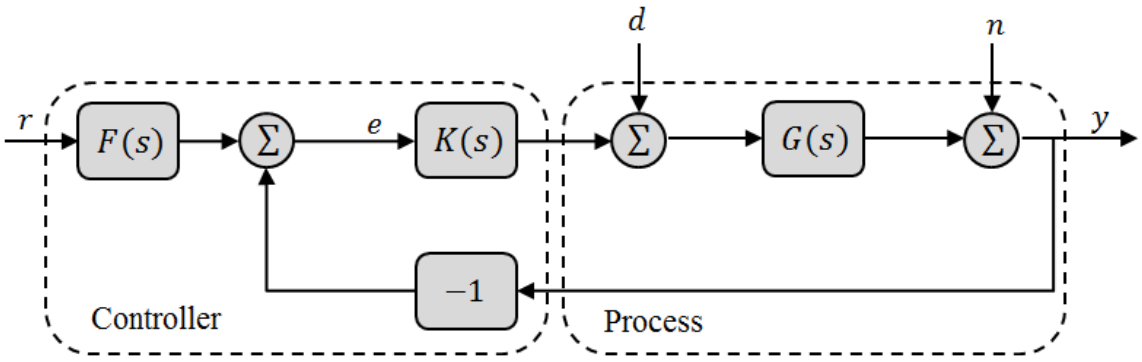

Figure 4-1 - Multivariable Feedback Configuration

In Figure 4-1, $G(s)$ represents the plant and is a matrix of transfer functions in which the (i,j) element g_{ij} relates the ith output to the jth input, $K(s)$ is a controller and $F(s)$ is a pre-filter that may or may not be necessary depending on the desired specification. Finally, d and n represent the disturbance and measurement noise respectively. The challenge to the control

designer is to understand the dynamics of the plant in question and produce a controller $K(s)$ that meets the design specifications [71].

In order to achieve a suitable design, a number of tuning techniques both parametric and non-parametric have been proposed in literature. Here, parametric methods are defined as being those that utilise either historical data or online identification for control design and require the use of linear models in transfer function or state space form across the frequency range of interest. Comparatively, non-parametric techniques are defined as those that require only partial model information around certain frequencies of interest either in steady state or at critical frequency points.

The first, non-parametric multivariable method was introduced by Davison in [72] as a robust control design for a servomechanism application. Davison designed a multivariable regulator for an unknown plant through experimental excitation at a particular frequency. This gave the desired asymptotic stability and asymptotic tracking in the presence of disturbances of a specific form. However, this work only considered tuning the integral part of the PID controller. Penttinen and Koivo then extended this to form a multivariable PI controller in [73] and [74]. Again this was based on simple step-response experiments on a linear time-invariant (LTI) stable plant. However, this was then expanded on by MacFarlane in [75] who developed the fundamentals of what is termed the characteristic locus method. Primarily, this work showed the importance that difference and return-ratio matrices play in terms of multivariable feedback control theory. This was subsequently developed by Kouvaritakis in [76] to form the characteristic locus method for multivariable systems. Essentially the characteristic locus method employs pre-compensators to adjust the characteristic loci to the desired specification. The gains are then derived by evaluating the

plant at some specific frequency which reduces interaction between the loops. Maciejowski discusses this in more detail in [71].

In comparison, parametric methods mostly employ classical tuning techniques such as the BLT method proposed by Luyben in [77] and the Direct Nyquist Array method described by Rosenbrock in [78]. Furthermore, Minimum Variance Control (MVC) can also be applied in a multivariable context, first being introduced by Borison [79]. This was then extended by Astrom and then by Yusef [80] who applied MVC to tuning a family of PID controllers. Finally, optimal control methods can be utilised, such as robust LQ designs used by Panagopoulos to optimise PID controllers [69]. This is in addition to H-infinity methods and Model Predictive Controllers that are also effective in the design of multivariable controllers.

A comprehensive review of these techniques was given in [68] with the main disadvantage discussed between non-parametric and parametric techniques being that there is a requirement for the open-loop system to be stable when the model is not fully available. This work informed the assessment of these techniques on a variety of systems, ranging from wastewater systems [81] to ship positioning [82]. However, all of these techniques are based on LTI systems in either state space or transfer function form. This means that the set of computed gains, regardless of technique, are only valid around one localised operating point. So if the system is nonlinear and has a wide operating envelope, an LTI controller may give sub-optimal performance at different operating conditions. Therefore, whilst it is true development is still required in multivariable control to deal with strongly coupled multivariable systems, it is also needed to optimise the controller and by extension the plant for its full range of operating conditions. This leads to adaptive control being a requirement for most modern-day systems.

4.1.2 Gain Scheduling and Adaptive Control

Historically, adaptive control in one form or another has been employed since Caldwell in the 1950's [83]. It can be broadly understood as the ability for a given regulator to change or 'adapt' its behaviour based on any change in the dynamics of the process. From a control perspective, adaptive control took significant steps forward in the 1960's when a rigorous mathematical description was presented by Kalman in [84] of linear time-invariant systems and their stability properties. Significant advances in this field were also made by the introduction of dynamic programming by Bellman in [85]. Nowadays, there are three approaches to adaptive control which are gain scheduling, model reference adaptive control (MRAC) and self-tuning regulators [86], [87].

Gain scheduling reduces the effect of parameter variations by updating the regulator based on auxiliary variables that correlate well with the measured change in dynamics. However, for this approach to be successful there is usually a requirement on the auxiliary variables to be slow varying with time. Understanding the plant in question can lead to a determination of what the suitable scheduling variables will be.

The regulator is scheduled on these variables to cover the full operating range and hence operating envelope of the plant. The gains are switched as the dynamics change and so the operation of the system remains stable. However, there are a few drawbacks to this method. The first is that feedback is only successful if it is scheduled correctly as it relies on look-up tables of gains correlating to specific operating conditions. Therefore, gain scheduling is classed as adaptive open-loop compensation. The second drawback is the amount of time it takes to generate the required number of regulators to cover the full operating envelope. For instance, some flight applications have potentially thousands of design points. Importantly

though, the gains can be updated quickly in response to any changes in plant dynamics so it is still a useful tool widely in use today.

Model Reference Adaptive Control (MRAC) differs from gain scheduling in that it uses a reference model as the starting point of its design. This reference model is assumed to give the ideal response to given command inputs. The output from the reference model is then compared with the physical output from the plant and an adjustment mechanism is employed to regulate the reference model parameters so that the error between the two becomes as small as possible. It has been shown that the adjustment mechanism cannot be simple linear feedback so the key issue is to create an adaption law this that produces a stable system and brings the error to zero. The key advantage of the MRAC method is that it is closed loop and can be retrofitted onto existing baseline control systems to account for any design changes made to the plant. However, there are still issues with MRAC that need to be resolved. Most important of which, is the model used for the reference. Depending on the type of system, there will be a different reference model for a particular mode of operation. For example, in flight systems a reference model will exist for take-off roll, rotation, climb-out, cruise, approach and landing which mean that scheduling these models becomes a scheduling issue in itself. Also, because there are several parameters and matrices used in the design process, tuning the controller is also an issue. Clear rules of thumb are needed for tuning these systems and more research is still required to improve the transient response of adaptive systems so that they are fully adopted as industrial design methods [88].

The third and final type of adaptive control is the use of self-tuning regulators. In a way this regulator is very similar to MRAC, in that there are two control loops, an inner loop and an outer loop. The inner loop contains the ordinary feedback regulator and the outer loop adjusts the parameters of the regulator. However, a difference exists in how the parameters

are adjusted. In self-tuning regulators, parameter estimation can be applied using a variety of methods. Stochastic approximation, least squares, extended and generalized least squares, instrumental variables, extended Kalman filtering and the maximum likelihood method have all been employed at some stage [79], [89]. As such, self-tuning regulators look at the adaptive problem from a stochastic viewpoint. However, as Wittenmark points out in [90] much work is still needed from both a theoretical and practical point of view if being applied routinely by inexperienced users.

Closed loop systems obtained with adaptive control are nonlinear so analysis of stability and performance are key problems. Although stability analysis has not been proved for gain scheduled systems it has been proved in the MRAC case. If Lyapunov theory is applied in the design and coupled with Barbalat's lemma, bounded output tracking is achieved and stability is guaranteed. This is case for many systems but none more so than flight systems.

4.1.3 Multivariable Control for Flight Applications

As most aerospace systems are heavily automated, control theory has taken on a more prominent role in development. For example, when addressing the stability and control issues associated with a typical aircraft system. Most modern, high performance aircrafts operate in flight regimes that exhibit significant nonlinearities such as extreme changes in pressure or wind speed. Control actuators in the form of an aileron, elevator and rudder as well as a throttle control are utilised to control the roll, pitch, yaw and forward thrust of the aircraft. Therefore, for adequate flight performance, a multivariable controller is necessary. Regardless of the design method employed, the controller must take into account uncertainties, disturbances, noise and adhere to all system constraints in order to guarantee performance over the operating envelope. This makes the control design iterative, as any change to system parameters may result in an insufficient controller. However, modern control systems are now not only concerned with stability during flight but also flight

quality. This is primarily addressed through dynamic stability analysis which enables the response of controls and disturbances to be determined for a range of flight conditions. Typically, this is achieved through the development of appropriate transfer functions, linking the actuators to outputs, that are then analysed in the frequency domain [91].

It is therefore necessary that in-flight applications, controllers offer good stability and robustness characteristics over the full flight envelope. The most common feedback regulator in flight systems is the LQR controller which gives excellent stability guarantees and performance [92]. Gain and phase margins are assessed for an LQR controller at each trim condition to ensure stability and then gain scheduled to cover the operating profile of the plant. The scheduled variables are usually the Mach number, altitude or angle of attack. Many other control designs have been carried to achieve the desired specification. For instance, H-infinity control was applied in [93] to derive a set of linearized controllers that were then scheduled to remove hidden coupling terms and thus enhance the overall performance of the system. Also, Linear Parameter Varying (LPV) analysis is provided in [94] to investigate the response of a gain scheduled controller for an aeroelastic aircraft. As it is a system within a rapidly changing environment, adaptive flight control has also been presented in many publications [53], [86], [87], [95], [96].

4.2 Plant Optimisation Methods

4.2.1 Model Predictive Control

MPC is widely used in many industrial sectors as a means of optimally driving the plant in question to a given condition under certain constraints. Compared to PID controllers which do not explicitly consider any future behaviour of the plant, MPC computes an optimal control, denoted u, based on the predicted intentions of the plant model dynamics.

Minimizing or maximising a pre-defined cost function at a given time step, the optimal control law is computed and applied to the plant.

One of the main principles of MPC is that it employs a receding horizon approach. This means that at each time-step, the controller will always look at a defined horizon, or time-step, into the future as the sample-time is updated [97]. This approach allows the controller to gain as much information as possible in order to make the optimum control move. Typically, the horizon selected for predictions should account for the response time of all significant dynamics in the system. Therefore, using the settling times of the system is usually a good starting point. A further benefit of MPC is that it handles constraints in a systematic way compared to PID controllers.

One clear example would be actuator performance. The response will be dictated by the PID gains as to whether it remains within desired constraints or not. However, in MPC, the optimal control solution can be explicitly solved subject to these constraints, as long as the states are estimated or measurable, therefore making it appealable for control problems.

4.2.2 MPC for Airborne Wind Energy Systems

Within the field of AWE, MPC provides a good way of dealing with constraints and it has been effectively used on the kite system and rigid body systems respectively in [98], [99]. In particular, algorithms such as Nonlinear Model Predictive Control (NMPC) facilitate optimised path planning as well as constraint handling allowing the nonlinear trajectory to be decoupled from the low level positional control. This work has been studied extensively in recent years with a focus on using these optimisation methods on simplified models of the kite/rigid-glider [98], [100]. As these systems typically have a constantly moving trajectory dependent on variables such as reel out speed, wind speed, lift, drag and angle of attack, it is important that the trajectory is optimised within feasible bounded constraints of the system.

In order to tackle the NMPC problem, a set membership approach was adopted by Fagiano in [43]. This allowed for the computation of an approximate control law that guaranteed performance and stabilizing properties. This has been successfully employed on kite applications [16]. However, the real-time applicability of algorithms such as this are highly dependable on the fidelity of the model in question meaning that the computed control decisions that are feasible in simulation may not necessarily be applicable in practice. This leads to the requirement of experimental validation in order to demonstrate the effectiveness of the proposed algorithms. Significant effort in recent years has gone into this application. The use of the NMPC algorithms is wide spread for constraint handling and path planning for a kite/rigid body system. However, thus far there has been little investigation into using hierarchical MPC for a lighter than air system. MPC has been as use as a direct replacement of the low level controller in [55].

4.2.3 Supervisory MPC

The most common implementation of MPC is in the direct computation of control inputs for the plant [97]. However, other approach's use MPC in a supervisory capacity [101]. Effectively, this places the MPC model within a hierarchical architecture which determines feasible set-points or optimal gains for a low-level controller. The following publications provide more detailed information on this [102]–[104].

There are several motivations behind the use of hierarchical MPC. Firstly, it allows desired set-points of the system to be optimised based on current operating conditions and secondly, the optimised control move can be computed based on certain constraint satisfaction of particular plant inputs, states or outputs. To that end, there are a number of methods in which a supervisory MPC can be developed to handle a nonlinear system. Largely these can be broken down into an inherently nonlinear or linear based approach. For instance, nonlinear model predictive control (NMPC) provides a methodology for computing a control move

over a nonlinear envelope. It offers global stability but suffers from large computation and processing times [86]. Alternatively, a linear approach can be taken such that assuming trim conditions are met, an estimated linear model describing the operating conditions of the plant can be used within the MPC framework. Successive linearizations at different operating points and appropriate scheduling should result in stability over the full operating envelope. If the model of the system is known, the linearizations can be done offline, offering an increased saving in computation time compared to an online model [105].

4.2.4 Extremum Seeking Control

Extremum seeking control forms part of a suite of optimisation methods (i.e. hill climbing) that look to find a real time solution to the derivation of a maxima or minima of local plant. The problem of extreme seeking for a plant was discussed in [106],[107], where research was conducted into the determination of appropriate tuning parameters for a extremum seeking perturbation scheme. In [106], Jacobs discusses the design of a single-input single-output sinusoidal perturbation scheme that maximises a standard parabolic function which can represent a given plant dynamic. Extremum methods were largely neglected until the late 1990's [108] primarily due to the lack of computing power required for a real time optimisation of this type. However, here has recently been a resurgence in the research of extremum seeking feedback control and the applications that this methodology can be applied to [109]–[113]., led predominately by work in [114] which provided the first proof of stability of an extremum seeking algorithm for a generalised nonlinear dynamic system using singular perturbation analysis.

ESC has since been applied to a number of systems ranging from gas turbines to anti-lock braking systems [115], [116]. However, in recent years, an interesting application of ESC has been in the field of renewable energy, specifically wind turbines and photovoltaic solar cells. This is because both systems have a region in which maximum power-point tracking is

demanded. This has been thoroughly investigated in [117]–[120] which shows that there is indeed a benefit in adding ESC loops into the maximum power-point tracking region of a wind turbine. In this work the ESC scheme is not directly applied to the rotor. Instead an optimisation function is created based on the trade-off of generated power from the rotor against the power losses incurred by reeling in/out the tether at high wind speeds. This is discussed in more detail in Chapter 6.

4.3 4.3 BAWT Application

A review of some of the key challenges associated with multivariable PID, MPC and ESC have been presented in Sections 4.1 – 4.3. This section motivates the need for these algorithms within the context of the BAWT. To that end, this work introduces the requirement for low level control derived from PID regulation with optimisation loops added in a supervisory capacity derived from the implementation of MPC and ESC. The proposed structure for this implementation is shown in Figure 4-2 below:

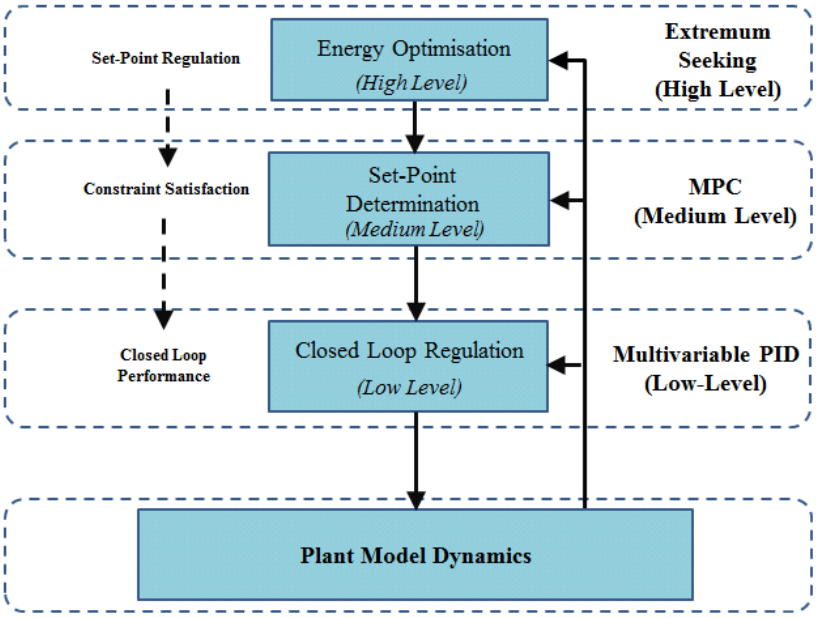

Figure 4-2 - Proposed hierarchical control design flow for a BAWT

Figure 4-2, outlines the design process to be followed in the remaining Chapters. Note that the plant model has been discussed in detail in Chapter 3 and interaction between controller

and plant is discussed in more detail in Chapter 4. Overall, the control design is broken up as follows:

- Chapter 5 – Low Level PID Design to regulate the roll, pitch and altitude set-points of the shroud. A discussion is provided on the operational bounds of the system and a simple method to derive suitable gains is presented.
- Chapter 6 – Medium and High level BAWT Optimisation. This chapter develops an MPC (Medium Level) and ESC (High Level) framework through which the low level set-points can be regulated. MPC provides the flexibility to constrain the operational envelope of the system by regulating defined set-points to the low level controller. Then, an ESC scheme is developed such that the altitude of the shroud is regulated autonomously through the maximisation of a power function. This trades off generated power from the rotor against power losses incurred at high wind speeds as a result of reeling the tether in and out.

4.4 Conclusion

This chapter has presented a review of three control design techniques (PID, MPC and ESC). A brief historical background was given and then a discussion on the application of each control method in terms of airborne wind energy was provided. The final section of this chapter motivates the development of the control architecture and analysis that follows in Chapter's 5 and 6. A low-level controller is designed in Chapter 5 to provide stability and desired closed loop set-point tracking of the roll, pitch and altitude of the shroud. Chapter 6, then discusses the development of two hierarchical control schemes. An MPC formulation is provided that regulates the roll, pitch and altitude set-points to the low-level controller. Then an ESC loop is designed such that the altitude of the system can be autonomously regulated.

5 Multivariable Control Design for a BAWT

This chapter presents a multivariable control design methodology for the BAWT. Two tuning methods are introduced in order to derive suitable multiloop controllers to stabilise the BAWT in roll, pitch and altitude. The discussion is centred on the augmented LQR method (guaranteeing zero tracking error) and the multi-loop PID method (MPID), a classical multivariable technique that up until now has previously had success on ship positioning systems and chemical processing plants.

The main contribution of this chapter rests in the multivariable analysis of the Altaeros system with results demonstrating that suitable control over the BAWT can be achieved by using very few tuning parameters. Indeed, simulations show that cheap and fast control design does not necessarily require knowledge of the exact state of plant dynamics, confirming that plant inversion techniques at a particular frequency such as the MPID method can be used to match the desired design specification.

5.1.1 Control of a BAWT System

The focus of this chapter centres solely on the control strategy employed for the Altaeros BAWT. This system is analogous with flight systems in that it is concerned with position control, stability and robustness over a full range of operating conditions. However, the primary focus of a BAWT is energy generation which means it is stationary in flight. So

much like an aircraft, position control is imperative but the added requirement for maximum energy generation makes the flight envelop unique. How this positional control is achieved differs when comparing the two systems directly. An aircraft controls its position through ailerons, elevators and rudders whereas a BAWT is controlled with regulation of three winches based at ground level. There is no reason why surface actuators cannot be placed physically on the shroud in the future but the main drawback comes down to the argument of enhanced performance versus added cost and weight, both of which are highly undesirable for a technology at this stage of development.

Other systems that share certain commonalities with the BAWT are aerostats and blimps. These have the same dependence on buoyant gas and also have to be controlled at high altitudes so are a good reference point for initial design. Previous control designs for applications these applications compared the use of PID controllers with LQG designs and showed that employing the LQR design yields greater performance than a manually tuned PID controller [121]. This informed the first baseline controller developed for the BAWT system by Vermillion in [52]. This work proposed a low level control strategy using an LQ method employed to derive the required set of gains. For implementation on the physical system, these were mainly used as a guide when developing a full discretized controller to cover the full operating envelope.

The remainder of this chapter looks at the BAWT dynamics in the frequency domain and the subsequent control of the shroud in roll, pitch and altitude. Taken from flight theory, the augmented LQR method is implemented and then compared to what is termed the multiloop method (MPID) based on system decoupling at a particular bandwidth frequency. Both techniques were chosen for their ease of implementation. An evaluation between them also

informs the potential benefits of simpler control design between more optimal design methods and classical techniques.

5.2 Operating Region of a BAWT

The BAWT will have a number of operating points within its operating envelope based on operating wind speed, altitude, pitch angle and tether tension. Each of these has limits that are inherently coupled to the dynamics of the system. Firstly, the operating wind speed range of the BAWT is primarily based on the operating wind speed range of the rotor. This is typically between 3-25 m/s depending on rotor configuration. However, although the turbine does not generate above or below these wind speeds, the shroud still has to endure until such times it is reeled back to ground or it is moved to an alternate altitude to start generating electricity again. Therefore, in periods of low wind speed the excess buoyancy must keep the system aloft. This places a limit on the attainable altitude as the tether weight is of course a function of altitude. If the system cannot sufficiently hold its weight at high altitudes, the tethers will become slack and there will be a significant safety concern. Similarly, at high wind speeds the mean breaking load of the tether must not be exceeded so tension regulation to preserve system operation becomes a priority. Tension regulation is achieved through constraining and varying the pitch angle of the shroud as a function of wind speed to ensure the maximum aerodynamic force does not exceed the limit placed on it.

Furthermore, Vermillion in [52] also discussed that the pitch of the shroud is not only limited at high wind speeds but also at low wind speeds. In [52] it was shown that a maximum and minimum pitch angle can be implicitly related to the parameters of the shroud. That is, the location of the tether attachment points and the corresponding relationship between the centre of buoyancy location and the centre of mass.

To show the effect of these limits on the operating envelope, an example is given for a BAWT rated at 30kW with parameters given in Table 5-1. The tether material is assumed to be SK75 fiber made by Dyneema, a typical tether for airborne applications. One tether is conductive facilitating an electricity transfer from shroud to ground. In this case the conductor is assumed to be aluminium. The breaking strength of the tether is assumed to be 30kN [37].

Table 5-1 - System Parameters for 30kW BAWT

Parameters	**Value**
$\boldsymbol{m}$ – Shroud Top Mass (*kg*)	600
$\boldsymbol{v_{range}}$ – Operating Wind Range (*m/s*)	0-30
$\boldsymbol{v_{rated}}$ – Rated Wind Speed (*m/s*)	12
$\boldsymbol{F_{net}}$ – Net Buoyancy (*N*)	1176
$\boldsymbol{\varphi_{diam}}$ – Tether diameter (*mm*)	12
$\boldsymbol{W_T}$ – Tether Weight (kg/100m)	16
$\boldsymbol{T_{MBL}}$ – Mean Tether Breaking Load (*N*)	30000
$\boldsymbol{\theta_{min}}$ – Minimum Pitch Angle (degrees)	5
$\boldsymbol{\theta_{max}}$ – Maximum Pitch Angle (degrees)	20

The parameters given in Table 5-1 provide all the information needed for the creation of a suitable operating envelope for a BAWT. The shroud mass includes the shroud material, fixings and buoyant gas. The operating range of the shroud is constrained to 30 m/s for safety reasons with a rated rotor speed of 12 m/s. The net buoyancy will dominate at low wind speeds so the tether diameter along with the weight is calculated to provide the adequate strength whilst allowing a sufficient operating range of altitudes. Finally, a minimum and maximum pitch angle of 5 and 20 degrees respectively is set so as not to adversely affect aerodynamic performance i.e. negative lift at low wind speeds and stall at

high wind speeds. Combining this information leads to an operating envelope shown in Figure 5-1:

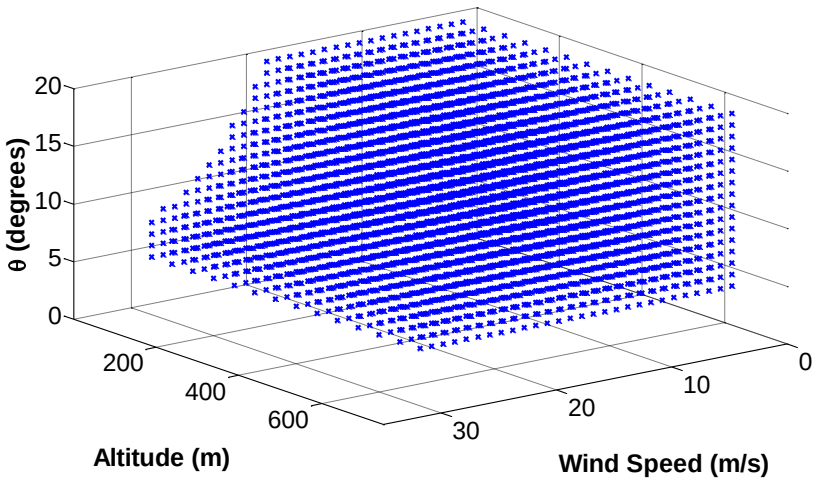

Figure 5-1 – Operating Envelope of a BAWT

As the altitude increases, the length and the subsequent weight of the tether will increase as a result. For the given parameters given in Table 5-1 the altitude is constrained to 650m. Similarly, as the aerodynamic lift varies with the square of the wind speed, at high wind speeds the pitch angle will need to be constrained to ensure the breaking load of the tether is not exceeded. The constraint on pitch can be seen more clearly as simply a function of wind speed as shown in Figure 5-2:

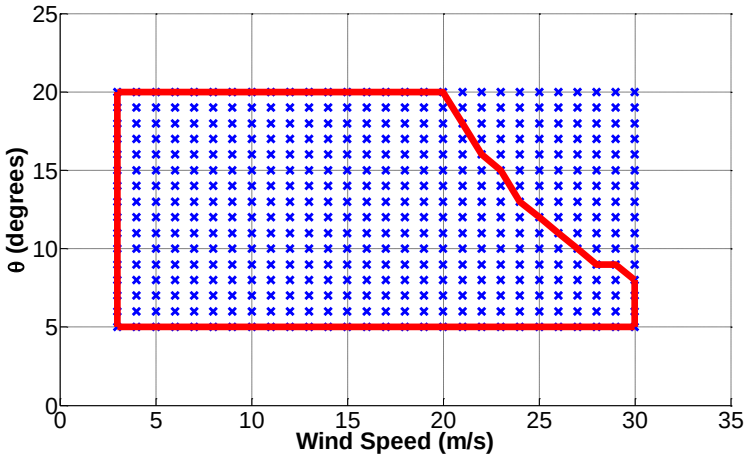

Figure 5-2 - Map of allowable pitch angles for a BAWT at 600m

In Figure 5-2 the region within the red line shows the allowable pitch angles for the BAWT as a function of wind speed. What is noticeable is that there is a reduction in allowable maximum pitch as the wind speed increases. The difference in aerodynamic behavior at different wind speeds informs this operating region and as such give a number of unique operating points of the system.

5.3 Control Aims and Objectives

5.3.1 Aims

The primary aim of the BAWT system is to generate electricity at high altitudes whilst ensuring safe operation. This leads to a requirement for closed loop roll, pitch and altitude control as well as ensuring tension in the tethers is maintained at all times. There are three distinct phases of operation of the system; Autonomous Release, Power Generation and Autonomous Landing. The autonomous release and landing phase require the winches to reel the system out or in whilst simultaneously adhering to the enforced safety and operational constraints. Typically, the system will be retracted in periods of high wind speed that are out-with the operational range of the rotor.

The Power Generation phase is the most pertinent phase from an operational perspective due to the fact this is when energy is being generated. To facilitate optimal power generation the shroud must be stable in flight whilst satisfying any constraints given by the operating envelope. In order to achieve this, a low level controller regulates the reel out speed of the three winches, located on the base station, to alter the unstretched tether length. This subsequently controls the overall length and tension of the tether. In total, there are three tethers located at the fore, aft-starboard and aft-port of the shroud. The difference in length between the three tethers controls the attitude and position of the shroud. The combination of

tether control inputs, to realize a change in roll, pitch and altitude are achieved with the following control actions:

- Roll (φ) – Regulation of tether length between aft-starboard and aft-port tethers
- Pitch (θ) – Regulation of tether length between fore tether and two aft tethers
- Altitude (z)– Synchronous regulation of all tether lengths

A control strategy must be implemented which defines the individual winch speeds to realize the given set-points, whilst also strictly adhering to any operational constraints. This leads to a hierarchical approach such as that shown in Figure 5-3:

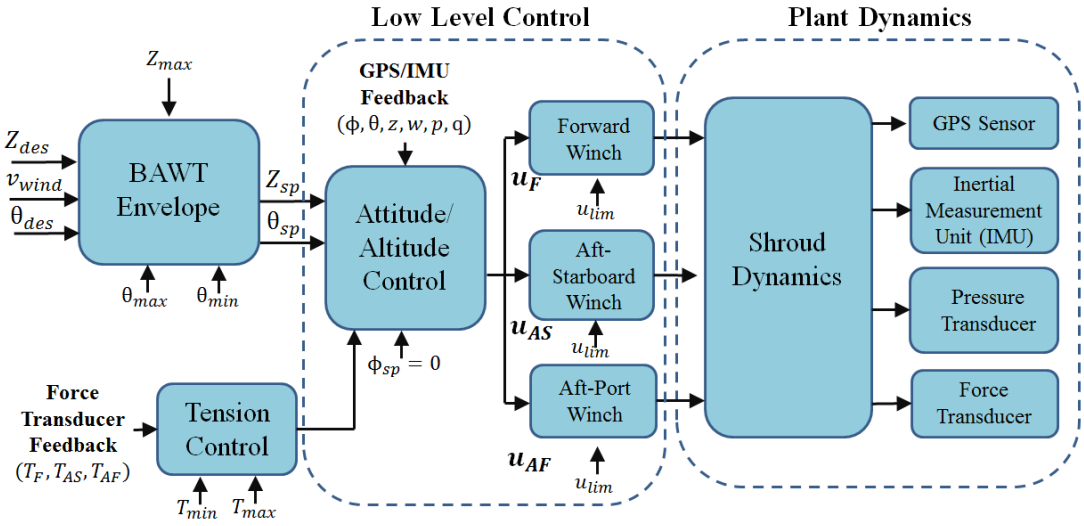

Figure 5-3 –BAWT Controller [44]

Figure 5-3 defines the control strategy for the BAWT system. The primary controller is seen as a low-level attitude and altitude regulator which relies on feedback from the GPS and Inertial Measurement Unit (IMU) sensors. A desired pitch and altitude set-point, Z_{des} and θ_{des}, are evaluated by the BAWT Envelope (Figure 5-1) as a function of wind speed v_{wind}. If the set-points are out-with the feasible range the controller will constrain these based on

allowable bounds. For altitude, the maximum is constrained at Z_{max} whilst for pitch a maximum and minimum can be set as θ_{max} and θ_{min} respectively. The roll ($\phi_{sp} = 0$) is always set at zero so as not to affect the overall aerodynamic lift from any lateral perturbations. Similarly, tension control can be added to provide constrain the allowable tension to the minimum (T_{min}) and maximum (T_{max}) values. Upon deriving a suitable controller, winch inputs are determined for the fore (u_F), aft-starboard (u_{AS}) and aft-port (u_{AF}) tethers. Each of these are limited to a maximum reel out speed u_{lim} which is typically set at 1 m/s. A low-level discretized controller to meet these particular objectives was first presented by Vermillion in [44]. This was a nonlinear controller, designed to account for any operating condition. In contrast, this works focus on model development at particular operating points, and then gain scheduling based on specific operating points.

5.3.2 Control Objectives

The overall objective of the control system is to facilitate conditions for the maximum amount of power generation as possible. In order to do so, the shroud must be operationally stable which means that appropriate regulation of roll, pitch and altitude must be provided. This is done by controlling three winch actuators located at the base station of the shroud. The fact that regulation of these three winches differs when attempting to achieve a given manoeuvre (i.e. altitiude regulation – synchronous movement of all tethers versus pitch regulation – differential movement of tethers) means that independent tuning of each loop will be insufficient to achieve the desired goal. This motivates the requirement for a multivariable approach to control design. The overall objective of this Chapter is to investigate two different multivariable tuning techniques such that control objective is satisfied namely; To ensure that simultaneous control over the roll, pitch and altitude of the shroud is provided under different wind conditions .

5.4 Trim and Linearization

5.4.1 Trim Condition

Autonomous control over the BAWT is imperative to ensure sufficient cost-savings compared with conventional wind generation. For this system the non-linear model developed in Chapter 3 (equations (3-8) - (3-13)) is linearized around distinct operating conditions. The trim condition is defined at a steady state value for pitch, altitude and roll ensuring all velocities and accelerations are equal to zero. This trim condition is defined at wind speed v_w in Equation (5-1) below:

$$l_F^u = l_{nom}^{uF}, \quad l_{AS}^u = l_{nom}^{uAS}, \quad l_{AP}^u = l_{nom}^{uAP}$$
$$v_w = 10\frac{m}{s},\ \phi_{sp} = 0,\ \theta = 10\ deg,\ z_{alt} = 600m,\ p = q = r = w = u = v = 0 \tag{5-1}$$

where, v_w is the operating wind speed set-point, θ and z are the steady state values of pitch and altitude and p, q and r are the rotational velocities with w the translational velocity for altitude. This trim condition is taken from one operating point defined in Figure 5-1.

5.4.2 Linearization

The state vector upon linearization of equations (3-8) - (3-13), is defined as:

$$x = [l_F^u, l_{AS}^u, l_{AP}^u, A_F, A_{AS}, A_{AP}, p, \phi, q, \theta, r, \psi, w, z_{alt}, v, y, u, x]^T \tag{5-2}$$

where A_F, A_{AS} and A_{AP} accounts for the 1st order winch dynamics. At the defined operating point (5-1) we have a state space model of the form

$$\dot{x} = Ax(t) + Bu(t) \tag{5-3}$$

$$y = Cx(t) + Du(t) \tag{5-4}$$

where, $A, B\ C$ and D are appropriate partial derivative matrices derived using Taylor's expansion. Note that there are no feed-forward terms so $D = 0$ and can be neglected. The input vector is defined as

$$u(t) = [u_1, u_2, u_3]^T \tag{5-5}$$

where, u_1, u_2 and u_3 are the three desired motor winch speeds of the fore, aft starboard and aft port motors respectively.

Manipulating equation (5-3) and (5-4) into transfer function form gives:

$$G(s) = \frac{Y(s)}{U(s)} = C(sI - A)^{-1}B \tag{5-6}$$

5.5 Validation with Nonlinear Model

To compare the validity of the linear model, a comparison is made with the nonlinear model at a nominal operating point. A trim condition is defined using Equation (5-1) with the operating points used for comparison defined in Table 5-2. The linearization was taken at a base wind speed of 10 m/s ($v_{wind} = 10\ m/s$):

Table 5-2 - Trim Condition around base wind speed of 10 m/s

l_F^u (m)	l_{AS}^u(m)	l_{AP}^u(m)	p(deg/s)	ϕ(deg)	q(deg/s)	θ_{ss}(deg)	w(m/s)	z_{sp}(m)
638	643	644	0	0	0	10	0	600

The resultant linearization is defined according to Equation's (5-3) and (5-4). This results in an 18 state system with the corresponding state space matrices taking the following form:

$$A = \begin{bmatrix}
0 & 0 & 0 & 10 & 0 & 0 & 0 & 0 & 0 & 0 & 0 & 0 & 0 & 0 & 0 & 0 & 0 & 0 \\
0 & 0 & 0 & 0 & 10 & 0 & 0 & 0 & 0 & 0 & 0 & 0 & 0 & 0 & 0 & 0 & 0 & 0 \\
0 & 0 & 0 & 0 & 0 & 10 & 0 & 0 & 0 & 0 & 0 & 0 & 0 & 0 & 0 & 0 & 0 & 0 \\
0 & 0 & 0 & -10 & 0 & 0 & 0 & 0 & 0 & 0 & 0 & 0 & 0 & 0 & 0 & 0 & 0 & 0 \\
0 & 0 & 0 & 0 & -10 & 0 & 0 & 0 & 0 & 0 & 0 & 0 & 0 & 0 & 0 & 0 & 0 & 0 \\
0 & 0 & 0 & 0 & 0 & -10 & 0 & 0 & 0 & 0 & 0 & 0 & 0 & 0 & 0 & 0 & 0 & 0 \\
-0.02 & 1.81 & -1.84 & 0 & 0 & 0 & 0 & -20.7 & 0 & -0.13 & 0 & 8.5 & 0 & 0.05 & 0.08 & -0.01 & -0.01 & 0.02 \\
0 & 0 & 0 & 0 & 0 & 0 & 1 & 0 & 0 & 0 & 0.29 & 0 & 0 & 0 & 0 & 0 & 0 & 0 \\
0.59 & -1.28 & -1.28 & 0 & 0 & 0 & 0 & 0.04 & -0.45 & -17.8 & -0.19 & -0.33 & 0.25 & 1.82 & 0 & -0.04 & 0.03 & 0.75 \\
0 & 0 & 0 & 0 & 0 & 0 & 0 & 0 & 1 & 0 & 0 & 0 & 0 & 0 & 0 & 0 & 0 & 0 \\
0.02 & -0.15 & 0.1 & 0 & 0 & 0 & 0 & 1.15 & 0.19 & 0.15 & -0.45 & -1.06 & 0 & 0.03 & -0.07 & 0 & 0 & 0.01 \\
0 & 0 & 0 & 0 & 0 & 0 & 0 & 0 & 0 & 0 & 1 & 0 & 0 & 0 & 0 & 0 & 0 & 0 \\
4.8 & 4.9 & 4.9 & 0 & 0 & 0 & 0 & 1.59 & 0 & 51.65 & 0 & 0.11 & -2.15 & -13.5 & 0 & 0.3 & -1.28 & -5.4 \\
0 & 0 & 0 & 0 & 0 & 0 & 0 & 0 & 0 & 0 & 0 & 0 & 1 & 0 & 0 & 0 & -0.28 & 0 \\
-0.1 & -0.09 & -0.12 & 0 & 0 & 0 & 0 & -4.2 & 0 & -0.78 & 0 & -13.9 & 0 & 0.29 & -1.85 & -0.02 & 0 & 0.12 \\
0 & 0 & 0 & 0 & 0 & 0 & 0 & 0 & 0 & 0 & 0 & 0 & 0 & 0 & 1 & 0 & 0 & 0 \\
0.46 & 0.48 & 0.48 & 0 & 0 & 0 & 0 & 0.2 & 0 & 8.14 & 0 & 0.25 & 0.35 & -1.3 & 0 & 0.03 & -0.5 & -0.55 \\
0 & 0 & 0 & 0 & 0 & 0 & 0 & 0 & 0 & 0 & 0 & 0 & 0.28 & 0 & 0 & 0 & 1 & 0
\end{bmatrix} \quad (5\text{-}7)$$

$$B = \begin{bmatrix}
0 & 0 & 0 & 1 & 0 & 0 & 0 & 0 & 0 & 0 & 0 & 0 & 0 & 0 & 0 & 0 & 0 & 0 \\
0 & 0 & 0 & 0 & 1 & 0 & 0 & 0 & 0 & 0 & 0 & 0 & 0 & 0 & 0 & 0 & 0 & 0 \\
0 & 0 & 0 & 0 & 0 & 1 & 0 & 0 & 0 & 0 & 0 & 0 & 0 & 0 & 0 & 0 & 0 & 0
\end{bmatrix}^T \quad (5\text{-}8)$$

$$C = \begin{bmatrix}
0 & 0 & 0 & 0 & 0 & 0 & 0 & 0 & 0 & 0 & 0 & 0 & 0 & 1 & 0 & 0 & 0 & 0 \\
0 & 0 & 0 & 0 & 0 & 0 & 0 & 1 & 0 & 0 & 0 & 0 & 0 & 0 & 0 & 0 & 0 & 0 \\
0 & 0 & 0 & 0 & 0 & 0 & 0 & 0 & 0 & 1 & 0 & 0 & 0 & 0 & 0 & 0 & 0 & 0
\end{bmatrix} \quad (5\text{-}9)$$

The state space matrices for a linearization at a wind speed of 10 m/s, altitude of 600m and pitch of 10 degrees are shown in Equations (5-7) - (5-9). It is noted that the actuator dynamics discussed in Section 3.10 have been incorporated into the dynamics with a time constant of 0.1. The linear model is then compared to the nonlinear model following a step disturbance in the input. The step disturbance lasts for 10 seconds. The defined input disturbance is shown in Figure 5-4 for the winch inputs and unstretched tether lengths. The nonlinear/linear comparison is then shown in Figure 5-5 for roll, pitch and altitude.

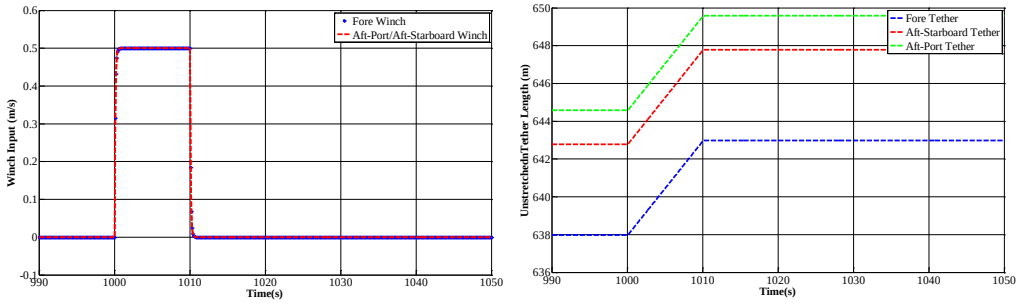

a) b)

Figure 5-4 -Step disturbance in control inputs a) Winch Response b) Unstretched Tether Lengths (Fore, Aft-Starboard, Port-Starboard tethers)

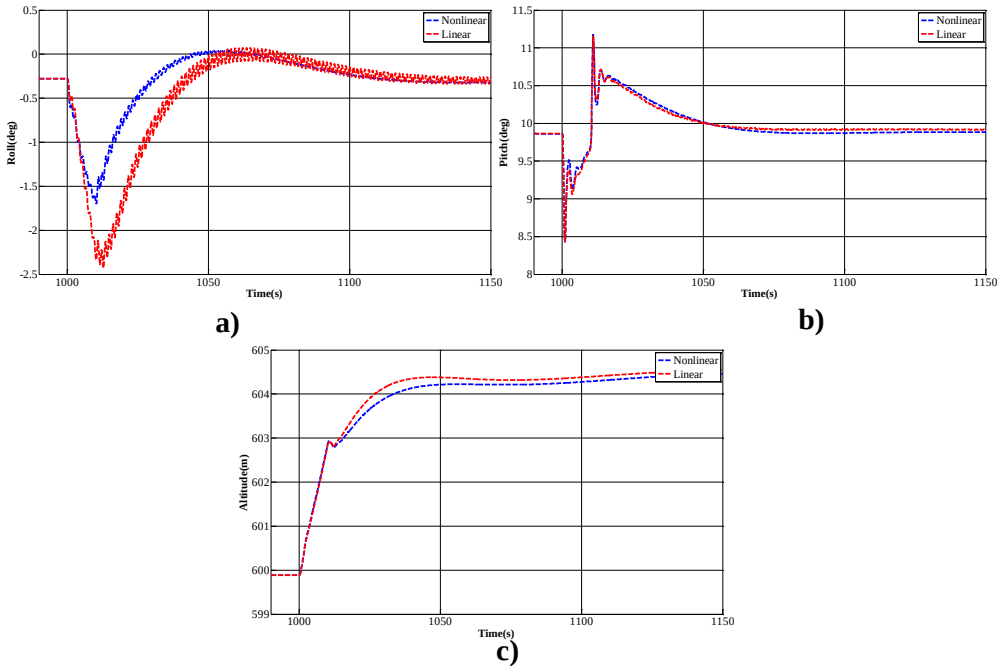

a) **b)**

c)

Figure 5-5 - Nonlinear-Linear Model Comparison Following Step Disturbance; a) Roll Response, b) Pitch Response, c) Altitude Response

5.6
5.6 Transfer Function Analysis

Three system outputs are considered on the plant namely; roll, pitch and altitude. Therefore, knowing (5-3) and placing into transfer function form (equation (5-6)) using the *tf* command in MATLAB, an open loop transfer function $G_{ij}(s)$ is computed. This takes the form of a square $[3 \times 3]$ matrix denoting interactions between the fore and aft winches to outputs in roll, pitch and altitude. Columns $j = 1{:}3$ denote the interactions from the fore, aft and aft-

port winches whilst, rows $i = 1{:}3$ denote the outputs altitude, roll and pitch respectively. This results in a full system defined as follows:

$$\begin{bmatrix} Y_{roll}(s) \\ Y_{pitch}(s) \\ Y_{alt}(s) \end{bmatrix} = \overbrace{\begin{bmatrix} g_{11} & g_{12} & g_{13} \\ g_{21} & g_{22} & g_{23} \\ g_{31} & g_{32} & g_{33} \end{bmatrix}}^{From\ output(i)to\ \ winch\ input\ (j)to} \begin{bmatrix} U_1(s) \\ U_2(s) \\ U_3(s) \end{bmatrix} \tag{5-10}$$

The multivariable system is defined by the interaction between the dynamics of the plant $G(s)$, shown here as the interactions from roll, $Y_{roll}(s)$, pitch, $Y_{pitch}(s)$, and altitude, $Y_{alt}(s)$, to the influence from the three winch inputs $U_1(s)$, $U_2(s)$ and $U_3(s)$.

There will be a degree of coupling between the desired inputs and outputs, therefore this motivates the need to consider the following:

- The interactions between the number of winch inputs and outputs will determine the overall influence on plant behavior and will be characterized by the linearization point on the system i.e. altitude, pitch and roll interaction between the three winch inputs U_1, U_2 and U_3 will be defined at a particular operating point
- The control of the system for a particular set-point will require different regulation of the three winches i.e. for a change in altitude all the winches must operate synchronously but for a change in pitch the fore and two aft winches will operate inversely. This presents a trade-off in the multivariable control strategy.
- The capability of the control of the system to regulate the altitude, pitch and roll of the system will be dictated by the time constant of both the actuator and the plant.

5.7 Optimal LQR Controller with Zero Tracking Error

The most relevant case study of LQR control design in relation to the BAWT is in aircraft control as discussed in Section 4.1.3. Indeed, in previous work on BAWT control Vermillion [44] designed gains based on an initial LQ design on a direct downward linearization which is defined when the roll of the shroud is zero and the shroud is sitting at a pre-defined pitch and altitude. This work extends this by designing an augmented LQR controller to provide the desired response in roll, pitch and altitude. Firstly, a method of deriving two optimal gains K_1 and K_2, one for state feedback and one for position control, is derived for a particular operating point. This process can be implemented across the operating envelop (Figure 5-2) to form gain tables, which are then interpolated based on current operating conditions. The design and implementation of the augmented LQR control is now discussed in more detail [53].

In order to provide tracking with zero steady state error, integral action is applied to the output error so that the resulting control action is of the following form:

$$u(t) = -K_1 x(t) + K_2 \int_0^t \big(y_r(\tau) - y(\tau)\big) d\tau \tag{5-11}$$

where y_r is the output reference. Assuming a constant y_r differentiating (5-11) and substituting into (5-3) and (5-4) gives

$$\dot{u}(t) = -K_1 \dot{x}(t) - K_2 y(t) \tag{5-12}$$

$$= [-K_1 A - K_2 C \quad -K_1 B] \begin{bmatrix} x(t) \\ u(t) \end{bmatrix}$$

$$= [-K_1 \quad -K_2] \begin{bmatrix} A & B \\ C & 0 \end{bmatrix} \begin{bmatrix} x(t) \\ u(t) \end{bmatrix}$$

To calculate the final controller, the system state is augmented so that the input is the derivative of the control. This gives an augmented system with

$$A_e = \begin{bmatrix} A & B \\ 0 & 0 \end{bmatrix} \qquad B_e = \begin{bmatrix} 0 \\ I \end{bmatrix} \qquad C_e = [C \quad 0] \tag{5-13}$$

$$x_e = \begin{bmatrix} x \\ u \end{bmatrix} \qquad u_e = \dot{u} \tag{5-14}$$

The second stage is to then use this form within a standard LQR cost for the augmented system, that is

$$L = \int_0^\infty ({x_e}^T Q_e x_e + {u_e}^T R_e u_e) \tag{5-15}$$

where Q_e is a positive semi-definite symmetric state weighting matrix and R_e is a symmetric control derivative weighting matrix. The well-known optimal state feedback controller is

$$K_e = {R_e}^{-1} {B_e}^T P_e \tag{5-16}$$

Where P_e is the positive definite symmetric solution of the algebraic Riccati equation

$${A_e}^T P_e + P_e A_e + Q_e - {R_e}^{-1} {B_e}^T P_e B_e P_e = 0 \tag{5-17}$$

The feedback is thus

$$\dot{u} = -K_e \begin{bmatrix} x \\ u \end{bmatrix} \tag{5-18}$$

The final step is to equate with (5-20) so that

$$K_e = [K_1 \quad K_2] \begin{bmatrix} A & B \\ C & 0 \end{bmatrix} \tag{5-19}$$

provided the plant is square and invertible,

$$[K_1 \quad K_2] = K_e \begin{bmatrix} A & B \\ C & 0 \end{bmatrix}^{-1} \tag{5-20}$$

The final closed loop system is therefore given by

$$\begin{cases} \begin{bmatrix} \dot{x} \\ \dot{e}_i \end{bmatrix} = \begin{bmatrix} A - BK_1 & BK_2 \\ -C & 0 \end{bmatrix} \begin{bmatrix} x \\ e_i \end{bmatrix} + \begin{bmatrix} 0 & I \\ I & 0 \end{bmatrix} \begin{bmatrix} y_r \\ d \end{bmatrix} \\ \begin{bmatrix} y \\ u \end{bmatrix} = \begin{bmatrix} C & 0 \\ K_1 & -K_2 \end{bmatrix} \begin{bmatrix} x \\ e_i \end{bmatrix} + \begin{bmatrix} 0 & 0 \\ 0 & 0 \end{bmatrix} \begin{bmatrix} y_r \\ d \end{bmatrix} \end{cases} \quad (5\text{-}21)$$

where, $e_i(t) = \int_0^t \big(y_r(\tau) - y(\tau)\big) d\tau$

Applying Equation (5-11) in practice results in a form of PID control form shown in Figure 5-6 below:

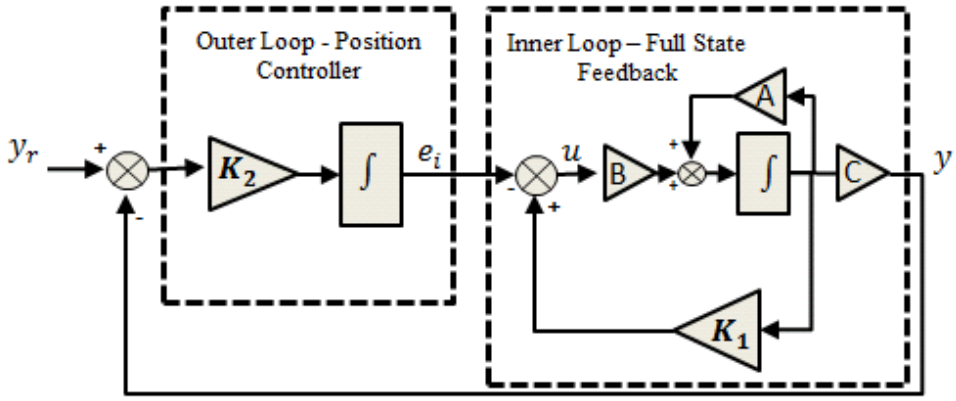

Figure 5-6 - Augmented LQR Controller

The design of K_1 and K_2 illustrated in Figure 5-6 is dependent on two weighting matrices Q_e and R_e, which place a weighting on the output and input respectively, see equation (5-15). These have to be tuned appropriately to achieve the desired multi-loop response. The method of doing this involves choosing an initial Q-matrix, solving the Algebraic Ricatti Equation and then evaluating the controller in both the frequency and time-domain. The weights are then altered if the desired design criteria are not met. The initial Q_e and R_e matrix are chosen according to Equations (5-22) - (5-23), adjustments are then made according to the methodology shown in Figure 5-7:

$$Q_e = 0.1 * C_e{}' C_e \quad (5\text{-}22)$$

$$R_e = \begin{bmatrix} 1 & 0 & 0 \\ 0 & 1 & 0 \\ 0 & 0 & 1 \end{bmatrix} \tag{5-23}$$

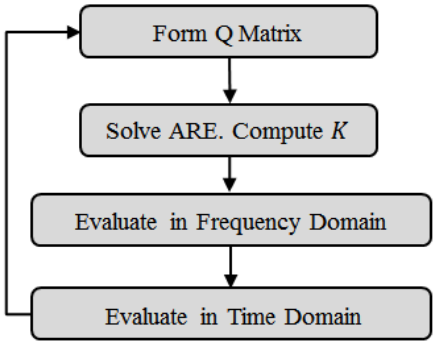

Figure 5-7 - LQR Design and Analysis for Altaeros System

Taking the example linearization given in Table 5-2, the resultant augmented LQR design results in two gain matrices K_1 and K_2. K_1 being of order 3×18 and K_2 being of order 3×3. The resultant K_2 matrix is shown in Equation (5-24)..

$$K_2 = \begin{bmatrix} 2.93 & -0.19 & 1.54 \\ 1.08 & 0.95 & -2.93 \\ 0.45 & -1.03 & -3.00 \end{bmatrix} \tag{5-24}$$

5.8 Multiloop PID Tuning Method (MPID)

The LQR method can be time consuming and difficult to tune, so it is necessary to provide alternative techniques to consider for control design. Such alternatives have been described in detail by Katebi in [68]. Specifically, in this case the desired goal was to compare the merits of optimal design methods, such as the augmented LQR method, with non-parametric methods that can be implemented without necessarily having access to a full state model of the plant. Of all the non-parametric methods described in Section 4.1.1 (Davison, Pettinnen-Koivo and Maciejowski) the Maciejowski (Modification of characteristic loci) method is the most applicable. In this case, the Davison and Pettinnen-Koivo method were discounted because both require exact plant inversion, which is impossible due to the pure integrators

contained within the actuator dynamics. Based on this reasoning, the Multiloop PID method was chosen for further exploration.

The Multiloop PID method, aims to decouple the system at the bandwidth frequency ω_b and in doing so altering the characteristic locus of the plant. This basic principle was developed by MacFarlane and Kouvaritakis [89]. If we have a square transfer matrix with m inputs and outputs which has the following spectral decomposition

$$G(s) = W(s)\Lambda(s)W^{-1}(s) \tag{5-25}$$

where, $W(s)$ is a matrix whose column vectors are the eigenvectors of $G(s)$ and

$$\Lambda(s) = diag\{\lambda_1(s), \lambda_2(s), \ldots, \lambda_m(s)\} \tag{5-26}$$

Where, the $\lambda_i(s)$ are the eigenvalues or characteristic functions of $G(s)$. If the compensator $K(s)$ is given the structure

$$K(s) = W(s)M(s)W^{-1}(s) \tag{5-27}$$

where,

$$M(s) = diag\{\mu_1(s), \mu_2(s), \ldots, \mu_m(s)\} \tag{5-28}$$

Then the open loop transfer function or return ratio is

$$-G(s)K(s) = -W(s)\Lambda(s)M(s)W^{-1}(s) \tag{5-29}$$

$$= -W(s)N(s)W^{-1}(s) \tag{5-30}$$

where,

$$N(s) = diag\{v_1(s), v_2(s), \ldots, v_m(s)\} \tag{5-31}$$

and,

$$v_i(s) = \lambda_i(s)\mu_i(s) \tag{5-32}$$

Therefore, if the plant and compensator share the same eigenvectors, the overall system connected in series is obtained by the product of the plant and compensator eigenvalues. The problem however arises when trying to determine the matrices $W(s)$ and $W^{-1}(s)$ which are

almost always irrational functions and have no practical realisations. In order to avoid issues such as this, a practical alternative is to give the compensator the following structure

$$K(s) = A(s)M(s)B(s) \tag{5-33}$$

where, $A(s)$ and $B(s)$ are chosen to be realizable and such that,

$$A(s) \approx W(s) \tag{5-34}$$

and,

$$B(s) \approx W^{-1}(s) \tag{5-35}$$

Maciejowski et al assessed this problem and determined that a good way of choosing $B(s)$ is to approximate $W^{-1}(s_0)$ at some particular point $s_0 = j\omega_0$, usually the desired bandwidth ω_b. This is approximated as real matrices through the ALIGN algorithm [76]. This algorithm finds a constant real gain matrix M, such that Equation (5-36) is minimized.

$$J(M,\theta) = \left(G(j\omega_b)M - e^{j\theta}\right)^T \left(G(j\omega_b)M - e^{j\theta}\right), \qquad \theta = diag(\theta_i) \tag{5-36}$$

The approach here uses the system bandwidth ω_B to decouple the system. The resultant matrix is then used as the basis for the compensator. Tuning parameters p, ε and δ provide the desired proportional, integral and derivative terms as follows

$$K_p = pK_m, \quad K_i = \frac{\varepsilon K_m}{s}, \quad K_d = \delta K_m s \tag{5-37}$$

The product of $G(j\omega_b)$ and K_m should be very close to a diagonal matrix resulting in full decoupling of each loop. Taking a linearization around an operating wind speed of 10 m/s at $\omega_b = 1.2$ rad/s results in the estimation of $G(j\omega_b)$ producing the complex gain matrix shown in Equation (5-38)

$$G(j1.2) = \begin{bmatrix} -0.4175 - 2.5010j & -0.0461 - 0.3969j & 0.0465 + 0.1886j \\ -0.0034 - 0.0041j & -0.0095 - 0.2312j & 0.0099 + 0.2358j \\ -0.04 - 0.3536j & 0.006 + 0.1435j & 0.0135 + 0.2068j \end{bmatrix} \tag{5-38}$$

Then using the ALIGN algorithm (formulated in Appendix 4) in MATLAB produces an approximate gain matrix K_m which can be modified according to p, ε and δ. The resulting K_m matrix based on alignment of Equation (5-38) is shown below

$$K_m = \begin{bmatrix} 0.3643 & -0.492 & 0.2181 \\ 0.3695 & 2.0314 & -2.6369 \\ 0.3688 & -2.2543 & -2.5843 \end{bmatrix} \tag{5-39}$$

To determine whether or not loop decoupling has been achieved, an assessment is made of $G(j1.2)K_m$. This is shown in Equation (5-40)

$$G(j1.2)K_m = \begin{bmatrix} -0.152 - 0.9883\text{j} & 0.0068 - 0.0011\text{j} & -0.0897 + 0.0138\text{j} \\ -0.0011 + 0\text{j} & -0.04 - 0.9991\text{j} & -0.0013 - 0.0006\text{j} \\ -0.0074 + 0.0004\text{j} & 0.0015 - 0.0007\text{j} & -0.0594 - 0.9899\text{j} \end{bmatrix} \tag{5-40}$$

Equation (5-40) shows that good decoupling has been achieved at the desired bandwidth of $\omega_b = 1.2$ rad/s. There is still some influence from the aft-port winch (3rd input) to desired altitude (1st output). However, this is nominal and upon appropriate tuning of the parameters $p = 0.95$, $\varepsilon = 0.1$ and $\delta = 0.6$ the desired closed loop response can be achieved. The tuning of these parameters can be first sweeping ε between 0 and 1 to get the desired overshoot. Then p can be increased to achieve the desired step response. Finally, δ can then be tuned, typically set between 0 and 1 to improve the resultant performance.

5.9 Principle Gains using Singular Value Decomposition (SVD)

In multivariable systems it is possible to define bounded ratios and replace a single gain in a SISO with a range of gains bounded below and above particular values for a MIMO system. These gains are called the singular values of the system and can be derived using singular value decomposition.

The main result of singular value decomposition can be stated that the gain of a multivariable system lies somewhere in-between the smallest and largest principle gains [8]

$$\sigma_{min}(\omega) \leq \frac{\|G(j\omega)u(j\omega)\|}{\|u(j\omega)\|} \leq \sigma_{max}(\omega) \tag{5-41}$$

where, $\sigma_{min}(\omega)$ is the minimum singular value,$\sigma_{max}(\omega)$ is the maximum singular value, $G(j\omega)$ is the transfer function G evaluated at frequency $j\omega$ and $u(j\omega)$ is the input vector evaluated at frequency $j\omega$. Analysing a multivariable feedback system in this way means that appropriate limits can be placed on factors such as sensitivity and disturbance rejection. This is in addition to providing a good method of assessing closed loop performance. To provide an initial assessment of the plant, the open loop singular values are plotted. This is shown in Figure 5-8 for three different linearised cases namely:

- A wind speed of 5 m/s at a shroud pitch of 5 degrees, a roll angle of zero and an altitude of 600m (linearization in the form of equation (5-3))
- A wind speed of 10 m/s at a shroud pitch of 5 degrees, a roll angle of zero and an altitude of 600m (linearization in the form of equation (5-3))
- A wind speed of 10 m/s at a shroud pitch of 10 degrees, a roll angle of zero and an altitude of 600m (linearization in the form of equation (5-3))

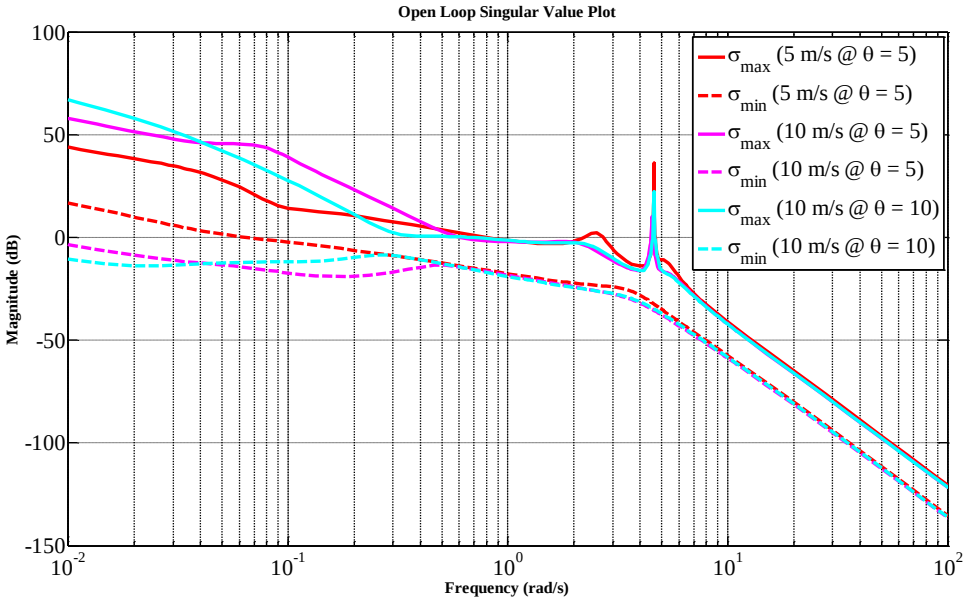

Figure 5-8 - Singular Value Plot of Multivariable Plant

The open loop dynamics of the BAWT can be seen in Figure 5-8 as a function of σ_{max} and σ_{min} for two different wind speeds under two different pitch angles. Note that the roll of the shroud is constrained to zero. The singular value plot bounds the open loop system between σ_{max} and σ_{min} for three different operating conditions. At low frequencies there is a difference in gain response for both the max and min singular values of the system. This is evidenced by a higher gain at low frequencies with a higher wind speed, which is seen to be independent of the pitch angles considered i.e. the gain is seen to be higher at low frequencies at a wind speed of 10 m/s. This change in behaviour lasts up until around 1 rad/s where the response is then seen to be largely similar. An undamped response is observed in each case at 4.65 rad/s, however, the damping is not seen to change significantly between the cases compared here. The high frequency roll off just after this event at 4.7 rad/s is approximately the same in each case. Aside from the low frequency response, the fact that the open loop transfer function suggests no significant differences perhaps suggests that a controller scheduled on wind speed may not be required. This point is discussed further in Section 5.10.

5.10 Requirement for Gain Scheduling for BAWT

There is a need to understand the underlying system behaviour to determine if there is a requirement for the implementation of a gain scheduling element. In Section 5.9 using singular value decomposition the open loop dynamics of the plant are shown. It was observed that at linearisations around higher wind speeds there is a change in gain response at low frequencies, whilst from approximately 1 rad/s and above, the frequency response is largely similar. Therefore, to understand whether a multivariable controller could be designed around one operating point and sensibly applied across the envelope, it is pertinent to understand how the open loop dynamics shift with wind speed. This is illustrated in more detail in Figure 5-9:

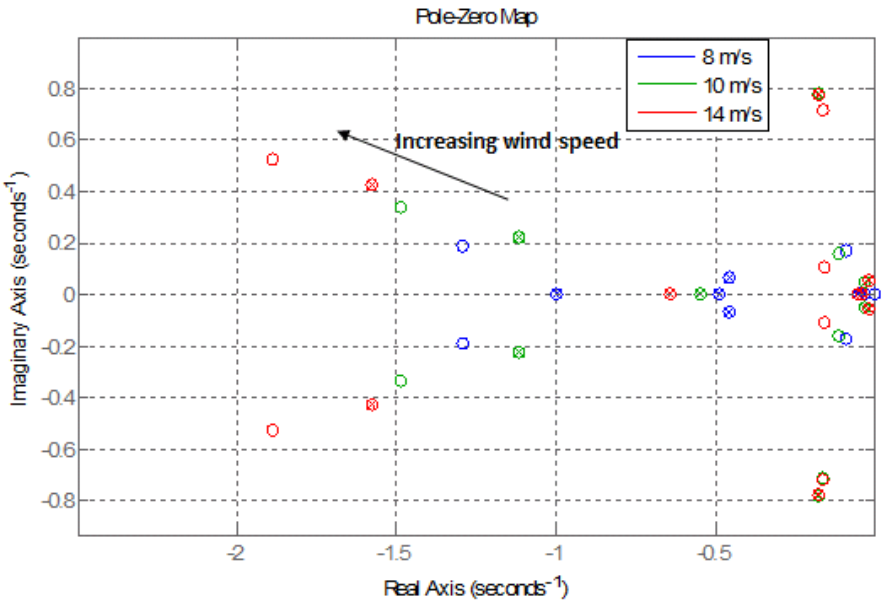

Figure 5-9 - Open loop pole/zero response of BAWT at 8 m/s (Blue), 10 m/s (Green), 14 m/s (Red)

It can be seen clearly in Figure 5-9 that the open loop poles move to the left as wind speed increases. This provides evidence of two things namely;

- The open loop system is stable as no right-hand plane zeros are observed

- The stability of the system is increased with wind speed evidenced by the left-hand plane poles moving further away from the origin.

One reason why system stability may improve as wind speed increases, could be related to the aerodynamic behaviour of the system. At higher wind speeds the aerodynamic damping of the system will be increased due to the increase in aerodynamic lift and drag forces on the shroud. This is evidenced in Appendix A3 which shows the open loop damping increase with respect to wind speed for the relevant transfer functions in roll, pitch and altitude. Furthermore, any increase in aerodynamic moment will be counteracted by an increase of the pitching moment applied by the tethers to the base-station. As a degree of damping will always be provided by the tethers and assuming the time constant of the system is in the order of minutes rather than seconds then system stability could be attained across the operating envelope for one set of controller gains for constant references in roll, pitch and altitude.

However, there may be a situation where the system will be sensitive to moving operating point. This is evidenced in Figure 5-10 below:

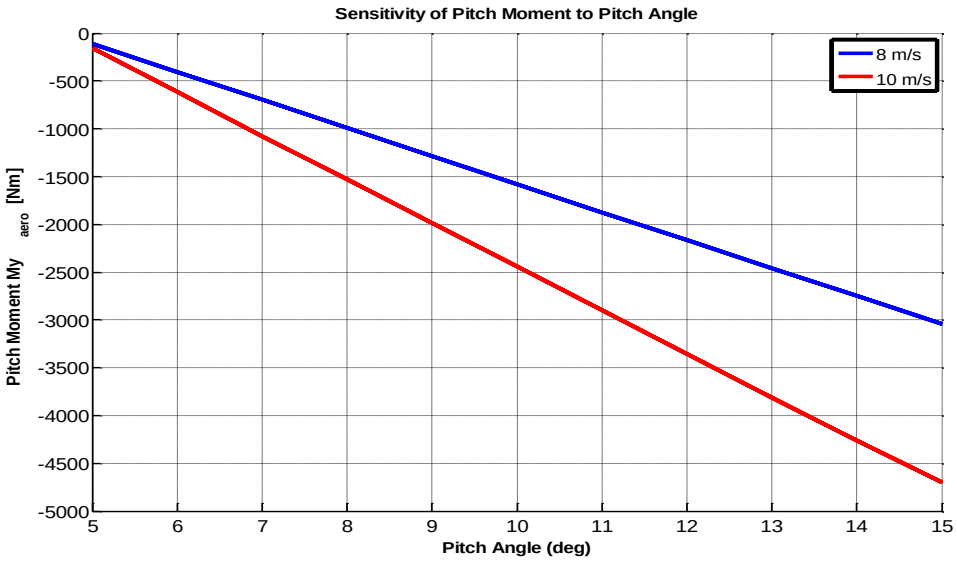

Figure 5-10 - Sensitivity of pitch moment to pitch angle

In Figure 5-10 it is clear that there is an increased sensitivity to pitch moment as a function of pitch angle as wind speed increases. An increase in sensitivity is observed from 300Nm/deg at 8 m/s to 600Nm/deg at 10 m/s. If the operating trajectory of the shroud was constantly varying and not held at a constant pitch, then there could be an argument for providing compensation to the controller as a function of this sensitivity. However, this case is not considered in this work, and a constant pitch angle is to set it at 10 degrees.

5.11 Stability and Robustness

The stability and robustness of the two proposed controllers will now be assessed. Firstly, this is done through an eigenvalue assessment of the open loop dynamics at 10 m/s and then comparing the response with either the applied MPID or Augmented LQR controller. Secondly, the closed loop assessment of the LQR and MPID controllers assessed using the principal gains of the sensitivity and complimentary sensitivity functions showing that both controllers exhibit good closed loop responses around the trim condition.

5.11.1 Eigenvalue Assessment

In order to stabilise the system at each defined condition, an LQR and MPID controller is designed at each operating point. Figure 5-11 shows the closed loop poles for both controllers taken at a linearization around a base wind speed of 10 m/s. The open loop poles are also shown for comparison. It can be seen that in both cases the controllers stabilise the system. This assessment can be extended to the full operating envelope, as discussed in Section 5.10.

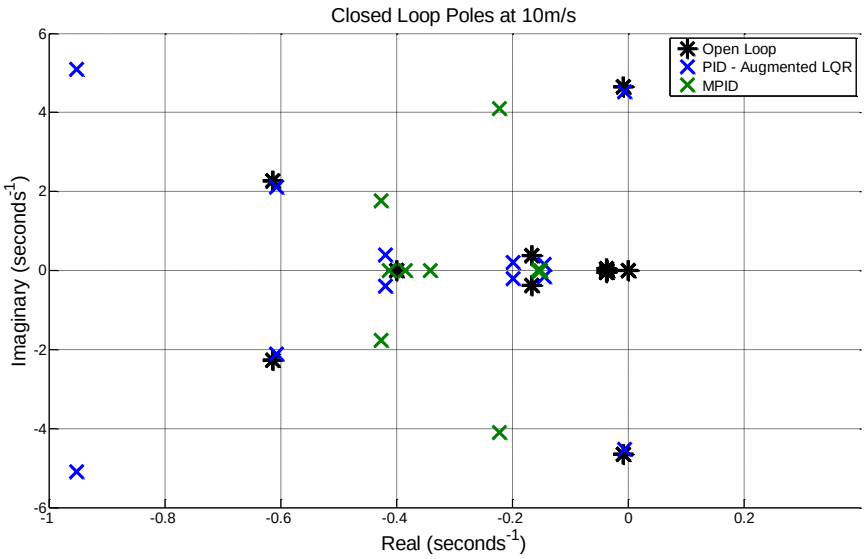

Figure 5-11 - Closed Loop Poles at 10 m/s

5.11.2 Frequency Domain Assessment

An important consideration for the control design is the ability to act against disturbances at high frequencies and provide good tracking at low frequencies. To assess the robustness of the controller, the sensitivity and complimentary sensitivity functions are compared for the maximum and minimum principal gains for the two controllers, denoted as the PID - LQR and MPID, at 10m/s. These are seen in Figure 5-12 and Figure 5-13 respectively. It is observed that the closed loop bandwidth of the MPID controller is greater than the LQR at 1.2 rad/s to 0.2 rad/s respectively. Therefore, an expected increase in closed loop

performance would be expected. However, this comes at the cost of some decrease in damping clearly seen between 1 to 5 rad/s Furthermore, in Figure 5-12, at low frequencies below the bandwidth the gain from both the LQR and MPD is low indicating good disturbance rejection. It can also be seen from Figure 5-12 that the maximum and minimum singular values for the system are relatively close. This is important because ideally there would be no difference, meaning that behaviour is akin to that of a SISO system.

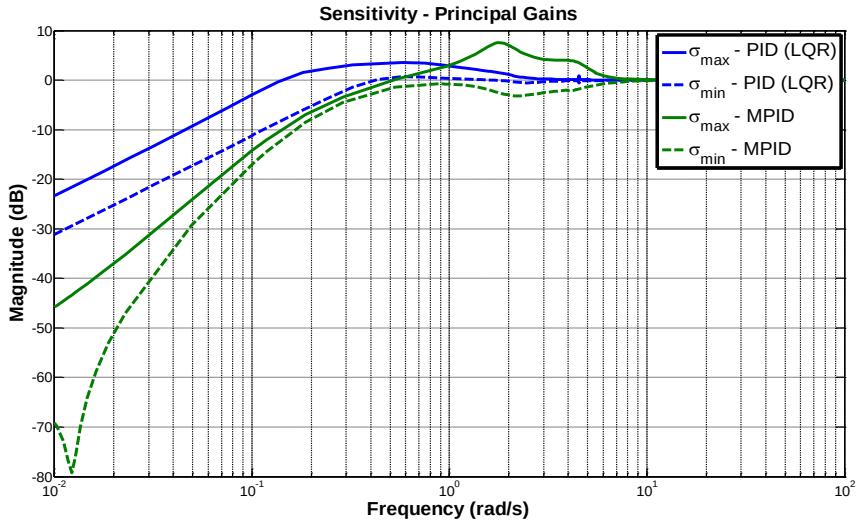

Figure 5-12 - Sensitivity Function

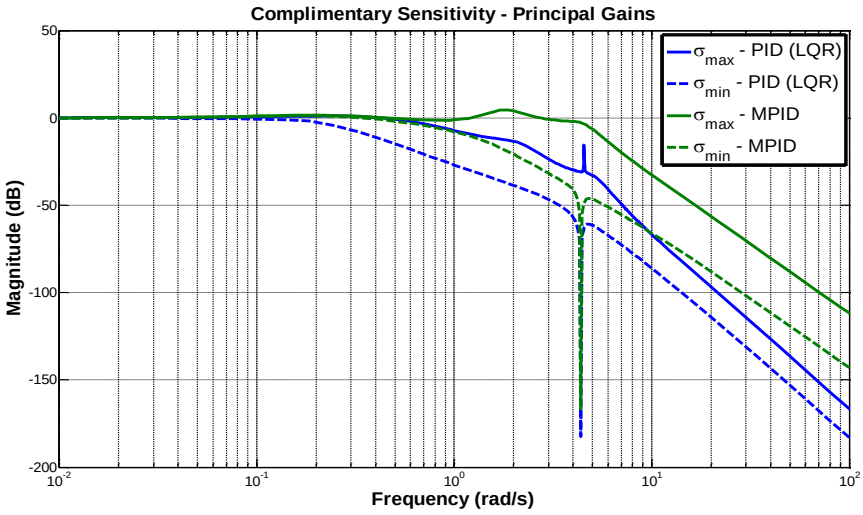

Figure 5-13 - Closed Loop Singular Value Plot

In Figure 5-13 it is seen that there is good closed loop tracking in both cases. A notch filter has been added to reduce the peak in roll at 4.4 rad/s, this takes the form $\frac{s^2+{\omega_0}^2}{s^2+2\omega_0\xi s+{\omega_0}^2}$ where ω_0 is the notch frequency and $\xi = 0.4$ is the damping factor. It can be argued that each controller provides good disturbance rejection and set-point tracking in the frequency range of interest. The next section evaluates the step response of each of the designed controllers.

5.12 Step Response of Linear Controllers

To make an initial assessment of each control design, the closed loop response for reference step inputs is evaluated from the reference set-points to both the output (Figure 5-14) and input (Figure 5-15) for each controller. In the case of the MPID the tuning values used were $p = 0.95$, $\varepsilon = 0.1$ and $\delta = 0.6$ for a linearisation around 10 m/s.

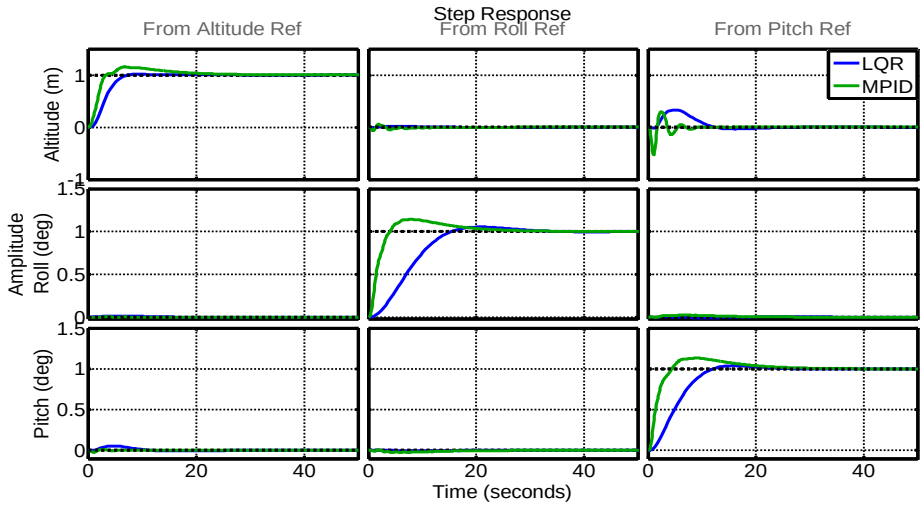

Figure 5-14 - Output Responses to Step command

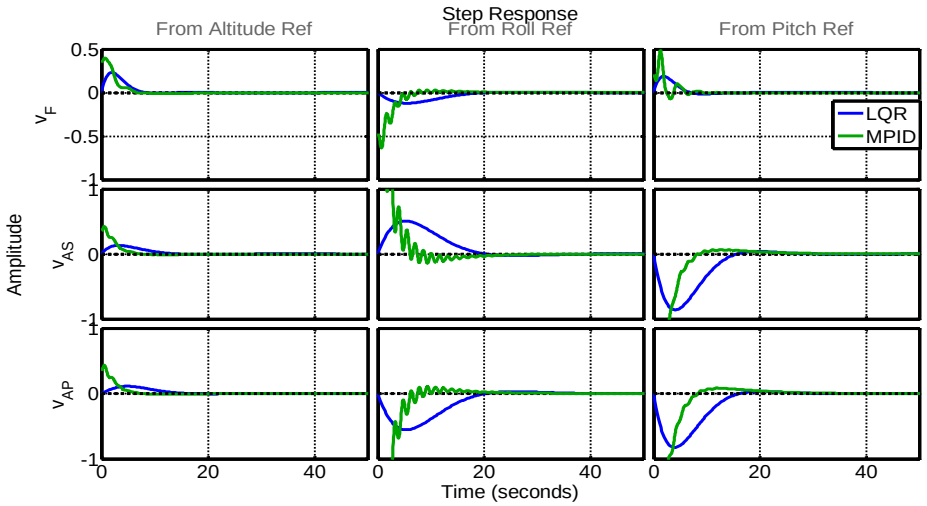

Figure 5-15 - Input Winch Responses to Step command

It can be seen from Figure 5-14 that there is good decoupling in all loops apart from the pitch ref to altitude loop which exhibits a small degree of cross-coupling (<0.3). It is also seen that the settling time response of the MPID and LQR controller are similar with the MPID clearly showing more overshoot. This primarily comes down to the trade-off when tuning the controller. A high proportional gain will lead to a faster response time and high integral action will lead to a reduced settling time. However, increasing integral action comes at the cost of overshoot in the closed loop response. In the MPID case, a higher integral gain is required to bring the response in line with the response of the LQR design.

Figure 5-15 compares the actuator response of each loop to a given step reference command. It is seen that with the LQR method there is low actuation compared to higher actuator activity with the MPID method, as a result of the increased controller gains. The actuator is constrained to a magnitude reel out speed of 1 m/s through a rate limiter. Thus, in this case, the MPID method could be required to reduce the proportional and integral gains to reduce actuator activity at the beginning of the simulation. This will have the adverse effect of increasing the rise time and settling time of the system.

5.13 Simulation and Results

5.13.1 Multivariable Control (With Turbulence)

One of the primary benefits of an airborne system is that its operation is flexible in comparison to conventional wind generation. This means that the system can respond to a change in environmental conditions, for example a measured change in wind speed, and alter the position of the system accordingly. Furthermore, in practice the system will also be subject to external disturbances, the primary cause of which will come from turbulence in the wind. This simulation seeks to demonstrate the performance of each controller to a measured change in wind speed by moving to a new operating altitude. As a result of the measured change in wind speed, the system responds by adjusting the altitude set-point whilst simultaneously ensuring that the roll and pitch of the BAWT are kept constant at 0 and 10 degrees respectively. The wind speed profile considered in this simulation is shown in Figure 5-16 below:

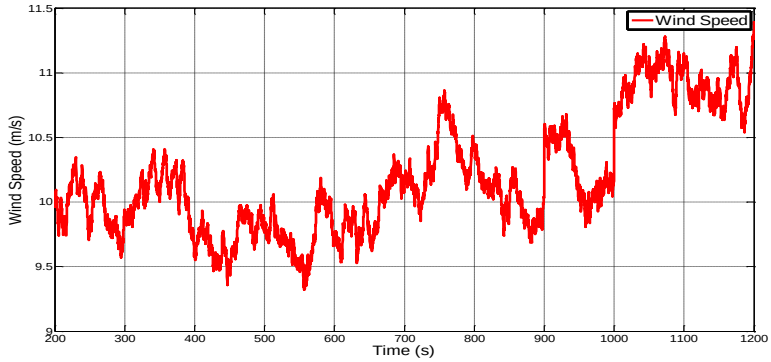

Figure 5-16 - Turbulent wind speed

At $t = 800s$ the system measures a step change in wind speed from 10 m/s to 11 m/s and the altitude is adjusted accordingly from 600m to 610m through a defined ramp input. The time responses of the system, in roll, pitch and altitude and the corresponding actuator response can be seen in Figure 5-17 and Figure 5-18 respectively:

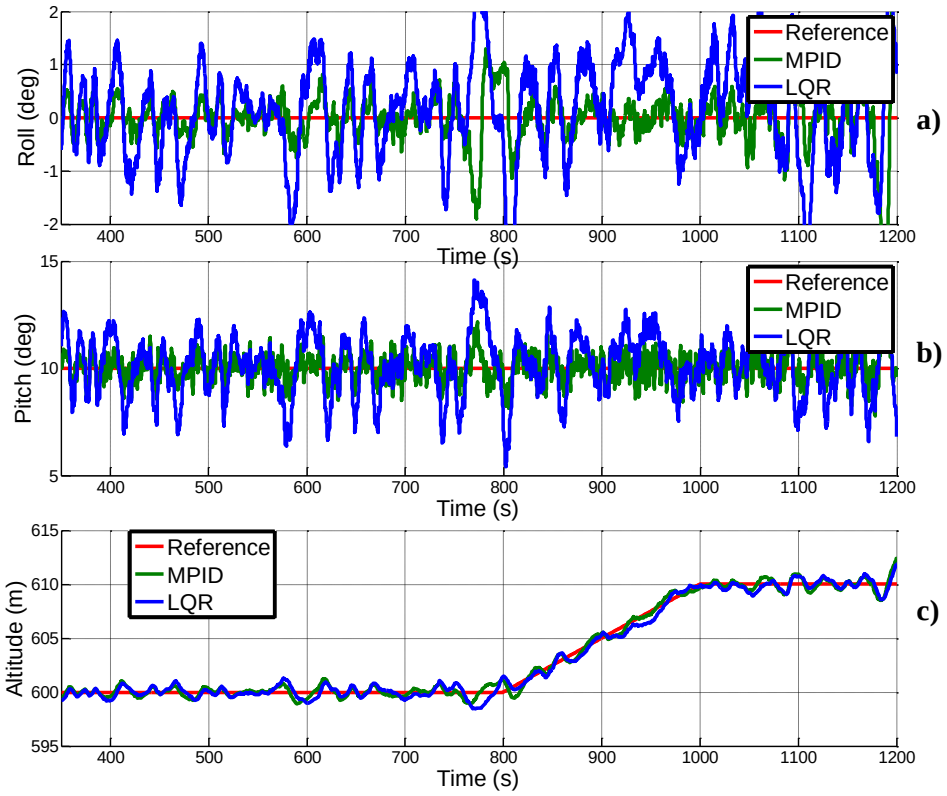

Figure 5-17 – Augmented LQR control with and without gain switching

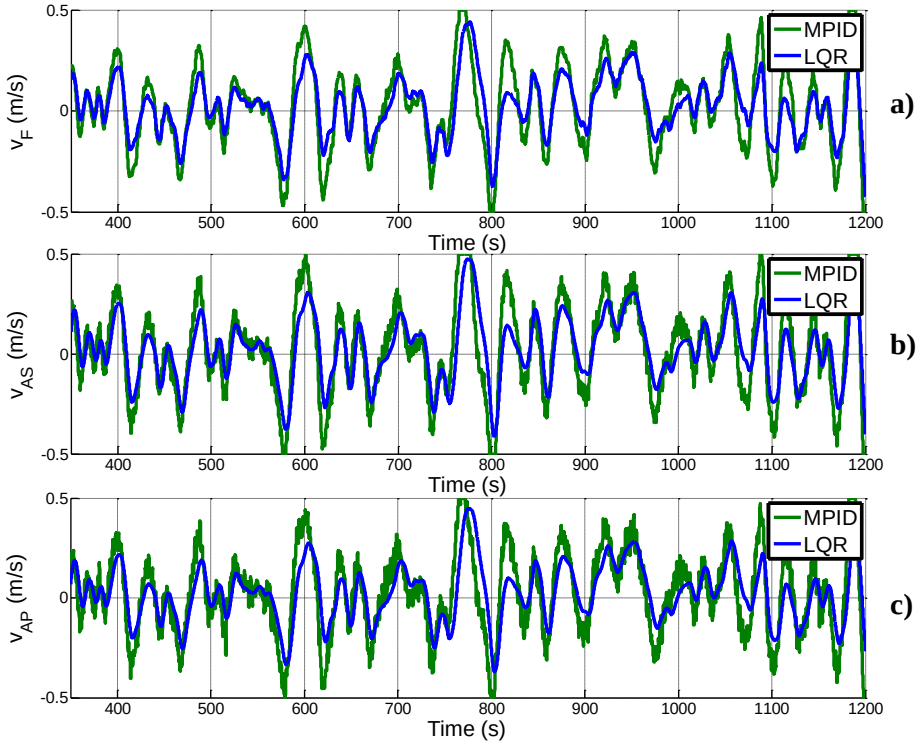

Figure 5-18 - Motor Winch Inputs

In Figure 5-17 the response of the LQR and MPD controllers are compared for turbulent conditions for roll, pitch and altitude. At $t = 800s$ the system follows the desired altitude profile up to a new operating altitude of 610m. As the system moves to a new altitude both the pitch and roll are kept constant at 10 and 0 degrees respectively. The performance of both controllers is similar, with the LQR controller exhibiting slightly more variation in roll and pitch. The corresponding time response of the winch inputs can be seen in Figure 5-18. It is clear that there is less actuator activity with the LQR design compared with the MPID method.

5.14 Comparison between Techniques

Throughout this Chapter the aim has been to compare a non-parametric tuning method termed the multiloop PID (MPID) method with the well-known augmented LQR method. It is clear that from the examples presented, both controllers offer good robustness and disturbance rejection properties at particular operating conditions. For the example shown in Section 4.14.2, the direct comparison of results between the controllers can be seen in Table 5-3:

Table 5-3 - Comparison of Results between Controllers

Tuning Method	**MPID**	**LQR**
Mean Altitude Squared Error (m)	0.24	0.29
Pitch Error Std. Deviation (deg)	0.012	0.025
Roll Error Std. Deviation (deg)	0.009	0.012
Mean Winch Speed – Fore (m/s)	0.16	0.11
Mean Winch Speed – Aft-Starboard (m/s)	0.18	0.13
Mean Winch Speed – Aft-Port (m/s)	0.16	0.11

The performance criterion laid out in Table 5-3 provides a good indicator as to the effectiveness of a particular controller. It is seen that there is a 17% reduction in mean altitude squared error with the MPID compared to the LQR. Similarly, with the MPID design there is a reduction in pitch error and roll error standard deviation of 50% and 25% compared to the LQR method. The mean winch speed is increased in the MPID case, reflecting the improvement in closed loop response i.e. closer set-point of tracking of roll and pitch.

In terms of performance, the MPID method compares favorably to the optimal augmented LQR design. However, there are certain factors that limit the performance of the LQR design in this application. Firstly, the LQR design is far more sensitive to variations in dynamics as it relies on all states being fully measurable. In reality this will be hard to guarantee and as such Kalman filters may be required to compensate for un-measurable states. Furthermore, the consequence of moving to a new operating point state means that some states have to be updated based on current conditions, particularly the unstrectched tether lengths. For instance, a given linearization at a particular wind speed and altitude will correspond to particular trimmed values of unstretched tether lengths. It is therefore difficult to fully update the system for all potential state variations during simulation and as a result some performance may be lost.

In contrast, the MPID method does not rely on full state-feedback and can be quickly designed based on approximate plant inversion at a particular bandwidth frequency. Furthermore, if the plant model is not available it would be possible to design the controller based on simple open loop tests once the physical system has been driven to the trimmed condition. This means that the design could be classed as ‘model-free’, another advantage for real-time tuning and debugging. However, the one major downside of this method is that if

the wrong decoupling bandwidth frequency is chosen it could result in unstable gain matrices. This subsequently means that all decoupling would be lost and the resultant controller will be unstable and ineffective.

This analysis illuminates the broader issues of optimal control design at individual operating conditions and provides insight into the benefits of two linear control design approaches. If employed at the correct bandwidth the MPID method offers a cheap, easy method of deriving the required gains without contending with full state feedback. Although, the closed loop properties of the controller are not guaranteed compared to the LQR design, this method is sufficient to ensure the desired response of the system.

5.15 Conclusion

This chapter has described a multivariable control methodology for a BAWT. Firstly, the operating region of a BAWT was explored and an assessment between wind speed and dynamic performance of the shroud was assessed through a frequency domain analysis. A multivariable control strategy was then designed using two well-known methods; the optimal LQR and multiloop PID (MPID) tuning method. In both cases the multivariable stabilised the plants. Furthermore, to compare the design of the two controllers the principle gains or singular values were used, as these give an indication of the limits of performance for a multivariable system. It was shown that for both controllers there was good disturbance rejection and closed loop tracking. The comparison between the controllers indicated that the MPID design matches the closed loop performance compared of the LQR design. This coupled with the fact that the LQR method is more difficult to tune and highly dependent on state measurements, makes the MPID approach more appealable for low level control design.

6 Optimisation of a BAWT

This chapter seeks to build on the low level multivariable controller derived in the previous chapter, through the investigation of two optimisation methods; Model Predictive and Extremum Seeking control. Each optimisation algorithm is placed within a hierarchical framework, which results in supervisory control over the altitude, pitch and roll of the system. The second stage, or medium level control, is achieved through a state space model predictive controller. A cost function is designed such that low-level system set-points are met under given constraints i.e. constraints on attainable altitude, pitch and roll, which facilitates the operation over a bounded operating envelope. The third stage in the hierarchical framework, termed high level controller, is designed to provide an optimum altitude set-point for the system. This is computed based on an optimisation function that trades off generated power from the rotor against the power consumed by the three winches. This relationship, driven by the co-dependence between wind speed and altitude motivates an extremum seeking approach for altitude set-point derivation. This extremum seeking controller completes the hierarchical framework and feeds into the medium level (MPC) and low level (PID) controller in order to provide a controller structure designed to optimise system performance under certain operating conditions.

6.1 Overview

In this work, the regulation of specific set-points of the shroud through a hierarchical model predictive control scheme is introduced followed by a discussion on how to efficiently compute the optimised altitude set-point within the context of an extremum seeking optimisation problem.

The low-level controller described in Chapter 5 regulates the altitude, pitch and roll of the system to some desired reference value. However, in practice the set-points for the system will be constrained across the operating envelope. These constraints will be enforced by the MPC on the altitude, pitch and roll set-points provided to the low-level controller. This justifies the need to frame the optimisation problem in terms of regulation on altitude, pitch and roll as follows:

- **Altitude regulation**: The desired altitude is bounded within the operational envelope. This is required to ensure that the system does not reach altitudes where loading restrictions become too high.
- **Pitch set-point regulation**: The pitch of the system is constrained within feasible bounds preventing an increased risk of stall.
- **Roll set-point regulation:** The roll of the shroud is always constrained close to zero to prevent adverse moments in yaw on the shroud.

The control architecture of how this is developed is shown in Figure 6-1, which demonstrates how the supervision structure is formulated, linking the roll, pitch and altitude set-points to the lower level control system, previously developed in Chapter 5. A further level of control is included to regulate the optimum altitude of the system. This is described in more detail in Section 6.8.

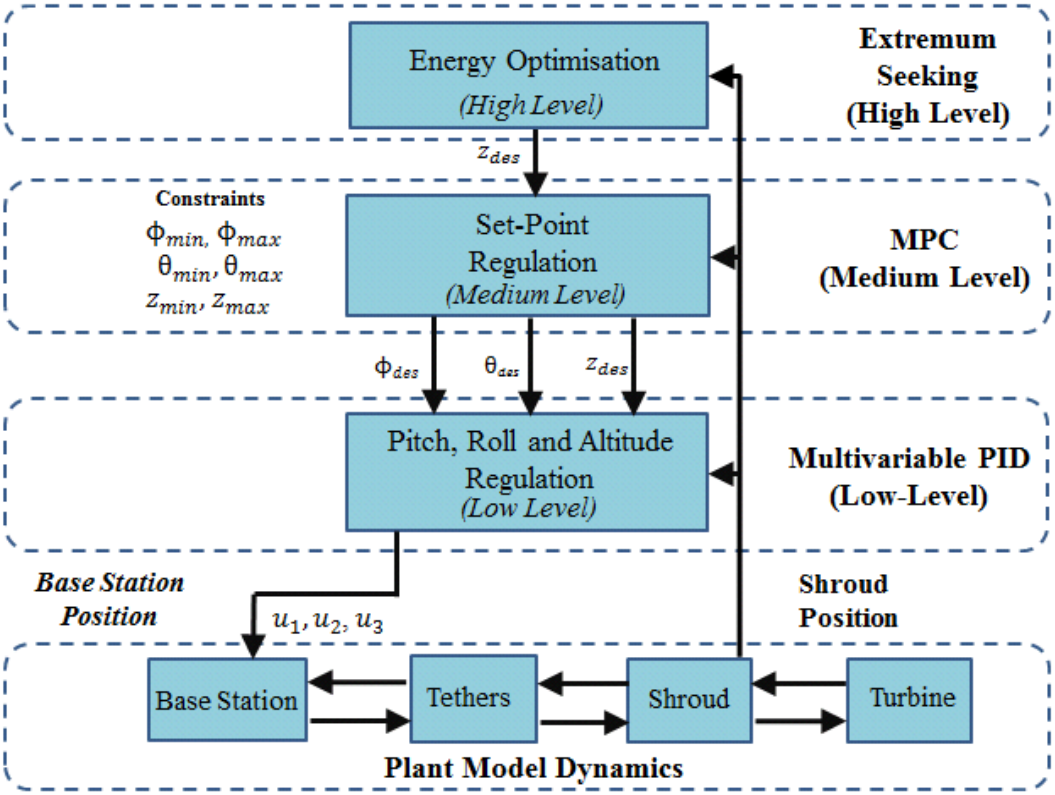

Figure 6-1 - Proposed Hierarchical Control Scheme for BAWT

Figure 6-1, illustrates how the hierarchical control structure is divided into three parts:

- Low Level Controller (PID) – The underlying plant dynamics and low-level control strategy here was developed in Chapter 5. The result was a low level PID multivariable controller that regulates the roll, pitch and altitude set-points of the system.
- Medium Level Controller (MPC) – This supervisor consists of an MPC formulation that regulates the set-points to the low-level controller. These set-points are computed under operational constraints defined by the systems operating envelope i.e. constraint on attainable altitude between minimum and maximum bounds (z_{min}, z_{max}), limits on attainable pitch to prevent stall ($\theta_{min}, \theta_{max}$), limits on attainable roll to prevent an adverse yaw moment ($\phi_{min,}\ \phi_{max}$). The MPC design is given in Sections 6.3 – 6.6.

- High Level Controller (ESC) – This controller computes an optimal altitude set-point based on the solution to an online optimisation problem computed in terms of net power from the system. This performance is given in terms of power optimisation with an argument provided on the trade-offs between choosing an optimal altitude (z_{des}) that both maximises power and loads on the system. The ESC design is given in Sections 6.8.

6.2 Optimal Altitude Regulation

Choosing the altitude of the system will be dictated by a trade-off of two key design drivers on system performance namely; energy maximisation and load alleviation. Energy maximisation will be dictated primarily by the wind speed, which is a function of altitude. This relationship is defined as wind shear, a concept introduced in Chapter 3. The underlying mathematical model is provided again in equation (6-1) below:

$$v_w = v_{ref} \frac{\log(\frac{z_{alt}}{z_0})}{\log(\frac{z_r}{z_0})} \tag{6-1}$$

The actual wind speed v_w can be computed as a function of the current altitude z_{alt}. Therefore, the effect from wind shear will vary on the choice of reference altitude (z_r) and wind speed (v_{ref}). This is shown in Figure 6-2, where v_w is computed for a range of v_{ref}, from 5 to 16 m/s, in steps of 1 m/s at a reference altitude of $z_{\mathrm{ref}} = 300m$..

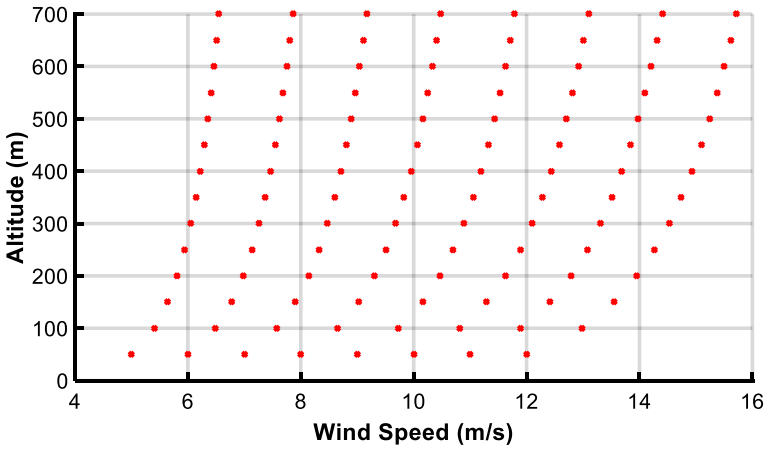

Figure 6-2 - Wind Speed vs Altitude

Figure 6-2 demonstrates the dependence altitude has on wind speed i.e. as altitude increases so does the computed wind speed. This motivates the primary design driver behind airborne wind energy systems namely; the design of light flexible systems that takes advantage of high wind speeds at high altitudes in order to increase energy capture for a site.

Furthermore, as wind speed increases with altitude, so too does the effect on energy capture over time. This is dictated by the Weibull distribution which provides a probability distribution of wind speed for a given site [122]. The Weibull distribution is defined in Equation (6-2):

$$p(U) = \left(\frac{k}{C}\right)\left(\frac{U}{C}\right)^{-1} e^{-\left(\frac{U}{C}\right)^{k}} \tag{6-2}$$

where, $p(U)$ is the probability of a given wind speed, k is the shape parameter and C is the scale parameter. Both the shape parameter and scale parameter can be related to a given site or location where the system will be operating for an extended period of time.

Figure 6-3, shows the Weibull distribution clearly for two cases. The first case is determined with a mean wind speed of 10 m/s ($v_{\text{ref}} = 10$) at a reference altitude of $z_{ref} = 100$m. The mean wind speed at an altitude of 600m ($z_{op} = 600$) is then computed by substituting in the

relevant values to equation (6-1). Note in this example a surface roughness of $z_0 = 0.05$ is assumed as it is reflective of a typical wind turbine site (Table 3-1). Substituting these mean wind speeds for U in Equation (6-2) will give the appropriate Weibull distributions at an altitude of 100m and 600m respectively. In each case the Weibull distribution was calculated with value of $k = 2$ and $C = 11.2$ which are also typical conditions associated with a wind turbine site [122]. The comparison can be seen in Figure 6-3:

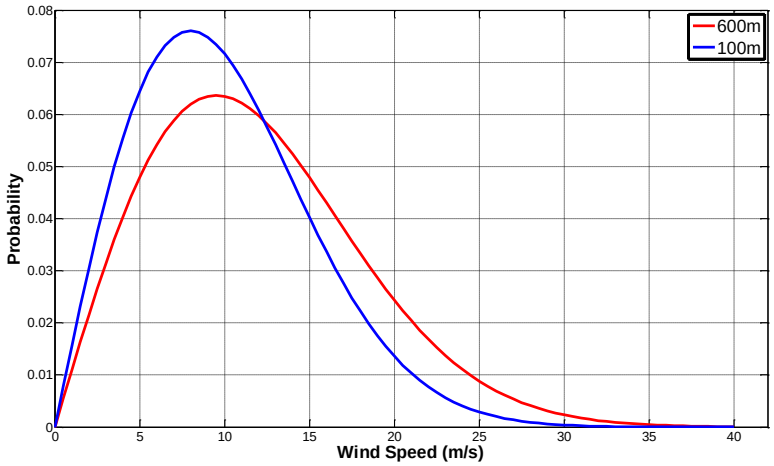

Figure 6-3 - Weibull Distribution at different altitudes

Figure 6-3 shows the Weibull distribution, with a higher probability of larger wind speeds (>15m/s) at an altitude of 600m compared with 100m. This could result in increased energy capture at higher altitudes for higher rated wind speeds.

However, in reality there will be a limitation on what altitude is attainable. This is primarily driven by tether losses and aerodynamic losses in the system at higher wind speeds. These tether losses can be approximated by the lift on the shroud as shown in equation (3-19), formulated in Chapter 3 and expressed here again as:

$$F_z^{aero} = \frac{1}{2}\rho_{air} {v_{app}}^2 A_{throat} C_L \tag{6-3}$$

The subsequent effect of combining equations (6-3) and (6-1), where $v_{app} = v_{w},$, calculated from a reference wind speed of $v_{\mathrm{ref}} = 10$ at a reference altitude of $z_{ref} = 100$m, is shown in Figure 6-4 which demonstrates that as altitude increases, the subsequent tether load increases as a function of both altitude and wind speed.

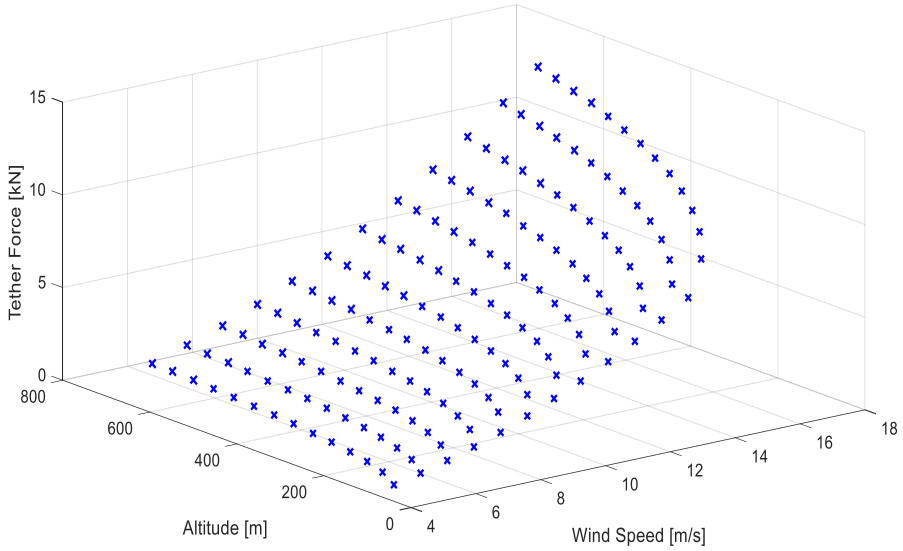

Figure 6-4 - Estimated Tether Tension [kN] as a function of Altitude [m] and Wind Speed [m/s]

It can be seen from Figure 6-4, that as both wind speed and altitude so too does the applied tether tension on the shroud. Therefore this motivates the one of the key optimisation problems for a BAWT namely; how to regulate the altitude of the system without affecting loading performance in addition to ensuring that bounds on attainable roll and pitch of the system are not compromised. The answer to this issue motivates the layered, hierarchical control design architecture developed within this chapter. Firstly a MPC medium level controller is developed in Section 6.3 and then a high level ESC is designed in Section 6.8 that 'seeks' to find the optimum altitude to deal with the issue presented in Figure 6-4.

6.3 MPC Model Design

The MPC hierarchical controller is designed to fit within the overall hierarchical framework defined in Figure 6-1. The main motivation behind employing MPC is that it allows efficient regulation of set-points, delivered to the low level controller developed in Chapter 5.

An unconstrained approach could be taken which would mean the development of an optimal cost function that computes the optimal set-point (without constraints) based on a demanded reference. If the BAWT has a significant range of allowable operating altitudes, pitch angles and roll angles then this approach could be justified. However, in practice there will be limitations on altitude (loading), pitch (aerodynamic stall) and roll (yawing moment) which will ultimately place constraints on the operational envelope.

To derive an appropriate MPC formulation, the continuous time model developed in Chapter 5 must be extended. First the model is combined to form a closed loop representation of the system i.e. with the inclusion of the controller dynamics. Here the linearization is undertaken at 12 m/s, with the trim conditions defined according to Table 1 below. Note that as before, the linearization is done within MATLAB using the Simulink toolbox.

Table 6-1 - Trim Conditions for State Space MPC Model

Trim Conditions	**Values**
z_{alt} (m)	600
θ (deg)	10
ϕ (deg)	0

The linearized BAWT model is represented as

$$\dot{x}_p(t) = A_p x_p(t) + B_p u_p(t) \tag{6-4}$$

$$y_p(t) = C_p x_p(t) \tag{6-5}$$

Note that the subscript p now represents the plant dynamics.

The state vector, $x_p(t)$ is the plant state vector defined as $x_p = [l_F^u, l_{AS}^u, l_{AP}^u, A_F, A_{AS}, A_{AP}, p, \phi, q, \theta, r, \psi, w, z, v, y, u, x]^T$, $u(t)$ is the motor winch speeds where $u(t) = [u_1, u_2, u_3]^T$ and as before, u_1, u_2 and u_3 are the three desired motor winch speeds of the fore, aft starboard and aft port motors respectively. Similarly, A_p, B_p and C_p are the linearised plant matrices at the given trim condition defined in Table 6-1. ***Note*** there is no D matrix indicating no feedforward term.

The low level PID controller, derived from Chapter 5 can also be represented in continuous state space as follows

$$\dot{x}_c(t) = A_c x_c(t) + B_c u_c(t) \tag{6-6}$$

$$y_c(t) = C_c x_c(t) \tag{6-7}$$

where, A_c, B_c and C_c are the PID state space matrices. Note in this formulation, the MPID gains are chosen, based on equation's (5-38) and (5-39), with the subscript c denoting the controller dynamics. The internal state space vector of the controller $x(t)$, represents the internal state of the PID controller. $u_c(t)$ represents the model errors from desired reference points in altitude, pitch and roll and can be expressed as

$$u_c(t) = \begin{bmatrix} e_z \\ e_\phi \\ e_\theta \end{bmatrix} = \begin{bmatrix} r_z - z \\ r_\phi - \phi \\ r_\theta - \theta \end{bmatrix} \tag{6-8}$$

where, e_z is the altitude error (from reference to measured altitude), e_ϕ is the roll error (from reference to measured roll) and e_θ is the pitch error (from reference to measured pitch). The reference values are defined as r_z, reference altitude set-point, r_ϕ reference roll set-point

and r_θ reference pitch set-point. The output of the controller is equal to the input of the plant that is, $y_c(t) = u_p(t)$, therefore equations (6-4) - (6-7) can be combined into a new state space system with $x(t)$ having two states, comprised from both the controller and plane, $[x_c\ x_p]^T$ and an input state $u(t)$ which is now comprised of the desired roll, pitch and altitude reference values $u(t) = [r_z\ r_\phi\ r_\theta]^T$. The final state space matrices used in the internal model of the MPC are given by:

$$A_{tot} = \begin{bmatrix} A_c & -B_c C_p \\ B_p C_c & A_p \end{bmatrix}, \quad B_{tot} = \begin{bmatrix} B_c \\ 0 \end{bmatrix}$$

$$C_{tot} = \begin{bmatrix} 0 & C_p \end{bmatrix}$$

And the final state model, in continuous time, is given as follows:

$$\dot{x}(t) = A_{tot}x(t) + B_{tot}u(t) \tag{6-9}$$

$$y(t) = C_{tot}x(t) \tag{6-10}$$

Evaluating (6-9) and (6-10) in terms of the trim condition defined in Table 1 results in the following state space equation:

$$A_{tot} = \begin{bmatrix}
0 & 0 & 0 & 0 & 0 & 0 & 0 & 0 & 0 & 0 & 0.1823 & 0 & -1.4646 & 0 & 0 & 0 & -0.2528 & 0 & 0 & 0 & 0 \\
0 & 0 & 0 & 0 & 0 & 0 & 0 & 0 & 0 & 0 & -2.1626 & 0 & 1.3711 & 0 & 0 & 0 & -0.1480 & 0 & 0 & 0 & 0 \\
0 & 0 & 0 & 0 & 0 & 0 & 0 & 0 & 0 & 0 & 2.300 & 0 & 1.4053 & 0 & 0 & 0 & -0.1191 & 0 & 0 & 0 & 0 \\
0 & 0 & 0 & 10 & 0 & 0 & 0 & 0 & 0 & 0 & 0 & 0 & 0 & 0 & 0 & 0 & 0 & 0 & 0 & 0 & 0 \\
0 & 0 & 0 & 0 & 10 & 0 & 0 & 0 & 0 & 0 & 0 & 0 & 0 & 0 & 0 & 0 & 0 & 0 & 0 & 0 & 0 \\
0 & 0 & 0 & 0 & 0 & 10 & 0 & 0 & 0 & 0 & 0 & 0 & 0 & 0 & 0 & 0 & 0 & 0 & 0 & 0 & 0 \\
0 & 0 & 0 & -10 & 0 & 0 & 0 & 0 & 0 & 0 & 0 & 0 & 0 & 0 & 0 & 0 & 0 & 0 & 0 & 0 & 1 \\
0 & 0 & 0 & 0 & -10 & 0 & 0 & 0 & 0 & 0 & 0 & 0 & 0 & 0 & 0 & 0 & 0 & 0 & 0 & 1 & 0 \\
0 & 0 & 0 & 0 & 0 & -10 & 0 & 0 & 0 & 0 & 0 & 0 & 0 & 0 & 0 & 0 & 0 & 0 & 1 & 0 & 0 \\
-0.02 & 1.81 & -1.84 & 0 & 0 & 0 & 0 & -20.7 & 0 & -0.13 & 0 & 8.5 & 0 & 0.05 & 0.08 & -0.01 & -0.01 & 0.02 & 0 & 0 & 0 \\
0 & 0 & 0 & 0 & 0 & 0 & 1 & 0 & 0 & 0 & 0.29 & 0 & 0 & 0 & 0 & 0 & 0 & 0 & 0 & 0 & 0 \\
0.59 & -1.28 & -1.28 & 0 & 0 & 0 & 0 & 0.04 & -0.45 & -17.8 & -0.19 & -0.33 & 0.25 & 1.82 & 0 & -0.04 & 0.03 & 0.75 & 0 & 0 & 0 \\
0 & 0 & 0 & 0 & 0 & 0 & 0 & 0 & 1 & 0 & 0 & 0 & 0 & 0 & 0 & 0 & 0 & 0 & 0 & 0 & 0 \\
0.02 & -0.15 & 0.1 & 0 & 0 & 0 & 0 & 1.15 & 0.19 & 0.15 & -0.45 & -1.06 & 0 & 0.03 & -0.07 & 0 & 0 & 0.01 & 0 & 0 & 0 \\
0 & 0 & 0 & 0 & 0 & 0 & 0 & 0 & 0 & 0 & 1 & 0 & 0 & 0 & 0 & 0 & 0 & 0 & 0 & 0 & 0 \\
4.8 & 4.9 & 4.9 & 0 & 0 & 0 & 0 & 1.59 & 0 & 51.65 & 0 & 0.11 & -2.15 & -13.5 & 0 & 0.3 & -1.28 & -5.4 & 0 & 0 & 0 \\
0 & 0 & 0 & 0 & 0 & 0 & 0 & 0 & 0 & 0 & 0 & 0 & 1 & 0 & 0 & 0 & -0.28 & 0 & 0 & 0 & 0 \\
-0.1 & -0.09 & -0.12 & 0 & 0 & 0 & 0 & -4.2 & 0 & -0.78 & 0 & -13.9 & 0 & 0.29 & -1.85 & -0.02 & 0 & 0.12 & 0 & 0 & 0 \\
0 & 0 & 0 & 0 & 0 & 0 & 0 & 0 & 0 & 0 & 0 & 0 & 0 & 0 & 1 & 0 & 0 & 0 & 0 & 0 & 0 \\
0.46 & 0.48 & 0.48 & 0 & 0 & 0 & 0 & 0.2 & 0 & 8.14 & 0 & 0.25 & 0.35 & -1.3 & 0 & 0.03 & -0.5 & -0.55 & 0 & 0 & 0 \\
0 & 0 & 0 & 0 & 0 & 0 & 0 & 0 & 0 & 0 & 0 & 0 & 0.28 & 0 & 0 & 0 & 1 & 0 & 0 & 0 & 0
\end{bmatrix}$$

$$B_{tot} = \begin{bmatrix} 1.4646 & -1.3711 & -1.4053 & 0 & 0 & 0 & 0 & 0 & 0 & 0 & 0 & 0 & 0 & 0 & 0 & 0 & 0 & 0 & 0 & 0 \\ -0.1823 & 2.1626 & -2.300 & 0 & 0 & 0 & 0 & 0 & 0 & 0 & 0 & 0 & 0 & 0 & 0 & 0 & 0 & 0 & 0 & 0 \\ 0.2528 & 0.1480 & 0.1191 & 0 & 0 & 0 & 0 & 0 & 0 & 0 & 0 & 0 & 0 & 0 & 0 & 0 & 0 & 0 & 0 & 0 \end{bmatrix}^T$$

$$C_{tot} = \begin{bmatrix} 0 & 0 & 0 & 0 & 0 & 0 & 0 & 0 & 0 & 0 & 0 & 0 & 0 & 0 & 0 & 0 & 1 & 0 & 0 & 0 & 0 \\ 0 & 0 & 0 & 0 & 0 & 0 & 0 & 1 & 0 & 0 & 0 & 0 & 0 & 0 & 0 & 0 & 0 & 0 & 0 & 0 & 0 \\ 0 & 0 & 0 & 0 & 0 & 0 & 0 & 0 & 0 & 1 & 0 & 0 & 0 & 0 & 0 & 0 & 0 & 0 & 0 & 0 & 0 \end{bmatrix}$$

For implementation with MPC, the state space model must be discretised. Here, discretization is done using the MATLAB command c2d, which implements an underlying zero order hold algorithm to convert the model in continuous time to discrete time. A discretized signal for both the input and output, as a function of time step k is achieved by holding the input constant over a defined sample time and recording the resultant output. This is represented in more detail in Figure 6-5 below:

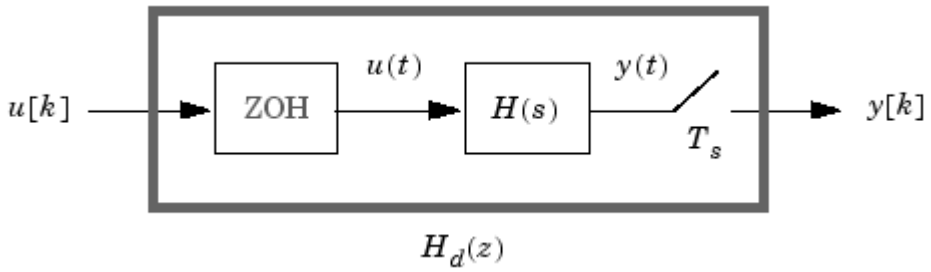

Figure 6-5 - Zero hold model for conversion to discrete time [123]

In this case the discretization is done at a sampling time of Ts = 0.1.

The combined state space model (including both plant and controller) described in (6-9) and (6-10) in continuous time is converted to discrete time using the method described above and now defined as follows:

$$x_{k+1} = Ax_k + Bu_k \tag{6-11}$$

$$y_k = Cx_k \tag{6-12}$$

where, A, B and C now represent the combined dynamics of the low level controller and plant. Note that $u_k = r_k$, where r_k is now the demanded reference values for the low level controller i.e. set-points in altitude, roll and pitch.

6.3.1.1 Augmented Model

So far a state model has been created that defines the system in terms of an input reference vector u_k to demanded outputs y_k. Within MPC the cost function to be optimised will only be as good as the formulation of the problem defined within it. In order to ensure offset free tracking, the state space model is augmented to define the input as the change of input Δu_k rather than the actual input u_k. This is done such that the steady state output y_k can reach the desired reference r_k when there is no change in reference i.e. $\Delta u_k = 0$. Knowing that Δu_k is the difference between the current control input and the previous one ($\Delta u_k = u_k - u_{k-1}$) and combining with (6-11) and (6-12) an augmented state space representation is defined as a function of Δu_k rather than u_k:

$$\begin{bmatrix} x_{k+1} \\ u_k \end{bmatrix} = \underbrace{\begin{bmatrix} A & B \\ 0 & I \end{bmatrix}}_{A} \underbrace{\begin{bmatrix} x_k \\ u_{k-1} \end{bmatrix}}_{x_k} + \underbrace{\begin{bmatrix} B \\ I \end{bmatrix}}_{B} \underbrace{\Delta u_k}_{u_k} \tag{6-13}$$

$$y_k = \underbrace{\begin{bmatrix} C & 0 \end{bmatrix}}_{C} \underbrace{\begin{bmatrix} x_k \\ u_k \end{bmatrix}}_{x_k} + \eta_k \tag{6-14}$$

Note the full state matrices are now defined as A, B and C with state ${x_k}^T$ and input ${u_k}^T$ now being the increments of the desired value.

6.3.1.2 Cost Function

In order to create the optimal set-point, MPC must look ahead or predict a given number of time steps into the future in order to inform both the current position and the next optimal step. This is done through recursive prediction equations. Combining (6-13) and (6-14) gives the *n*-step ahead predictions resulting in:

$$x_{k+n} = A^n x_k + A^{n-1} B\Delta u_k + A^{n-2} B\Delta u_{k+1} + \cdots + B\Delta u_{k+n-1} \tag{6-15}$$

$$y_{k+n} = C[A^n x_k + A^{n-1} B\Delta u_k + A^{n-2} B\Delta u_{k+1} + \cdots + B\Delta u_{k+n-1}] \tag{6-16}$$

This can then be grouped to form a vector of future predictions up to horizon n_y which allows for the definition of appropriate prediction models. These prediction models are derived from equations (6-15) and (6-16) and denoted as

$$X = P_{xx}x_k + H_x\Delta U \tag{6-17}$$

$$Y = Fx_k + H\Delta U \tag{6-18}$$

where,

$$X = \begin{bmatrix} x_{k+1} \\ x_{k+2} \\ x_{k+3} \\ . \\ . \\ x_{k+n_y} \end{bmatrix}, \quad P_{xx} = \begin{bmatrix} A \\ A^2 \\ A^3 \\ . \\ . \\ A^{n_y} \end{bmatrix} H_x = \begin{bmatrix} B & 0 & 0 \\ AB & B & 0 \\ A^2B & AB & B \\ . & . & . \\ . & . & . \\ A^{n_y-1}B & A^{n_y-2}B & A^{n_y-3}B \end{bmatrix}, \Delta U = \begin{bmatrix} \Delta u_k \\ \Delta u_{k+1} \\ \Delta u_{k+2} \\ . \\ . \\ \Delta u_{k+n_y-n} \end{bmatrix}$$

$$Y = \begin{bmatrix} y_{k+1} \\ y_{k+2} \\ y_{k+3} \\ . \\ . \\ y_{k+n_y} \end{bmatrix} F = \begin{bmatrix} CA \\ CA^2 \\ CA^3 \\ . \\ . \\ CA^{n_y} \end{bmatrix} H = \begin{bmatrix} CB & 0 & 0 \\ CAB & CB & 0 \\ CA^2B & CAB & CB \\ . & . & . \\ . & . & . \\ CA^{n_y-1}B & CA^{n_y-2}B & CA^{n_y-3}B \end{bmatrix}$$

The main control law for generalised predictive control is given by the minimisation of the state space realisation given in (6-13) and (6-14) to compute an optimal reference in altitude, pitch and roll for the low level controller. The cost function shown for the BAWT is given below:

$$J = \sum_{i=1}^{n_y} \|r_{k+i} - y_{k+i}\|^2{}_W + \sum_{i=1}^{n_u-1} \|\Delta u_{k+i}\|^2{}_R \tag{6-19}$$

where, n_y is the prediction horizon, n_u is the control horizon, r_{k+i} is the reference vector $r_{k+i} = [\, r_z \quad r_\phi \quad r_\theta]$, y_{k+i} is the output in altitude, roll and pitch from the plant, and Δu_{k+i} is the change in demanded reference in altitude, pitch and roll to the low level controller. W and R are two weighting matrices used to tune the behaviour of the cost function.

The control objective can be expressed in terms of the prediction matrices (6-17) and (6-18) as follows [124]:

$$J = \big(R_s - Fx(k_i)\big)^T W\big(R_s - Fx(k_i)\big) - 2\Delta U^T H^T\big(R_s - Fx(k_i)\big) + \Delta U^T(H^T H + R)\Delta U \tag{6-20}$$

where, R_s is the reference vector $r = [\, r_z \quad r_\phi \quad r_\theta]$ defined up to the prediction horizon n_y as

$$R_s = r_{3\times n_y}$$

W is the weighting matrix on the relative error between reference and output:

$$W = \begin{bmatrix} W1 & 0 & 0 \\ 0 & W2 & 0 \\ 0 & 0 & W3 \end{bmatrix}$$

And R is a weighting matrix on the difference of the control input defined as a function of the control horizon n_u and a tuneable parameter r_w described below.

$$R = r_w I_{\mathrm{n}_u \times \mathrm{n}_u}$$

Note in this work r_w is tuned equal to 1 since the admissible output to the PID controller should be dominated by the output i.e. the delivered set-point.

Equation (6-17), presents an MPC cost function that, when minimised, derives suitable references to the low-level controller in roll, pitch and altitude. The solution of this cost function can be solved in two ways. An optimal solution can be found analytically [97]. This could be done to compute the reference values free from constraints. This would only make sense if the BAWT system had an infinitely large operating envelope where there are no restrictions on a specific output. This is clearly not the case in practice. Therefore, the solution of this cost function is computed as a function of constraints (described in Section 6.4), which can be solved using a quadratic programming solver [124]. In this work the MATLAB MPC toolbox was used to provide the desired solution [125].

6.4
6.4 Constraints within MPC

One key aspects of MPC is that there is the possibility of adding constraints on the input and outputs of the system. In the BAWT case, the roll, pitch and altitude of the system set-points

are controlled such that the desired reference values can be met within the feasible bounds of the operational envelope. Limits can be placed on the three variables as follows:

- Altitude – Constrain allowable maximum and minimum altitude to prevent excessive tether loading
- Pitch – Constrain allowable maximum and minimum pitch to prevent aerodynamic stall
- Roll – Constrain allowable maximum and minimum roll to prevent adverse yaw moments

This motivates the requirement of adding constraints on the output i.e. absolute value and rate of change such that these operational constraints can be enforced. In practice this means placing constraints as follows:

$$y^{min} \leq y(k) \leq y^{max} \tag{6-21}$$

Where the limits are given for the following outputs as:

$$\left[{y_{alt}}^{min}, {y_{roll}}^{min}, {y_{pitch}}^{min}\right]$$

$$\left[{y_{alt}}^{max}, {y_{roll}}^{max}, {y_{pitch}}^{max}\right]$$

The output constraints can be expressed in terms of ΔU as:

$$\mathrm{Y}^{min} \leq Fx(k_i) + \phi\Delta U \leq \mathrm{Y}^{max} \tag{6-22}$$

Therefore the model predictive control scheme in the presence of hard constraints can be proposed as finding ΔU that minimises equation (6-20).

Subject to the inequality constraints

$$[M_1]\Delta U \leq [N_1] \tag{6-23}$$

where the data matrices are

$$\mathrm{M}_1 = \begin{bmatrix} -H \\ H \end{bmatrix} ; \mathrm{N}_1 = \begin{bmatrix} -\mathrm{Y}^{min} + Fx(k_i) \\ \mathrm{Y}^{max} - Fx(k_i) \end{bmatrix}$$

The matrix $H^T H + R$ is the Hessian matrix and assumed to be positive definite. As the cost function is quadratic and the constraints are linear, the problem of finding the optimal predictive control move becomes one of solving a standard quadratic programming problem

6.5
6.5 Tuning and Controller Stability

The tuning and stability of the system under the proposed hierarchical framework will now be assessed. Firstly, the tuning parameters of the controller will be evaluated to determine what impact they have on system performance and how efficiently tuning the gains leads to the desired closed loop behaviour. Then a discussion into the stability of the controller for a chosen operating point will be given.

6.5.1 Tuning

The performance of the supervisory MPC controller is based on the accuracy of the internal model in relation to the plant and the three main tuning parameters W, n_y and n_u which define the output weighting, prediction horizon and control horizon respectively.

6.5.1.1 Prediction Horizon n_y

The horizon n_y defines how many steps ahead into the future the model should look. Typically increasing n_y generally enhances performance and leads to less aggressive control action but may result in an insufficient computation time.

6.5.1.2 Control Horizon n_u

It is always the case that during the optimisation problem $n_u \leq n_y$. That is the limit of the prediction is placed on the prediction horizon n_y and not the number of control moves available defined by n_u. Usually n_u should be large which ensures better closed loop performance.

6.5.1.3 Output Weighting W

The choice of output weighting directly influences how important tracking the reference is i.e. the importance of tracking a specific loop (altitude, roll or pitch). However, the control weighting can be of little influence if the optimisation problem is dominated by the control error. To understand the effect in more detail a brief tuning process is followed to achieve the desired closed loop behaviour from the MPC controller.

6.5.2 Tuning of MPC Controller

The tuning of the MPC controller comes down to a choice between constraint satisfaction and closed loop performance. For the proposed controller outlined here, the results for trim condition presented in table Table 6-1. The resultant closed loop state space matrices, are given in (6-9) and (6-10). In this case, the hierarchical MPC was implemented using the MATLAB MPC toolbox [126]. A snapshot of the model is shown in Figure 6-6:

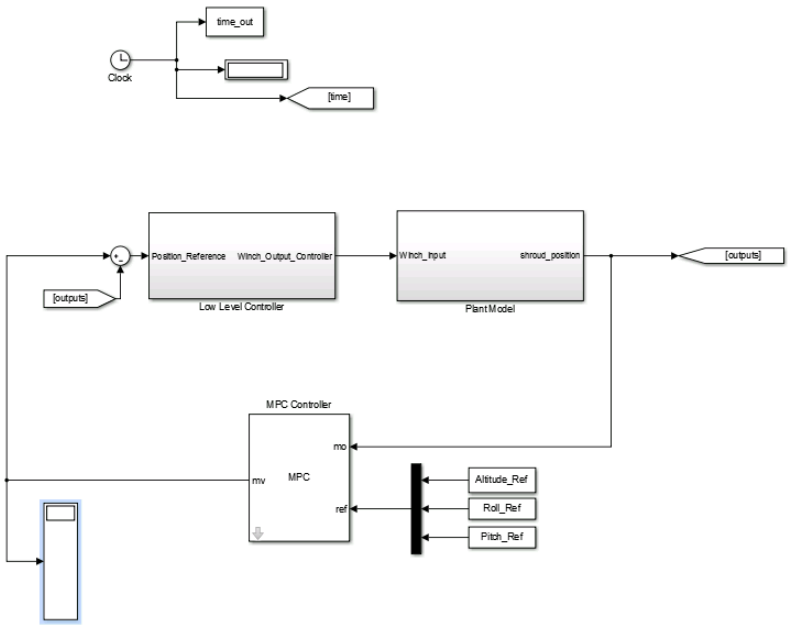

Figure 6-6 - MPC Hierarchical State Space Model driving low level controller

In order to determine appropriate tuning parameters n_y, n_u, and W, the tuning procedure outlined in Figure 6-7 as follows:

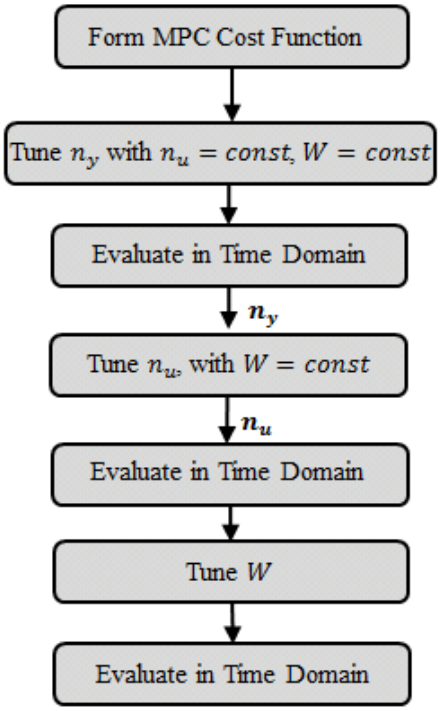

Figure 6-7 - Tuning Procedure for Hierarchical MPC

First, a suitable cost function is formed such that the outputs in roll, pitch and altitude can be independently regulated. After this has been formulated, equation (6-20), the prediction horizon is then tuned. This is carried out by holding the control and weighting function at a constant value and sweeping the prediction horizon until the desired response is obtained. Once the prediction horizon is found (chosen based off evaluation of the resultant time trace), the control prediction horizon is then varied to investigate if any increasing this improves the response. Note that an improved response is defined by a decrease in the rise time of the closed loop step response. Finally, the weighting function is evaluated with the prediction and control horizon fixed to the values found in the earlier iteration. Again, inspecting the resultant time traces is sufficient to determine the response of the system. The tuning values chosen are given according to Table 6-2 below:

Parameters	**Prediction Horizon Tuning (Stage 1)**			**Control Horizon Tuning (Stage 2)**		**Weight Tuning (Stage 3)**		
	Test 1	Test 2	Test 3	Test 4	Test 5	Test 6	Test 7	Test 8
n_y	10	40	80	10	10	10	10	10
n_u	2	2	2	4	8	4	4	4
$W1$(Altitude)	1	1	1	1	1	10	5	1
$W2$(Roll)	1	1	1	1	1	4	1	0.3
$W3$(Pitch)	1	1	1	1	1	6	3	0.7

Table 6-2 – Tuning Parameters for Hierarchical MPC

Table 6-2, shows the three different tuning scenarios undertaken in order to derive an appropriate tuning for implementation within the hierarchical MPC structure. The results are presented in the subsequent sections below:

6.5.2.1 Tuning of prediction horizon

The prediction horizon was varied according to Test 1,2 and 3 defined in Table 6-2. The result is shown in Figure 6-8 below. It can be seen that at a low prediction horizon the step response in roll and pitch is improved. As the prediction horizon is increased further, from $n_y = 40$ to $n_y = 80$, no further improvement is observed. Therefore, a prediction horizon of $n_y = 10$ is chosen.

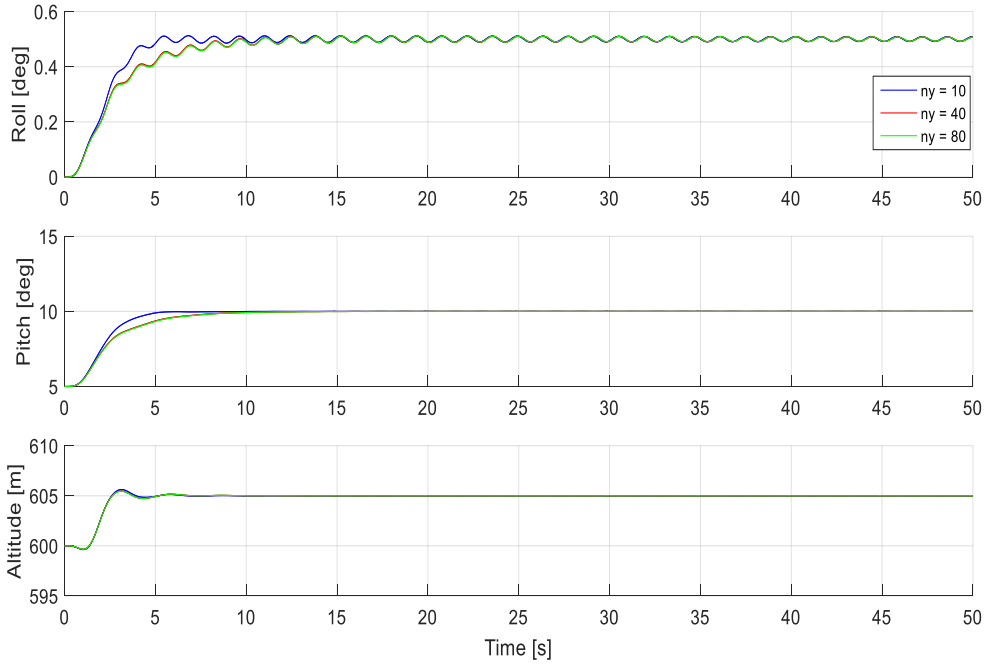

Figure 6-8 - MPC Tuning of ny

6.5.2.2 Tuning of control horizon

Similarly, the tuning of the control horizon is defined according to Test 4 and 5 (Table 6-2). With a chosen prediction horizon of $n_y = 10$ the difference in varying the control prediction horizon is shown in Figure 6-9. It is observed that there is negligible difference from increasing the control horizon from $n_u = 4$ up to $n_u = 8$, therefore a control prediction horizon of $n_u = 4$ is chosen.

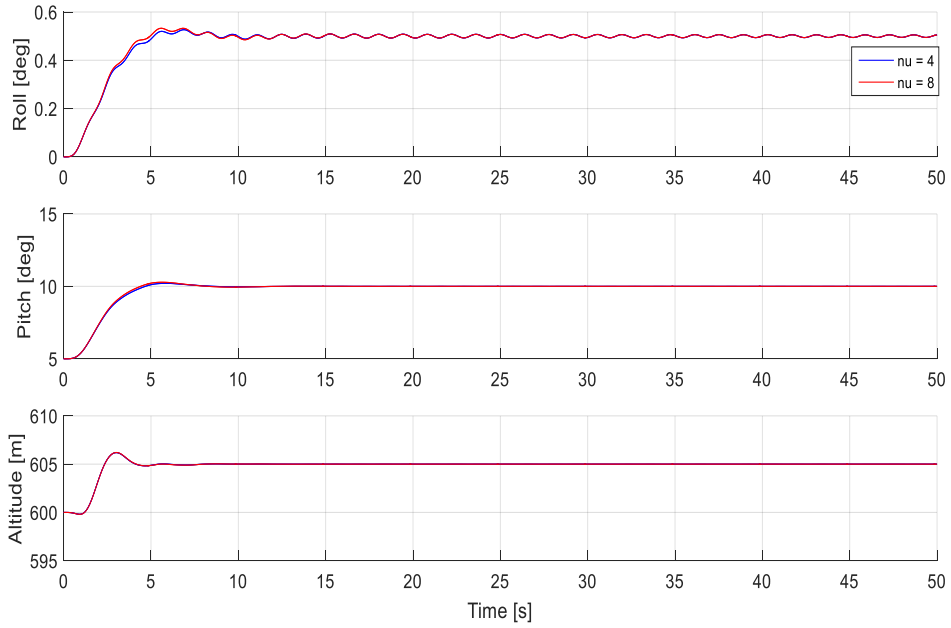

Figure 6-9 - MPC Tuning of nu

6.5.2.3 Tuning of applied weights

Finally, the performance of different applied weights is assessed according to Tests 6,7 and 8 (Table 6-2). In this case, three different sets of weights are applied shown in blue, red and green. It is observed from Figure 6-10, that the closed loop response is best achieved using the lower combination of weights. However, although the performance in roll is affected, this is balanced by a smoother response. Therefore, on balance the final tuning for this trim condition of the Altaeros system is given by $n_y = 10$, $n_u = 4$ and $W1 = 1$ (Altitude), $W2 = 0.3$ (Roll) and $W3 = 0.7$ (Pitch).

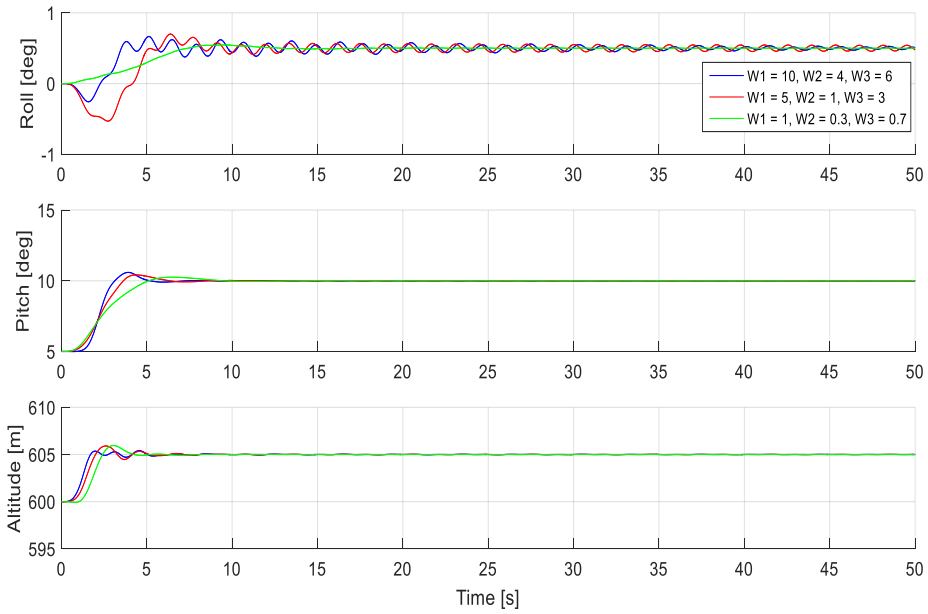

Figure 6-10 - MPC Tuning of W1, W2 and W3

6.6 Constraint Handling

As discussed, one of the key features of the MPC controller allows for the addition of system constraints. Within this hierarchical framework, the constraints are defined on the set-points driving the system on altitude, pitch and roll. In doing so, the operational envelope is well defined and constrained i.e. Figure 5-1. This will prevent significant loading at higher altitudes (Figure 6-4) and instabilities caused by stall as the pitch angle is increased. In this controller design the constraints defined are applied according to Table 6-3.

Constraints	Value
z_{max}	605
z_{min}	600
θ_{max}	10
θ_{min}	0
ϕ_{max}	0.3

ϕ_{min}	-0.3

Table 6-3 – Constraints on Hierarchical MPC Set-points

The comparison of applying the constraints defined in Table 6-3 against the unconstrained formulation is shown in Figure 6-11.

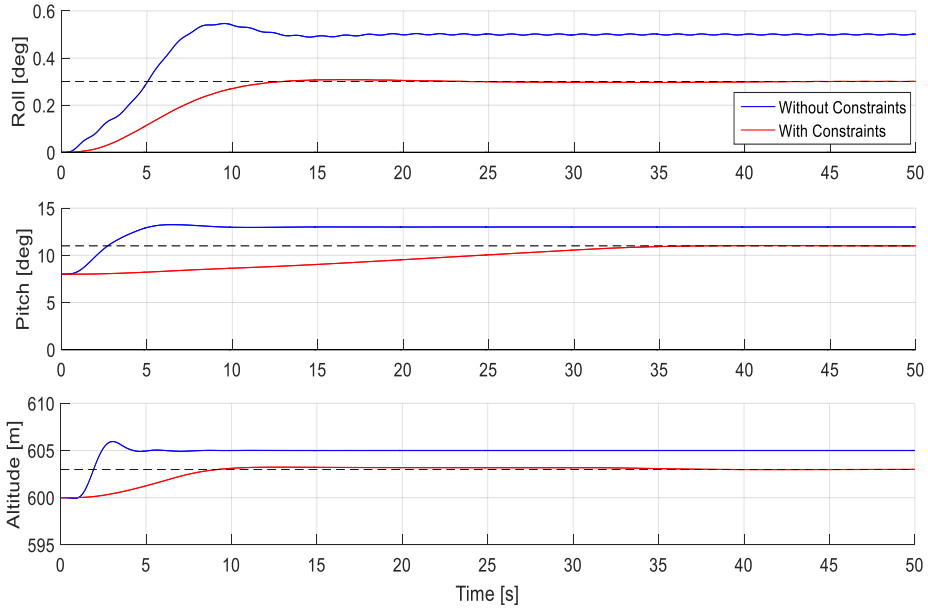

Figure 6-11 – MPC Hierarchical Controller with constraints

From Figure 6-11, the effect of constraining the system can be clearly seen on roll, pitch and altitude. The fact that constraints can be applied easily within this framework means that the hierarchical controller could be adopted to regulate the system within the operational envelope. This is important as it will prevent adverse loading effects from the tethers and the aerodynamics, which come as a result of poor choice of nominal operating conditions.

6.7 Extremum Seeking Control

The final part of the hierarchical control framework presented here, discusses a method through which the altitude set-point of the system can be self-regulated i.e. independent of a

pre-defined set-point. The primary benefit in this approach for a BAWT is related to the energy capture of the system over a certain period of time, ranging from short term performance e.g. hours, to a more long-term view e.g. months and years. In this section an optimum altitude set-point is found by an extremum seeking loop that maximises the net power of the system. The net power of the system is defined as being the power from the wind turbine rotor minus the losses associated with reeling the tether/in out. As the tether losses dominate at high wind speeds, this creates a net power loss on the power curve which in turn motivates the requirement to operate a specific point on the power curve i.e. at rated speed where the power is maximised and the loads are minimised.

6.7.1 ESC Overview

As discussed in Chapter 4, ESC methodologies have been applied to airborne wind energy systems in previous work [127]. This final section presents the control design for the final layer of the hierarchical controller shown in Figure 6-1. Here the power performance of the turbine is evaluated and framed within an altitude optimisation context through the wind shear law introduced in equation (6-1). This illustrates the relationship between wind speed and altitude i.e. the wind speed increases with altitude.

The key element of the system performance will be to keep the turbine close to rated wind speed. The reason behind this can be better understood by evaluating the power generated and consumed by the system. The generated power from the BAWT is modelled as in equation (6-24). Note that in this work an ideal generator is assumed and therefore no significant losses are accounted for within the generator itself. Furthermore, the time constant for the rotor is assumed to be very low as a small change in wind speed would result in a near instantaneous change in power. This would clearly not be the case in reality.

The loss in power is represented by the sum of power loss from each winch as a function of the force on the tether, as in equation (6-25). The tether force can be approximated by the lift on the shroud, given in equation (6-3).

The net power is therefore denoted as the difference between the generated power from the turbine and the power consumed by the winches. This simple power model is shown in equation (6-26) below:

$$P_{turbine} = \frac{1}{2}\rho A v_w(z_{alt})^3 C_p(\lambda, \beta_{blade}) \tag{6-24}$$

$$P_{loss} = \sum_{u=1}^{x} u_x F_z^{aero} \tag{6-25}$$

$$P_{net} = P_{turbine} - P_{loss} \tag{6-26}$$

where, $v_w(z_{alt})$ can be expressed as a function of altitude upon substitution of v_w into equation (6-1).

If there were no losses in the system i.e. $P_{loss} = 0$ then it could simply be argued that the ESC would be unnecessary because you would be able to choose the altitude corresponding with any speed above rated. However, following the previous discussion in Section 6.2, it was argued that as wind speed increases, the force on the tethers increases, which leads to greater loads and an increase in power consumption from the winch to reel in/reel out the tether in high wind speeds. This means that the power curve of the BAWT will show a clear power loss at higher wind speeds, driven by tether losses, compared with a conventional rotor. This is demonstrated in Figure 6-12 computed by running the BAWT model developed in Chapters 3, with the power modelled as in equation (6-24) for a turbulent wind speed in steps of 2 m/s. The rotor is assumed to have a rated speed of 12.5 m/s, a rated power of 30kW and an area A assumed to be 37.5m^2.

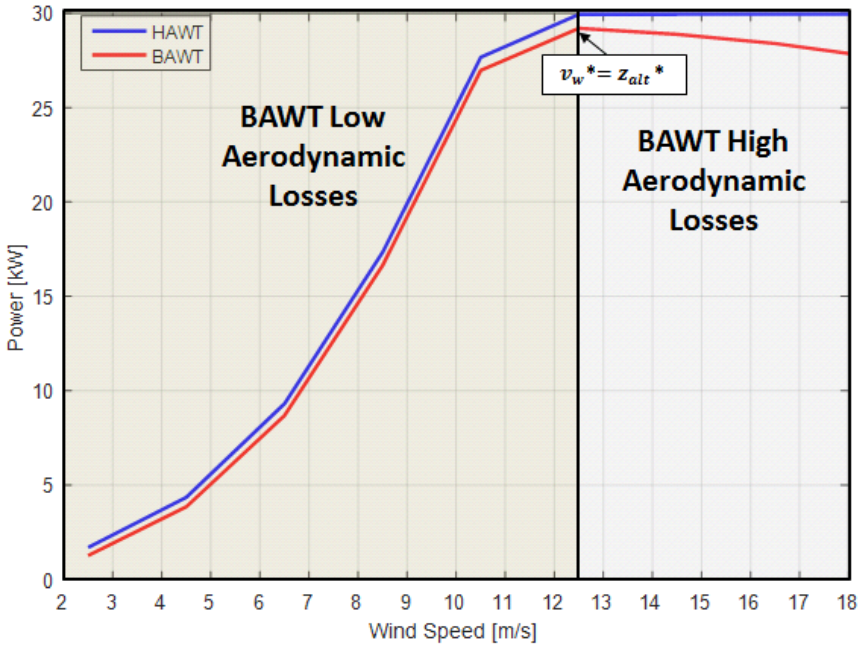

Figure 6-12 - Power Curve for a BAWT and HAWT

From Figure 6-12, it can be seen that a local optimum is defined at $\boldsymbol{v_w}$*= $\boldsymbol{z_{alt}}$* where * denotes the optimum value for both wind speed ($\boldsymbol{v_w}$), which in this case is equal to 12.5 m/s and an optimum altitude z_{alt} which can be derived from equation (6-1).

As the power drops off at higher wind speeds, the optimisation problem becomes clear. That is, how can a suitable altitude be found that maximises the power performance of the system whilst keeping the power losses low. This work makes two key assumptions in order to address this issue:

- The power performance from the BAWT can be measured instantaneously i.e. a small change in wind speed will result in an immediate change in measureable power.
- The wind speed monotonically increases with altitude and is represented by wind shear. The shear present will be based on a assumption of reference altitude and wind speed, as per equation (6-1).

6.8 ESC Control Design

The simple extremum seeking strategy is incorporated into the current control design of the BAWT and illustrated in Figure 6-13 below. Note that the control structure now includes the MPC hierarchical layer described in Section 6.7.

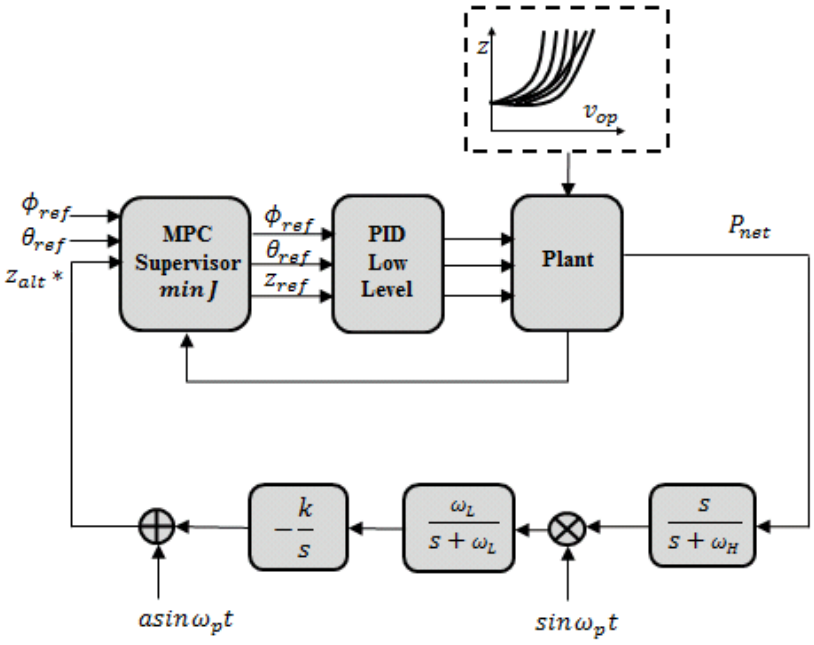

Figure 6-13 - BAWT Extremum Control Seeking Scheme

Figure 6-13 shows an extremum seeking controller for a static map. Consider that $P_{net}(z_{alt})$ takes the following form [108]:

$$P_{net}(z_{op}) = P_{net}{}^{*} + \frac{P_{net}{}''}{2}(z_{alt} - z_{alt}{}^{*})^2 \qquad (6\text{-}27)$$

where, $P_{net}{}'' > 0$. Any quadratic function can be approximated locally by (6-27). The purpose of the algorithm is to minimize $(z_{alt} - z_{alt}{}^{*})$ so that the output $P_{net}(z_{alt})$ is driven to $P_{net}{}^{*}$.

From Figure 6-13, it can be seen there are four significant parts to tune, within the presented ESC loop. These are broken down into the following:

- Perturbation Amplitude and Frequency ($asin\omega_p t$) – As part of the ESC scheme it is important to introduce a perturbation in order to estimate the gradient of the function that is being optimised. This perturbation will have a tuneable frequency ω and a corresponding amplitude a. The implication of the choice of a for a given perturbation frequency ω_p is investigated in more detail in Section 6.8.1.
- High Pass Filter Constant (ω_h) – A high pass filter is introduced in order to filter out the DC component of the signal before it is passed through the integrator. Thus allowing the perturbation applied to drive the signal to the optimal value. This can be tuned based on ω_h, which denotes a tuneable filter time constant.
- Low Pass Filter Constant (ω_L) – Before the signal is passed through the integrator a low pass filter is added to smooth out the low frequency variation introduced by the perturbation signal.
- Integrator adaption gain (k) – Finally, the incoming signal is passed through an integrator which greatly attenuates the high frequency components of the signal. The output of this signal is multiplied by a tuneable gain k such that gradient of the trajectory is affected i.e. speeding up or slowing down the response.

6.8.1 Tuning of ESC

Tuning the extremum loop becomes a balance of response time and performance. As the optimised output is naturally perturbed around the extremum point there will be a need to ensure that this perturbation is limited to within a reasonable tolerance. This tolerance is analysed in more detail here. To ensure that the response of the ESC loop is matched with the dynamics of the shroud, care is chosen on the units of each tuneable parameter to ensure consistency with the model. In this case the following units are assigned:

Parameters	Description	Units
a	Perturbation Amplitude	m
ω_p	Perturbation Frequency	rad/min
ω_h	High Pass Filter Frequency	rad/min
ω_L	Low Pass Filter Frequency	rad/min
k	Integral Gain	m/kW

Table 6-4 – Parameter units for ESC loop tuning

There are a couple of important points to note from the units provided in Table 6-4. Firstly, the perturbation frequencies are given in units of rad/min to account for the fact that the shroud dynamics responds in the order of minutes to a given change in reference command. Note that this was confirmed through the PID control design conducted for the nonlinear model in Chapter 5. Secondly the integral gain will naturally be low to account for the conversion from power (kW) to meters (m). The response of the ESC loop is investigated to understand the tolerance and response of the system to a variation in the amplitude a. This parameter was chosen specifically for this investigation because the degree of perturbation seen, around a specific operating point should ideally be as small as possible. In order to justify a small value for this, a tuning was conducted. The other parameters in the ESC loop were held constant and defined according to Table 6-5 below:

Parameters	Description	Units
ω_p	1.668	rad/min
ω_h	48	rad/min
ω_L	0.0480	rad/min
k	0.0080	m/kW

Table 6-5- Parameter values for ESC tuning

Note that the perturbation frequency is approximately 1.5 order of magnitudes larger than the low pass filter frequency. Similarly the high pass filter frequency is much larger than the perturbation frequency. A good bandwidth between these frequencies will ensure good robustness of the ESC tuning.

A tuning process is then conducted on the perturbation amplitude a, with the other tuning parameters defined as Table 6-5. As discussed before, the reasoning behind this was to gain an increased understanding of the tolerance of the ESC loop to a large change in amplitude. If the peak-peak amplitude variation are large (>20m) then this could have a negative effect on system performance i.e. introduction of load cycling and increased power variations. These simulations were conducted under the following conditions:

- Nonlinear shroud model defined in equation's (3-8) - (3-13)
- Low Level PID controller defined in (5-39)
- Reference wind speed (v_{ref}) of 11.5 m/s at a reference altitude (z_{ref}) of 300m defined according to equation (6-1).
- Constant wind speed defined as v_w according to equation (6-1)

The perturbation amplitude a was varied from 2 to 20 to understand if the desired set-point can be found that maximises power for a given altitude set-point. The simulation was run for 4.5 hours to track the variation in altitude and power output accordingly. Note that there is an initial transient of around (300seconds) before the ESC begins to drive the set-point of the system i.e. the altitude set-point.

Figure 6-14 and Figure 6-15 show the altitude and power response of the BAWT system for the ESC scheme defined in Figure 6-13. As the perturbation amplitude (a) increases so too

does the deviation away from the desired reference. A low perturbation amplitude shows that an attainable altitude of 900m can be obtained which maximises the power of the system after 3.5 hours. However, as the amplitude increases so too does the variation around the desired amplitude. This subsequently translates into increased variation on the power output. Therefore, the justification for setting a low perturbation amplitude is demonstrated as the performance in closed loop at a low perturbation improves the response of the system and settles at a desired altitude that optimises the power output from the system.

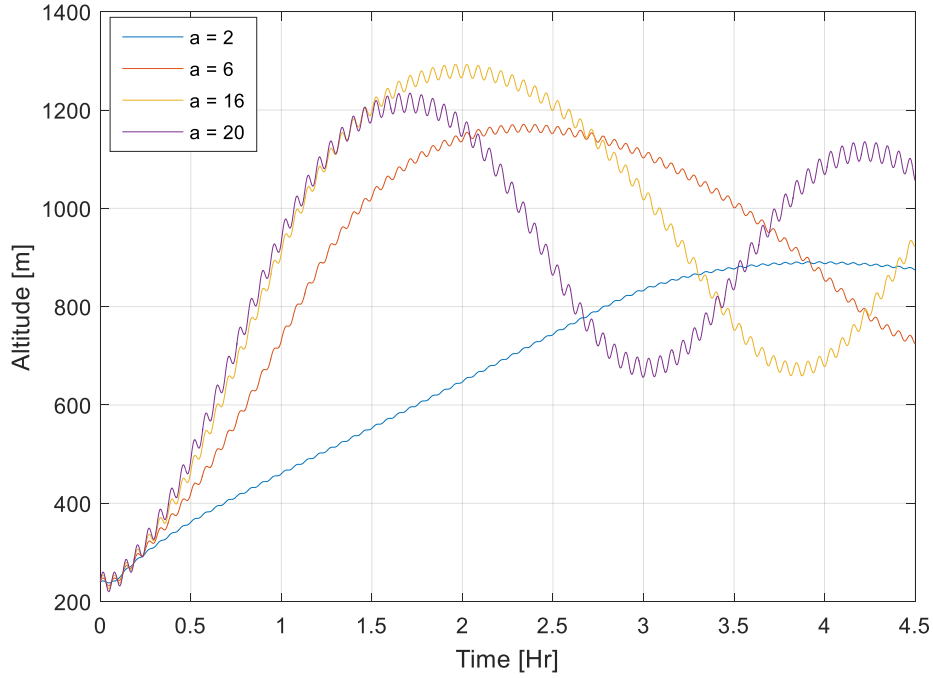

Figure 6-14 - Altitude set-point determination from ESC for different amplitude perturbations (No Turbulence conditions)

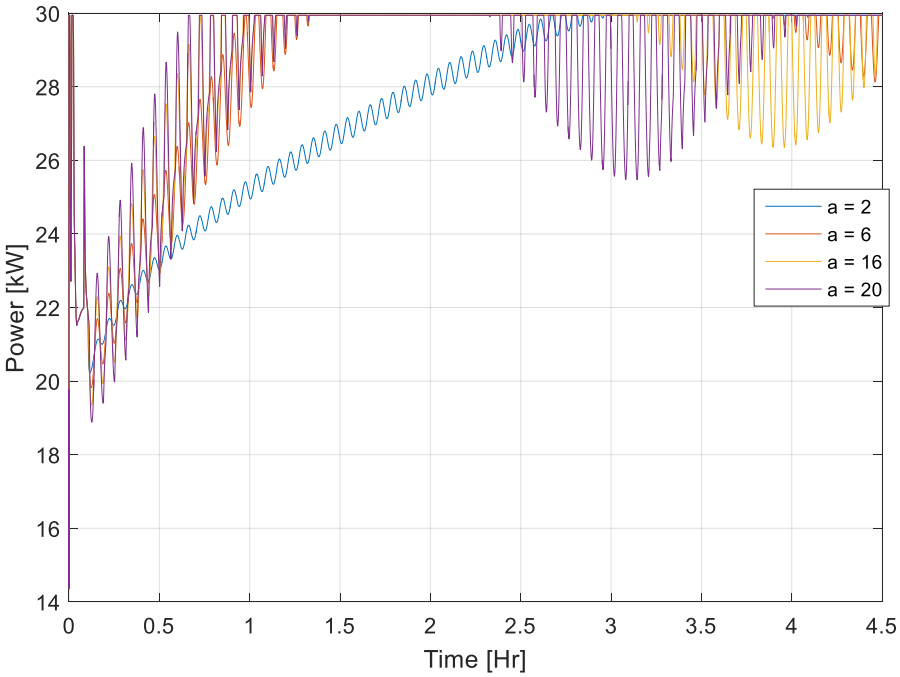

Figure 6-15 - Power response from ESC for different amplitude perturbations (No Turbulence)

Finally, to demonstrate that the ESC scheme is indeed providing a desired altitude reference that optimises power, a graph of altitude against power is shown in Figure 6-16. This is clearly showing that the ESC drives the altitude set-point of the system to an operating point where maximum power from the turbine is reached.

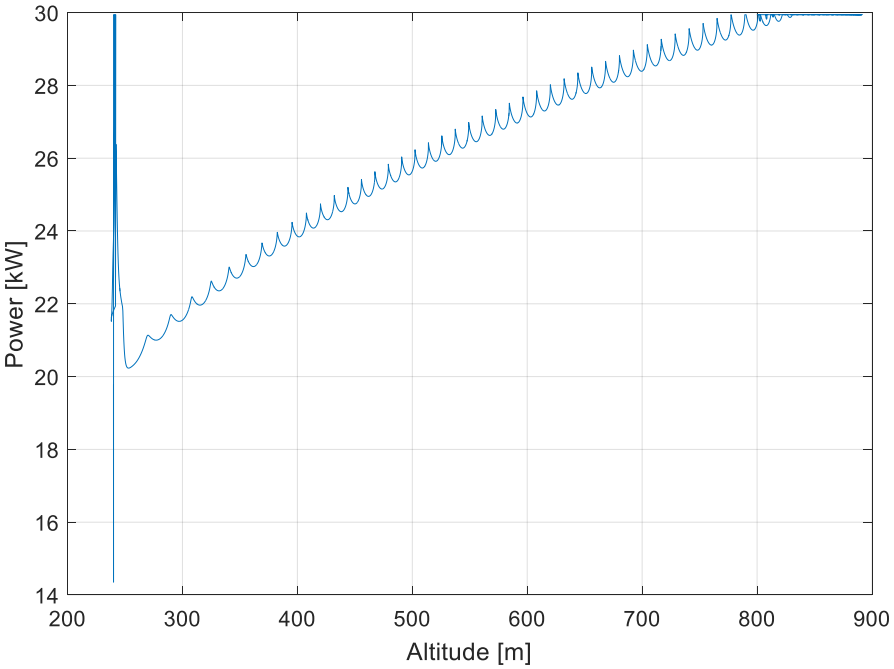

Figure 6-16 - Altitude Vs Power from ESC Scheme

6.9 Hierarchical Controller for a BAWT

The final result shows the impact of the hierarchical controller defined according to Figure 6-13 which is:

- Low Level PID Control – Driving the system to the desired set-point in altitude, roll and pitch (5-39)
- Medium Level Control – MPC control that enforces constraints on these set-points according to equation (6-19)
- High Level Control – ESC loop that defines the optimum altitude of the system (6-27)

The conditions for this simulation are defined from the nonlinear model developed in Chapter 3, akin to that defined in Section 6.8. However, in this instance a turbulent wind speed profile is applied, instead of a constant wind speed. The wind speed is applied at a

reference wind speed of 11 m/s at a reference altitude of 300m. The wind speed turbulence is defined around v_w, computed from (6-1), according to equation's (3-2) - (3-4).

The wind speed profile observed in Figure 6-17 is a function of changing altitude set-point from the ESC. This clearly demonstrates the effect of wind shear, correlated to Figure 6-2 shown earlier.

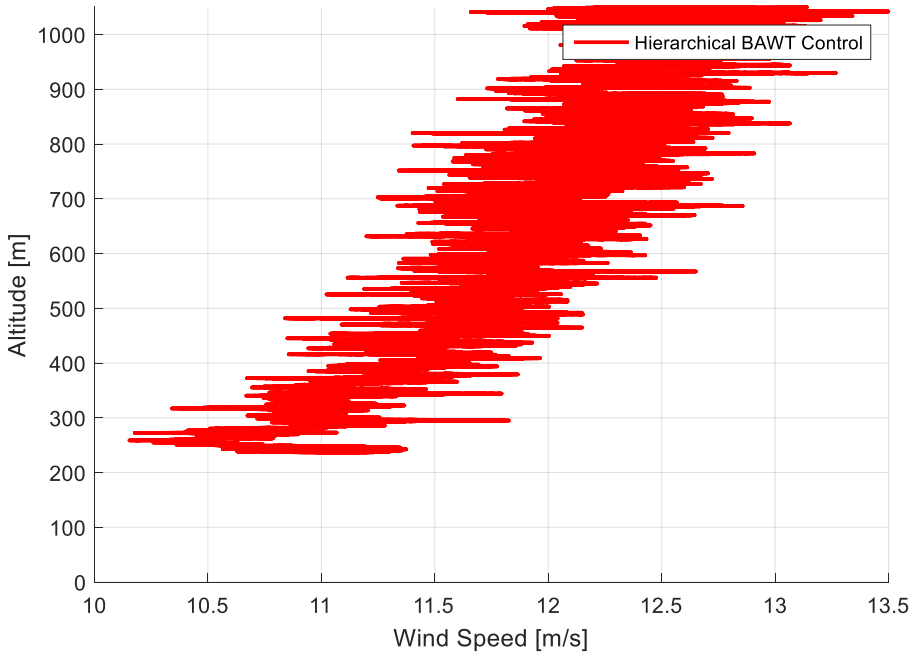

Figure 6-17 - Wind Shear as a function of altitude change from ESC

Figure 6-17, shows that as the turbine reaches an altitude of 1000m, the average wind speed is computed around 12.5 m/s, corresponding to peak power of the system (Figure 6-12). It is interesting to note that by adding turbulence there is, on average, a variation of around +/- 1m/s in peak-peak wind speed. In reality, there will be different variations of turbulence which means that this wind shear, with this turbulence profile may not accurately represent real-time operating conditions.

Finally, the results are presented for the BAWT hierarchical control strategy, demonstrating performance of the low level (set-point regulation), medium level (constraint satisfaction) and high level (energy optimisation) control strategies discussed throughout this work Two figures are presented to demonstrate this performance. Figure 6-18, shows results for the attitude and altitude of the shroud, with Figure 6-13 showing the subsequent impact on altitude, instantaneous and ten-minute average power.

From Figure 6-18, the influence of the low-level controller, alongside that of the supervisory control strategies can be observed. The closed loop system is driven to the desired values in roll, pitch and altitude, with the altitude set-point being chosen as a result of the net power optimisation strategy presented in Figure 6-13.

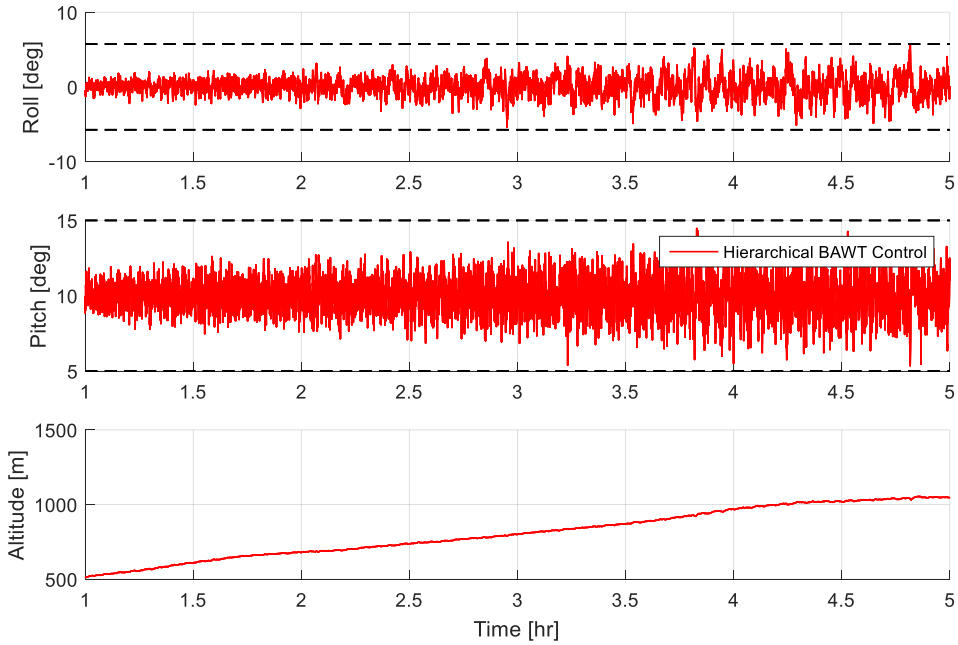

Figure 6-18 - Attitude and Altitude performance of the BAWT hierarchical controller

To confirm that the power capture is indeed being maximised with respect to time, an analysis is conducted on the power performance of the system. This is shown in Figure 6-19 below.

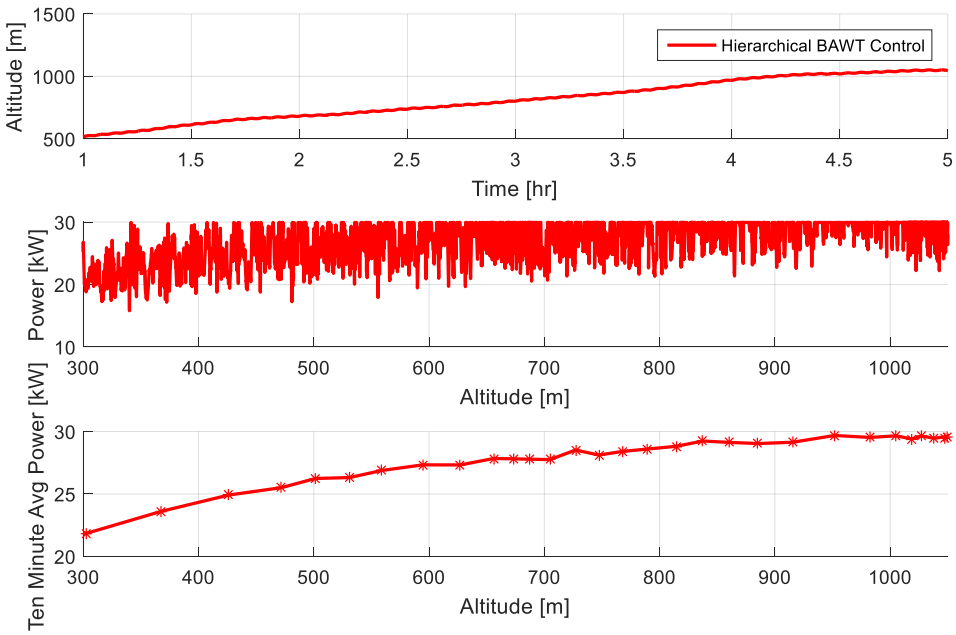

Figure 6-19 - Power performance of rotor with respect to Altitude set-point from ESC scheme

Figure 6-19 shows the altitude with respect to time, the instantaneous power and ten-minute average. The instantaneous power is unfiltered and is seen to be significantly affected by the turbulence profile applied. Therefore, to understand the underlying trend, in terms of performance, a ten-minute average power is shown. This is shown with respect to altitude. It is clear that as the ESC drives the altitude set-point towards the rated wind speed of the rotor, the power is maximised as a result. Note this is also observed in the unfiltered case, but the ten-minute average provides a clearer insight into the resulting system response.

Implementing a hierarchical control strategy such as this allows the control designer flexibility in terms of providing limitations on performance (constraints) and a method for optimising power performance (ESC). The merits of this have been demonstrated in this work for sample simulations which show low level control providing stability to the system and supervisory levels of control providing constraint satisfaction and power optimisation.

6.10 Conclusions

This chapter has discussed the implementation of a hierarchal control framework for the BAWT control system. Two methods are presented that offer a benefit in terms of optimising system performance, that is; A hierarchical MPC design that can enforce, when required, envelope constraints on the roll, pitch and altitude and an ESC, that seeks to regulate the altitude set-point of the system as a function of power. The design approach taken presents a methodology for developing an appropriate MPC cost function that allows the system to provide a reference in roll, pitch and altitude that is regulated by weighting parameters and constraints on the system. An ESC is then designed to exploit the joint relationship between wind speed, altitude, and power performance of the system which worsens at higher wind speeds due to power losses from reeling in/out the tether. This resulted in an optimal altitude set-point that regulates optimises the system to around rated wind speed of the rotor.

Note that there are a number of assumptions made in this chapter to facilitate the hierarchical control design. Firstly, the MPC framework has only been shown at one operating point which was sufficient to create the plots shown. In practice, there will be a number of operating points within the system envelope that will affect controller behaviour. The hierarchical MPC framework could be extended into a nonlinear framework that understands the behaviour of the system in more detail making it less susceptible to changes in operating conditions. For instance, quick changes in roll, pitch and altitude, tether impact etc. In addition, the ESC scheme presented could present an issue because the assumed shear may not accurately represent real-life performance. Therefore, in practice the controller may drive the system to an incorrect operating point as a result. This could be mitigated by accurate site measurements, but at a significant additional cost.

7 Conclusions and Future Work

This thesis has sought to address the challenges associated with the new field of wind energy research known as Airborne Wind Energy (AWE). These systems, due to their unique tethered design, are able to reach altitudes that are not attainable by conventional wind turbines. Although a significant amount of research has already been published in this area there are still challenges to face. One contribution of this work highlights the challenges that Airborne Wind Energy companies face from both an economic and technological point of view. This is achieved through a full consideration of potential energy capture from airborne wind energy systems. The scaling arguments of these systems mean there is great potential for investment. However, as kite/rigid-body systems are inherently dynamic by design the control problem becomes more challenging in high and low winds. Conversely, the stability of the BAWT, developed by Altaeros Energies, is guaranteed at low winds due to the buoyancy present from the shroud. The introduction of two novel force ratio's for this system shows that system stability is directly related to aerodynamic design and the volume of the shroud.

The main contribution of this thesis rests in the development of suitable control algorithms for the Buoyant Airborne Wind Turbine (BAWT). This research is required to ensure autonomous operation and reduce costs associated with maintenance of the system. The primary aim of this work was to develop suitable control designs that can both stabilise the system under nominal operating conditions whilst also maximising power. A low level controller has been designed using two known multivariable techniques, the Maciejowski

and LQR methods. This work demonstrates the applicability of each algorithm to low level control design of the BAWT whilst also providing a quantitative analysis between classical and optimal PID tuning techniques.

The question of optimal energy capture is then addressed through two further algorithms. A model predictive control scheme is implemented to provide the altitude, roll and pitch set-points for the low-level controller under given constraints. This provides a methodology for bounding the operational envelope to prevent excessive loading i.e. maximum and minimum altitude to prevent high tether loads, maximum and minimum pitch to prevent aerodynamic stall and maximum and minimum roll to prevent adverse yaw moments. This methodology is presented for one operating on the system. Although this may not provide optimal performance across the operating envelope, the stability of the BAWT was observed over a wide range of conditions for the low-level control design and the hierarchical MPC simply extends the state space model to apply within a pre-defined cost function.

This hierarchical strategy is then extended with the implementation of an ESC loop which seeks to find an altitude that maximises the net power output of the BAWT. This idea is motivated by the fact that a trade-off exists between power capture from the rotor, against power consumed by the tethers from reeling the tether in and out. As the operating wind speed increases, so too does the force on the tether and by extension, the power consumed by the winch when adjusting the altitude and attitude of the system. This results in a net power loss at high winds. The derived optimal altitude is based off an applied wind shear at an assumed reference wind speed and altitude. This optimal altitude is seen to correspond well with the rated speed of the turbine.

A summary of each chapter is now given and the conclusions from each are discussed and summarised. Potential avenues for further research are then highlighted for future work.

7.1 Conclusions

Firstly, Chapter 2 provides a brief introduction and state of the art literature review into Airborne Wind Energy Systems (AWES). The main benefits of airborne wind energy are highlighted to show that due to the nature of the wind resource, it is possible using tethered systems, to exceed the power output of conventional turbines at higher altitudes due to superior average wind speeds. The overriding motivation in discussing each type of design individually is to highlight the very fact that a variety of designs exist. As Airborne Wind Energy is a new field of research it is clear there is yet to be a consensus as to which design is most efficient both in terms of cost, performance and safety. Whilst the kite, rigid body and buoyant systems are all interesting from an academic point of view due to their challenging multivariable and dynamic nature, to compete as a stand-alone product these systems require much more field validation so that an optimum design can be found. However, the final discussion highlights that the two most viable and commercial designs are the Makani power rigid body rotor and the BAWT. As this work has been in collaboration with Altaeros Energies, the modelling and control design of the BAWT is explored in subsequent chapters.

Chapter 3 develops the six degree of freedom model of the Altaeros system in a MATLAB/SIMULINK environment. Each component is discussed and modelled in detail, with the dynamics of the tethers in particular being highlighted as a design issue from both a cost and weight perspective. Furthermore, a contribution to the understanding of the system operation is given through the development of two novel force ratios which highlight the buoyant-aerodynamic transition points of the system. This analysis is helpful from a scaling perspective as it clearly shows the transition points of the system regardless of the turbine's

rating assuming the shroud is scaled with similarity. The reasoning behind why the shroud is aerodynamically designed becomes easily apparent using this method, with stability shown to be compromised if the shroud is not designed to generate aerodynamic lift.

Chapter 4 reviews the current industry practice in terms of PID, MPC and ESC control design. This is done to inform the work in the proceeding chapters. The merits of each technique are discussed and the outline of the hierarchical approach to control design is laid out such that the reader can understand the motivation behind implementing a control architecture of this type for a BAWT.

Chapter 5 then introduces a multivariable control strategy to control the altitude, pitch and roll of the Altaeros system. Two PID/PD tuning techniques are then compared namely; the optimal LQR method and a more classical approach based on plant inversion techniques derived from work by Maciejowski. The final results demonstrate adequate control over roll, pitch and altitude of the shroud, concluding that the MPID controller due to both its ease of implementation and performance means it is used as the basis for the proceeding control development.

Finally. Chapter 6 builds upon the work done in Chapter 5 to develop a hierarchical controller using a hierarchical MPC and an ESC loop implemented to optimise the altitude of the system. In this context, hierarchical MPC is defined as a controller that provides desired set-points to the low level controller in altitude, roll and pitch under given constraints. These constraints on the output references present a method by which the operational envelope can be enforced such that excessive loading is not observed. The results presented here builds upon the low level in Chapter 5 at one operating condition. The ESC loop then seeks to optimise the altitude set-point which in turn increases the overall energy capture. This

presents a hierarchical control strategy that provides low-level stability and high level constraint satisfaction and optimisation. This will be important from a system design perspective as it provides a methodology for bounding the operational envelope of the system which in turn will increase confidence in the autonomous operation in deployment.

7.2 Future Work

The following points are now given as potential future avenues of research

1. Following on from the discussion provided in Chapter 2, one interesting avenue of research may be to fully explore the cost of energy of each type of system. In practical terms this may offer greater insight as to which system might be more efficient.
2. Extending the model of the Altaeros system further may also yield interesting insights into its operation. For instance, a full model of the turbine, with wake effects may give greater information as to how the turbine interacts with the shroud. This will lead to a more coordinated control strategy between the turbine and shroud.
3. The low-level control design could be extended to look at other techniques. This particular work looked at two tuning techniques showing that classical techniques, work well against optimal tuning methods. However, looking at combined tuning methods may lead to greater control in the desired directions.
4. The MPC strategy defined here could be extended to cover the full operational envelope. This could be achieved through the extension to a nonlinear framework or a linear parameter varying strategy to increase robustness to operating conditions.

References

[1] EWEA, “Wind in power, 2015 European Statistics,” 2015.

[2] EWEA, “The European offshore wind industry - key trends and statistics 1st half 2013,” 2013.

[3] T. Burton, N. Jenkins, D. Sharpe, and E. Bossanyi, “Wind Energy Handbook (Google eBook),” *John Wiley Sons*, pp. 11–38, 2011.

[4] Siemens, “The new Stantard for Offshore: Siemens 7MW DD Platform,” 2015.

[5] P. Jamieson, “Innovation in Wind Turbine Design,” *John Wiley Sons*, pp. 211–222, 2011.

[6] M. Loyd, “Crosswind kite power,” *J. Energy*, vol. 4, no. 3, pp. 106–111, 1980.

[7] M. Diehl, “Airborne Wind Energy,” *Springer*, 2013.

[8] M. Maciejowski, *Multivariable feedback design*. Addison, 1989.

[9] C. L. Archer and K. Caldeira, “Global Assessment of High-Altitude Wind Power,” *Energies*, vol. 2, no. 2, pp. 307–319, May 2009.

[10] C. L. Archer, “An Introduction to Meteorology for Airborne Wind Energy,” *Airborne Wind Energy*, pp. 81–94, 2013.

[11] C. L. Archer, L. Delle Monache, and D. L. Rife, “Airborne wind energy: Optimal locations and variability,” *Renew. Energy*, vol. 64, pp. 180–186, Apr. 2014.

[12] L. Fagiano and M. Milanese, “Airborne Wind Energy: An overview,” *Am. Control Conf. 2012*, pp. 3132–3143, 2012.

[13] L. Fagiano, M. Milanese, and D. Piga, “Optimization of airborne wind energy generators,” *Int. J. robust nonlinear Control*, vol. 22, no. 18, 2011.

[14] L. Fagiano and M. Milanese, “Control of power kites for naval propulsion,” *Am. Control Conf.*, pp. 4325–4330, 2010.

[15] P. Williams, B. Lansdorp, and W. Ockesl, “Optimal Crosswind Towing and Power Generation with Tethered Kites,” *J. Guid. Control. Dyn.*, vol. 31, no. 1, pp. 81–93, Jan. 2008.

[16] M. Canale, L. Fagiano, and M. Milanese, “High Altitude Wind Energy Generation Using Controlled Power Kites,” *IEEE Trans. Control Syst. Technol.*, vol. 18, no. 2, pp. 279–293, Mar. 2010.

[17] “Makani Power.” [Online]. Available: http://www.makanipower.com/. [Accessed: 12-Apr-2012].

[18] “Altaeros Energies.” [Online]. Available: http://www.altaerosenergies.com/.

[19] M. Canale, L. Fagiano, M. Milanese, and M. Ippolito, “KiteGen project: control as key technology for a quantum leap in wind energy generators,” *2007 Am. Control Conf.*, pp. 3522–3528, Jul. 2007.

[20] “SkySails.” [Online]. Available: http://www.skysails.info/english/.

[21] “Windlift.” [Online]. Available: http://windlift.com/index.html.

[22] M. Erhard and H. Strauch, “Control of towing kites for seagoing vessels,” *IEEE Trans. Control Syst. Technol.*, vol. 21, no. 5, pp. 1629–1640, 2013.

[23] F. Fritz, “Application of an automated kite system for ship propulsion and power generation,” in *Green Energy and Technology*, 2013, pp. 359–372.

[24] [electronic Resource], “KiteGen.” [Online]. Available: http://www.kitegen.com/en/.

[25] E. J. Terink, J. Breukels, R. Schmehl, and W. J. Ockels, “Flight Dynamics and Stability of a Tethered Inflatable Kiteplane,” *J. Aircr.*, vol. 48, no. 2, pp. 503–513, Mar. 2011.

[26] “Ampyx Power.” [Online]. Available: http://www.ampyxpower.com/.

[27] J. Breukels and W. Ockels, “Design of a large inflatable kiteplane,” *48th*

AIAA/ASME/ASCE/AHS/ASC Struct. Struct. Dyn. Mater. Conf., p. 2246, 2007.
[28] B. Lansdorp, R. Ruiterkamp, and W. Ockels, "Towards flight testing of remotely controlled surfkites for wind energy generation," in *AIAA Modelling and Simulation Technologies Conference and Exhibit, Hilton Head*, 2007.
[29] B. Houska and M. Diehl, "Optimal Control of Towing Kites," *Proc. 45th IEEE Conf. Decis. Control*, no. 3, pp. 2693–2697, 2006.
[30] B. Houska and M. Diehl, "Optimal Control for Power Generating Kites," in *9th European Control Conf*, 2007, pp. 3560–3567.
[31] "Omnidea." [Online]. Available: http://omnidea.net/site/index.php.
[32] "SkyWindPower." [Online]. Available: http://www.skywindpower.com/.
[33] "Magenn." [Online]. Available: http://www.magenn.com/.
[34] C. Vermillion, "Modeling and control design for a prototype lighter-than-air wind energy system," *Am. Control Conf. (ACC), 2012, vol,, no., pp.5813-5818, 27-29 June 2012*, pp. 5813–5818, 2012.
[35] J. Samson and R. Katebi, "Shroud Design Criteria for a Lighter than Air Wind Energy System," *J. Phys. Conf. Ser.*, 2014.
[36] S. Wunder and N. Hanley, *The Future of Helium as a Natural Resource*. Routledge, 2010.
[37] R. Bosman, V. Reid, M. Vlasblom, and P. Smeets, "Airborne wind energy tethers with high-modulus polyethylene fibers," in *Green Energy and Technology*, 2013, pp. 563–585.
[38] H. . McKenna, J. W. . Hearle, and N. O´Hear, *Handbook of fiber rope technology*. Woodhead Publishing, 2000.
[39] "DynaOne." [Online]. Available: http://www.gleistein.com/en-geo-yacht-productsheet-for-rope-product/dynaone-hs. [Accessed: 13-Feb-2015].
[40] S. G. C. De Groot, J. Breukels, R. Schmehl, and W. J. Ockels, "Modelling Kite Flight Dynamics Using a Multibody Reduction Approach," *J. Guid. Control. Dyn.*, vol. 34, no. 6, pp. 1671–1682, Nov. 2011.
[41] P. Williams, B. Lansdorp, R. Ruiterkamp, and W. Ockels, "Modeling, simulation, and testing of surf kites for power generation," *AIAA 2008-6693, AIAA Model. Simul. Technol. Conf. Exhib.*, 2008.
[42] J. Breukels and W. J. Ockels, "A multi-body dynamics approach to a cable simulation for kites," *Proc. IASTED Asian Conf. Model. Simul.*, pp. 168–173, Oct. 2007.
[43] L. Fagiano, "Control of Tethered Airfoils for High–Altitude Wind Energy Generation," Politecnico di Torino, 2009.
[44] C. Vermillion, T. Grunnagle, R. Lim, and I. Kolmanovsky, "Model-Based Plant Design and Hierarchical Control of a Prototype Lighter-Than-Air Wind Energy System , with Experimental Flight Test Results."
[45] L. Fagiano, A. U. Zgraggen, M. Morari, and M. Khammash, "Automatic control of tethered wings for airborne wind energy: design and experimental results," in *Proceedings of the European Control Conference (ECC13)*, 2013, pp. 167–180.
[46] L. Fagiano and M. Milanese, "High-Altitude Wind Energy for Sustainable Marine Transportation," *IEEE Trans. Intell. Transp. Syst.*, vol. 13, no. 2, pp. 781–791, 2012.
[47] L. Fagiano, A. U. Zgraggen, M. Morari, and M. Khammash, "Automatic crosswind flight of tethered wings for airborne wind energy: Modeling, control design, and experimental results," *IEEE Trans. Control Syst. Technol.*, vol. 22, no. 4, pp. 1433–1447, 2014.
[48] R. Ruiterkamp and S. Sieberling, "Description and Preliminary Test Results of a Six Degrees of Freedom RigidWing Pumping System," in *Airborne Wind Energy*, 2013, pp. 443–458.
[49] D. Vander Lind, "Analysis and Flight Test Validation of High Performance AirborneWind Turbines," in *Airborne Wind Energy*, 2013, pp. 473–490.

[50] C. Vermillion, B. Glass, and A. Rein, “Lighter-Than-Air Wind Energy Systems,” *Springer - Verlag Berlin*, pp. 501–513, 2014.
[51] J. Samson and R. Katebi, “Multivariable control of a lighter than air system,” *2014 UKACC Int. Conf. Control. Control 2014 - Proc.*, pp. 256–261, 2014.
[52] C. Vermillion, T. Grunnagle, R. Lim, and I. Kolmanovsky, “Model-based plant design and hierarchical control of a prototype lighter-than-air wind energy system, with experimental flight test results,” *IEEE Trans. Control Syst. Technol.*, vol. 22, no. 2, pp. 531–542, 2014.
[53] J. Samson and R. Katebi, “Adaptive envelope control design for a Buoyant Airborne wind energy system,” in *Proceedings of the American Control Conference*, 2015, vol. 2015–July, pp. 2395–2400.
[54] U. Kalabic and C. Vermillion, “Reference governor design for computationally efficient attitude and tether tension constraint enforcement on a lighter-than-air wind energy system,” *Control Conf. (ECC), 2013 Eur.*, pp. 1004–1010, 2013.
[55] R. Weng and C. Vermillion, “Model Predictive Longitudinal Control of a Lighter-Than-Air Wind Energy System,” *Am. Control Conf. 2012*, 2012.
[56] R. Schmehl, M. Noom, and R. Van Der Vlugt, “Traction Power Generation with TetheredWings,” in *Airborne Wind Energy*, 2013, pp. 23–45.
[57] U. Zillmann and S. Hach, “Financing strategies for Airbornewind energy,” in *Green Energy and Technology*, 2013, pp. 117–137.
[58] “Techcrunch,” 2013. [Online]. Available: http://techcrunch.com/2013/05/22/google-x-acquires-makani-power-and-its-airborne-wind-turbines/. [Accessed: 13-Feb-2016].
[59] P. Jamieson, *Innovation in Wind Turbine Design*, 1st Ed. John Wiley & Sons, 2011.
[60] J. Samson, R. Katebi, and C. Vermillion, “A Critical Assessment of Airborne Wind Energy Systems,” in *IET Renewable Power Generation Conference*, 2013, pp. 4–7.
[61] T. Burton, N. Jenkins, D. Sharpe, and E. Bossanyi, “The wind resource,” in *Wind Energy Handbook*, 2011, pp. 9–36.
[62] “Mathworks: Dryden Wind Turbulence Model (Continuous).” [Online]. Available: https://www.mathworks.com/help/aeroblks/drydenwindturbulencemodelcontinuous.html.
[63] M. Nahon, G. Gilardi, and C. Lambert, “Dynamics/Control of a Radio Telescope Receiver Supported by a Tethered Aerostat,” *J. Guid. Control. Dyn.*, vol. 25, no. 6, pp. 1107–1115, 2002.
[64] P. Dewdney, M. Nahon, B. Veidt, and I. Ntroduction, “The Large Adaptive Reflector : A Giant Radio Telescope with an Aero Twist,” vol. 48, no. 4, pp. 239–250, 2002.
[65] S. Widnall, “Potential Flow Calculations of Axisymmetric Ducted Wind Turbines,” *Electr. Resour. web.mit.edu/aeroastro/sites/widnall/turbine3.pdf*, 2009.
[66] C. Vermillion, B. Glass, and S. Greenwood, “Evaluation of a Water Channel-Based Platform for Characterizing Aerostat Flight Dynamics: A Case Study on a Lighter-Than-Air Wind Energy System,” *21st AIAA Light. Syst. Technol. Conf.*, pp. 1–10, 2014.
[67] C. Vermillion, B. Glass, and A. Rein, “Lighter than Air Wind Energy Systems,” in *Airborne Wind Energy*, 2013, pp. 501–514.
[68] R. Katebi, “PID Control in the Third Millennium,” *Springer*, 2012.
[69] T. Hägglund, H. Panagopoulos, and K. J. Åström, “Design of PID controllers based on constrained optimisation,” *IEE Proc. - Control Theory Appl.*, vol. 149, no. 1, pp. 32–40, Jan. 2002.
[70] K. J. Åström and T. Hägglund, “The future of PID control,” *Control Eng. Pract.*, vol. 9, no. 11, pp. 1163–1175, 2001.
[71] J. Perkins, *Multivariable Feedback Design*, vol. 1, no. 1. 1991.
[72] E. Davison, “The robust decentralized control of a general servomechanism

problem," in *IEEE Transactions on Automatic Control*, 1976, vol. 21, no. 1, pp. 14–24.
[73] J. Penttinen and H. N. Koivo, "Multivariable tuning regulators for unknown systems," *Automatica*, vol. 16, no. 4, pp. 393–398, 1980.
[74] R. N. Koivo, "A multivariable pid-controller for unknown systems," in *19th IEEE Conference on Decision and Control including the Symposium on Adaptive Processes*, 1980, pp. 1158–1159.
[75] A. G. J. MacFarlane, "Return-difference and return-ratio matrices and their use in analysis and design of multivariable feedback control systems," *Proc. Inst. Electr. Eng.*, vol. 117, no. 10, p. 2037, 1970.
[76] B. Kouvaritakis, "Theory and practice of the characteristic locus design method," *Proc. Inst. Electr. Eng.*, vol. 126, no. 6, pp. 2–8, 1979.
[77] W. I. Luyben, *Process Modeling, Simulation, and Control for Chemical Engineers*. 1999.
[78] H. Rosenbrock, *Computer-aided control system design*. Academic Press, 1974.
[79] U. Borison, "Self-tuning regulators for a class of multivariable systems," *Automatica*, vol. 15, no. 2, pp. 209–215, 1979.
[80] R. Yusof, S. Omatu, and M. Khalid, "Self-tuning PID control: A multivariable derivation and application," *Automatica*, vol. 30, no. 12, pp. 1975–1981, 1994.
[81] N. A. Wahab, M. R. Katebi, and J. Balderud, "Multivariable PID control design for wastewater systems," *2007 Mediterr. Conf. Control Autom.*, pp. 1–6, Jun. 2007.
[82] P. Martin and R. Katebi, "Multivariable PID tuning of dynamic ship positioning control systems," *Proc. IMarEST - Part A - J. Mar. Eng. Technol.*, pp. 11–24, 2005.
[83] W. I. Caldwell, "Control system with automatic response adjustment," 743862, 1950.
[84] R. E. Kalman, "Contributions to the Theory of Optimal Control," *Bol. Soc. Mat. Mex.*, vol. 5, pp. 102–119, 1960.
[85] C. J. Rose, "Dynamic programming processes within dynamic programming processes," *Journal of Mathematical Analysis and Applications*, vol. 26, no. 3. pp. 669–683, 1969.
[86] A. Astolfi, D. Karagiannis, and R. Ortega, *Nonlinear and Adaptive Control with Applications*. 2007.
[87] G. Tao, "Chapter 9 - Adaptive control design and analysis," *Wiley*, pp. 371–504, 2003.
[88] K. J. Åström and B. Wittenmarkt, "A survey of adaptive control applications," *Proc. 1995 34th IEEE Conf. Decis. Control*, no. December, pp. 649–654, 1995.
[89] R. E. Kalman, "A New Approach to Linear Filtering and Prediction Problems," *J. Basic Eng.*, vol. 82, no. 1, p. 35, 1960.
[90] B. Wittenmark and K. J. Åström, "Practical issues in the implementation of self-tuning control," *Automatica*, vol. 20, no. 5, pp. 595–605, 1984.
[91] M. V Cook, "Flight dynamics principles," *Elsevier*, vol. 2nd Ed., 2007.
[92] E. Lavretsky, "Properties of LQG / LTR Controllers," *IEEE Trans. Automat. Contr.*, vol. 57, no. 6, pp. 1587–1591, 2012.
[93] R. A. Nichols, R. A. Nichols, R. T. Reichert, and W. J. Rugh, "Gain Scheduling for H-Infinity Controllers: A Flight Control Example," *IEEE Trans. Control Syst. Technol.*, vol. 1, no. 2, pp. 69–79, 1993.
[94] A. Hjartarson, P. Seiler, and G. J. Balas, "LPV analysis of a gain scheduled control for an aeroelastic aircraft," *Proc. Am. Control Conf.*, pp. 3778–3783, 2014.
[95] K. Wise, E. Lavretsky, and N. Hovakimyan, "Adaptive control of flight: theory, applications, and open problems," *2006 Am. Control Conf.*, pp. 8–10, 2006.
[96] Z. T. Dydek, A. M. Annaswamy, and E. Lavretsky, "Adaptive Control and the NASA X-15-3 Flight Revisited: Lessons learned and Lyapunov-stability-based design," *IEEE Control Syst.*, vol. 30, no. 3, pp. 32–48, 2010.

[97] J. A. Rossiter, *Model- Based Predictive Control - A practical approach*. 2003.
[98] L. Fagiano, "MPC for airborne wind energy generation," *Electron. Resour.*, 2013.
[99] S. Gros, M. Zanon, and M. Diehl, "Orbit control for a power generating airfoil based on nonlinear MPC," *2012 Am. Control Conf.*, pp. 137–142, 2012.
[100] A. Ilzhoefer, B. Houska, and M. Diehl, "Nonlinear MPC of kites under varying wind conditions for a new class of large scale wind power generators," *Int. J. Robust Nonlinear Control*, pp. 1–9, 2006.
[101] M. Trifkovic, M. Sheikhzadeh, K. Nigim, and P. Daoutidis, "Hierarchical control of a renewable hybrid energy system," *Proc. IEEE Conf. Decis. Control*, pp. 6376–6381, 2012.
[102] A. S. Morse, "Supervisory control of families of linear set-point controllers - Part 2: Robustness," *IEEE Trans. Automat. Contr.*, vol. 42, no. 11, pp. 1500–1515, 1997.
[103] A. S. Morse, "Supervisory control of families of linear set-point controllers - Part 2: Robustness," *IEEE Trans. Automat. Contr.*, vol. 42, no. 11, pp. 1500–1515, 1997.
[104] T. Besselmann, J. Löfberg, and M. Morari, "Explicit MPC for LPV systems: Stability and optimality," *IEEE Trans. Automat. Contr.*, vol. 57, no. 9, pp. 2322–2332, 2012.
[105] F. Bruzelius, "Linear Parameter-Varying Systems an approach to gain scheduling," 2004.
[106] O. L. R. Jacobs and G. C. Shering, "Design of a single-input sinusoidal-perturbation extremum-control system," in *Proceedings of IEE*, 1968, vol. 115, no. 1, pp. 212–217.
[107] R. W. Mayne, "A fluidic extremum controller," *Automatica*, vol. 8, no. 3, pp. 349–356, 1972.
[108] K. Ariyur and M. Krstić, "Real-Time Optimization by Extremum-Seeking Control," *John Wiley Sons*, 2003.
[109] M. Krstić, "Performance improvement and limitations in extremum seeking control," *Systems & Control Letters*, vol. 39, no. 5. pp. 313–326, 2000.
[110] Joon-Young Choi, M. Krstic, K. B. Ariyur, and J. S. Lee, "Extremum seeking control for discrete-time systems," *IEEE Trans. Automat. Contr.*, vol. 47, no. 2, pp. 318–323, 2002.
[111] A. Banaszuk, K. B. Ariyur, M. Krstid, and C. A. Jacobson, "An adaptive algorithm for control of combustion instability," *Automatica*, vol. 40, no. 11, pp. 1965–1972, 2004.
[112] Y. Tan, D. Nešić, and I. M. Y. Mareels, "On non-local stability properties of extremum seeking control," *IFAC Proc. Vol.*, vol. 16, pp. 550–555, 2005.
[113] A. Ghaffari, M. Krstić, and D. Nešić, "Multivariable Newton-based extremum seeking," *Automatica*, vol. 48, no. 8, pp. 1759–1767, 2012.
[114] M. Krstić and H.-H. Wang, "Stability of extremum seeking feedback for general nonlinear dynamic systems," *Automatica*, vol. 36, pp. 595–601, 2000.
[115] A. Banaszuk, Y. Zhang, and C. a. Jacobson, "Adaptive control of combustion instability using extremum-seeking," *Am. Control Conf.*, vol. 1, no. 6, pp. 416–422, 2000.
[116] H. Yu and U. Ozguner, "Extremum-seeking control strategy for ABS system with time delay," *Proc. Am. Control Conf.*, vol. 5, pp. 3753–3758, 2002.
[117] A. Ghaffari, M. Krstić, and S. Seshagiri, "Power optimization and control in wind energy conversion systems using extremum seeking," *IEEE Trans. Control Syst. Technol.*, vol. 22, no. 5, pp. 1684–1695, 2014.
[118] F. Fateh, W. N. White, and D. Gruenbacher, "A nonlinear control scheme for extremum power seeking in wind Turbine Energy Conversion Systems," in *Proceedings of the American Control Conference*, 2014, pp. 1180–1185.
[119] M. Krstic and A. Ghaffari, "Extremum Seeking for Wind and Solar Energy Applications," *Proc. 11th World Congr. Intell. Control Autom.*, 2014.

[120] H. Hashimoto and T. Hayakawa, “Extremum Seeking for Maximizing Wind Energy Generation,” *IEEE Conf. Control Appl.*, pp. 1389–1393, 2014.
[121] C. Lambert, M. Nahon, and D. Chalmers, “Implementation of an aerostat positioning system with cable control,” *IEEE/ASME Trans. Mechatronics*, vol. 12, no. 1, pp. 32–40, 2007.
[122] L. Seguro and T. Lambert, “Modern estimation of the parameters of the Weibull wind speed distribution for wind energy analysis,” *J. Wind Eng. Ind. Aerodyn.*, vol. 85, no. 1, pp. 75–84, 2000.
[123] “Mathworks: Documentation c2d.” [Online]. Available: uk.mathworks.com/help/control/ref/c2d.html.
[124] L. Wang, “Model Predictive Control System Design and Implementation using MATLAB,” *Springer*, 2009.
[125] A. Bemporad, M. Morari, and N. L. Ricker, “Model Predictive Control Toolbox User’s Guide.” [Online]. Available: uk.mathworks.com/help/pdf_doc/mpc/mpc_ug.pdf.
[126] “Mathworks, Model Predictive Control Toolbox.” [Online]. Available: www.mathworks.com/products/mpc.html.
[127] A. Bafandeh and C. Vermillion, “Altitude Optimization of Airborne Wind Energy Systems via Switched Extremum Seeking; Design, Analysis, and Economic Assessment,” *IEEE Trans. Control Syst. Technol.*, vol. 25, no. 6, pp. 2022–2033, 2017.

Appendix A1

A1.1 Maximum Power of AWES

Consider a force balance in which a wing with a given, lift coefficient C_L, drag coefficient C_D flies at a steady speed v_k perpendicular to the wind v_w. Assuming perfect efficiency and that the force from power generation is $F_P = \frac{P}{v_a}$. Consider the force balance along v_k in

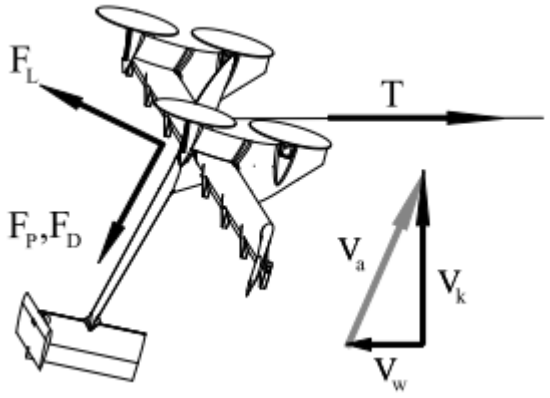

Figure A1 – 1 – Basic downwind force balance used to derive majority of wing performance estimates

$$\frac{P}{v_a} + \frac{\rho_{air} {v_a}^2 A}{2} C_D \cos\left(tan^{-1}\left(\frac{v_w}{v_k}\right)\right) = \frac{\rho_{air} {v_a}^2 A}{2} C_L \sin\left(tan^{-1}\left(\frac{v_w}{v_k}\right)\right) \quad \text{(A1.1)}$$

Using a small angle approximation and letting $v_a \approx v_k$ results in

$$P_{AWES} = \frac{1}{2}\rho_{air} A C_L(\alpha) v_a^2 (v_w C_L(\alpha) - v_a C_D(\alpha)) \quad \text{(A1.2)}$$

The force balance along the tether is

$$T = \left(\frac{\rho_{air} {v_a}^2 A}{2} C_D + F_P\right) \sin\left(tan^{-1}\left(\frac{v_w}{v_k}\right)\right) + \frac{\rho_{air} {v_a}^2 A}{2} C_L \cos\left(tan^{-1}\left(\frac{v_w}{v_k}\right)\right) \quad \text{(A1.3)}$$

Again using the small angle approximation and assuming $C_D \ll C_L$the tension can be simplified as lift:

$$T = \frac{1}{2}\rho_{air} A {v_k}^2 C_L \quad \text{(A1.4)}$$

Differentiating Equation with respect to velocity v_a yields the theoretical maximum

$$v_a = \frac{2}{3}\frac{C_L(\alpha)}{C_D(\alpha)}v_w \tag{A1.5}$$

This can be substituted back in to get

$$P_{AWE} = \frac{2}{27}\rho_{air}A_{wing}{v_w}^3\frac{C_L(\alpha)^3}{C_D(\alpha)^2} \tag{A1.6}$$

$$T = \frac{4}{9}\rho_{air}A_{wing}{v_w}^2\frac{C_L(\alpha)^3}{C_D(\alpha)^2} \tag{A1.7}$$

Whilst the zeta factor in Equation (2-7) is a measure of the power capture, the power is limited relative to the force. This can be defined as the tau factor:

$$\tau = \frac{Tv_w}{P_{turb}} \tag{A1.8}$$

τ is the ratio between the achieved tension and theoretical minimum tension $T_{min} = \frac{P}{v_a}\tau$ which when solved from A1.6 and A1.7 results in a maximum value of

$$\tau = 3 \tag{A1.9}$$

A1.2 Maximum τ of a Wind Turbine

From actuator disc theory [3] the force of the disc on the wind is:

$$F_{turb} = 2\rho_{air}A{v_w}^2a(1-a) \tag{A2.10}$$

And knowing that the Betz limit is achieved at $a = \frac{1}{3}$ giving a C_P of $\frac{16}{27}$ results in a τ for a wind turbine of

$$\tau = \frac{2\rho_{air}A{v_w}^3a(1-a)}{\frac{1}{2}\rho A{v_w}^3C_P} = \frac{3}{2} \tag{A2.12}$$

Appendix A2

A2.1 Equations of Motion - Proof

Three Euler angles are defined to describe the orientation of the shroud in the air relative to an earth axis. The earth axis will be coincident with the base station through the length of the tether l. The attitude of the shroud may be established by considering the rotation about each axis in turn required to bring (x_0, y_0, z_0) into coincidence with (x_3, y_3, z_3). The two axes (x_0, y_0, z_0) and (x_3, y_3, z_3) are shown in Figure A2.1 below:

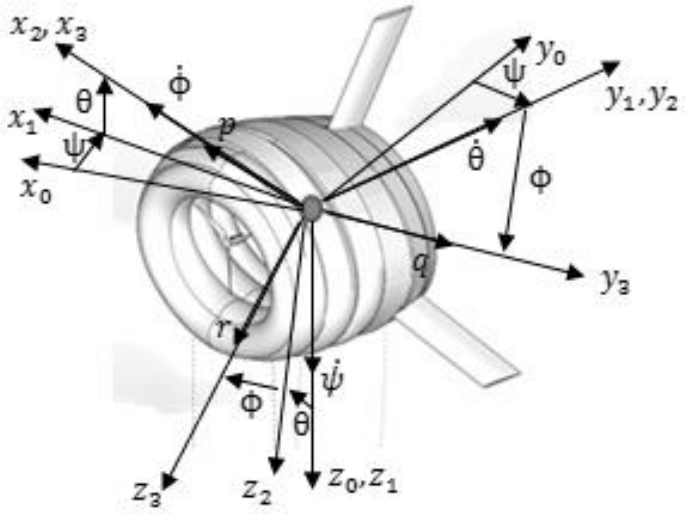

Figure A2.1 - Altaeros shroud with angle rates transformation

It will be necessary to transform variables from one system of axes to another. This is done through rotation matrices defined in the x, y and z directions as follows:

$$R_x = \begin{bmatrix} 1 & 0 & 0 \\ 0 & \cos\phi & -\sin\phi \\ 0 & \sin\phi & \cos\phi \end{bmatrix} \tag{A2.1}$$

$$R_y = \begin{bmatrix} \cos\theta & 0 & \sin\theta \\ 0 & 1 & 0 \\ -\sin\theta & 0 & \cos\theta \end{bmatrix} \tag{A2.2}$$

$$R_z = \begin{bmatrix} \cos\psi & \sin\psi & 0 \\ -\sin\psi & \cos\psi & 0 \\ 0 & 0 & 1 \end{bmatrix} \tag{A2.3}$$

The earth fixed coordinates (x_0, y_0, z_0) can be expressed in terms of (x_3, y_3, z_3) through rotations in the following order; *yaw*,*pitch* and *roll*.

$$\begin{bmatrix} x_0 \\ y_0 \\ z_0 \end{bmatrix} = R_{zyx} \begin{bmatrix} x_3 \\ y_3 \\ z_3 \end{bmatrix} \tag{A2.4}$$

In our application, the most important result will be to relate the angular velocities p, q and r of the shroud axis to the resolved components of the attitude rates $\dot{\phi}, \dot{\theta}, \dot{\psi}$ with respect to the datum axis. This is done by considering how to make (x_3, y_3, z_3) with corresponding angular velocity vectors (p, q, r) coincident with the earth axis (x_0, y_0, z_0). First, *roll* about $0x_3$, through the angle ϕ with angular velocity $\dot{\phi}$. Second *pitch* about $0y_2$ through angle θ with angular velocity $\dot{\theta}$. Finally *yaw* about $0z_1$ through angle ψ with angular velocity $\dot{\psi}$. This is shown algebraically below:

$$\begin{bmatrix} p \\ q \\ r \end{bmatrix} = \left[R_x \begin{bmatrix} \dot{\phi} \\ 0 \\ 0 \end{bmatrix} + R_x R_y \begin{bmatrix} 0 \\ \dot{\theta} \\ 0 \end{bmatrix} + R_x R_y R_z \begin{bmatrix} 0 \\ 0 \\ \dot{\psi} \end{bmatrix} \right] \tag{A2.5}$$

Evaluating in terms of p, q and r yields

$$\begin{bmatrix} p \\ q \\ r \end{bmatrix} = \left[\begin{bmatrix} \dot{\phi} \\ 0 \\ 0 \end{bmatrix} + \begin{bmatrix} 0 \\ \dot{\theta}\cos\phi \\ -\dot{\theta}\sin\phi \end{bmatrix} + \begin{bmatrix} -\dot{\psi}\sin\theta \\ \dot{\psi}\cos\theta\sin\phi \\ \dot{\psi}\cos\phi\cos\theta \end{bmatrix} \right] \tag{A2.6}$$

Condensed into matrix form the fixed body angular velocities depend on the Euler rotations plus the relative attitude rates as follows

$$\begin{bmatrix} p \\ q \\ r \end{bmatrix} = \begin{bmatrix} 1 & 0 & -\sin\theta \\ 0 & \cos\phi & \cos\theta\sin\phi \\ 0 & -\sin\phi & \cos\phi\cos\theta \end{bmatrix} \begin{bmatrix} \dot{\phi} \\ \dot{\theta} \\ \dot{\psi} \end{bmatrix} \tag{A2.7}$$

Where the inverse is

$$\begin{bmatrix} \dot{\phi} \\ \dot{\theta} \\ \dot{\psi} \end{bmatrix} = \begin{bmatrix} 1 & \sin\phi\tan\theta & \cos\phi\tan\theta \\ 0 & \cos\phi & -\sin\phi \\ 0 & \sin\phi\sec\theta & \cos\phi\sec\theta \end{bmatrix} \begin{bmatrix} p \\ q \\ r \end{bmatrix} \tag{A2.8}$$

When the shrouds perturbations are small i.e. when the Euler angles are small then equations (A2.7) and (A2.8) can be approximated by

$$p = \dot{\phi} \tag{A2.9}$$

$$q = \dot{\theta} \tag{A2.10}$$

$$r = \dot{\psi} \tag{A2.11}$$

The angular velocities are now used in the determination of the moments about each axis present on the shroud. The moments on the shroud will arise from the aerodynamics of the shroud, the three tethers located at the fore and aft port/starboard and the buoyancy moment resulting from the difference in centre of buoyancy and centre of mass. The sum of all moments on a rigid body is equal to the rate of change of the body's angular momentum

$$\sum M_G = \dot{H_G} \tag{A2.12}$$

where M_G is the sum of all moments and $\dot{H_G}$ is the rigid-body's angular acceleration. H_G is defined relative to the moving frame as follows

$$H_x = \bar{I_x}p - \overline{I_{xy}}q - \overline{I_{xz}}r \tag{A2.13}$$

$$H_y = -\overline{I_{yx}}p + \bar{I_y}q - \overline{I_{yz}}r \tag{A2.14}$$

$$H_z = -\overline{I_{zx}}p - \overline{I_{xy}}q + \bar{I_z}r \tag{A2.15}$$

where, $\bar{I_x}$, $\bar{I_y}$ and $\bar{I_z}$ are the inertias in the x, y and z axis and $\overline{I_{xy}}$, $\overline{I_{xz}}$, $\overline{I_{yx}}$, $\overline{I_{yz}}$, $\overline{I_{zx}}$, $\overline{I_{xy}}$ are cross coupling terms. It can be seen from Equations (A2.13) – (A2.15) that the momentum is characterized by the inertia and cross-coupled inertia of different axes. The inertia matrix can then be defined as

$$I = \begin{bmatrix} \bar{I}_x & -\bar{I}_{xy} & -\bar{I}_{xz} \\ -\bar{I}_{yx} & \bar{I}_y & -\bar{I}_{yz} \\ -\bar{I}_{zx} & -\bar{I}_{zy} & \bar{I}_z \end{bmatrix} \tag{A2.16}$$

The shroud is axisymmetric and selecting an appropriate principal axis, all products of inertia on the body reduce to zero and the main inertial matrix is left as follows

$$I = \begin{bmatrix} \bar{I}_x & 0 & 0 \\ 0 & \bar{I}_y & 0 \\ 0 & 0 & \bar{I}_z \end{bmatrix} \quad \text{(A2.17)}$$

Subbing Equation (A2.17) into Equations (A2.13) – (A2.15), the angular momentum equation in each axis is reduced to

$$H_x = \bar{I}_x p \quad \text{(A2.18)}$$

$$H_y = \bar{I}_y q \quad \text{(A2.19)}$$

$$H_z = \bar{I}_z r \quad \text{(A2.20)}$$

Taking the derivative of H_x, H_y and H_z with respect to time we obtain the rate of change of angular momentum relative to a rotating frame. However, when considering a rotating frame of reference an added component must be included to account for the angular velocity of the rigid body when viewed from the fixed frame of reference. Thus the overall rate of change of angular momentum in a rotating reference frame is defined as

$$\dot{H}_G = \dot{H}_G(xyz) + \Omega_{rot} \times H_G \quad \text{(A2.21)}$$

Where, $\Omega_{rot} = [p\ q\ r]$, $\dot{H}_G = [\dot{H}_x\ \dot{H}_y\ \dot{H}_z]$ and $H_G = [H_x\ H_y\ \ H_z]$

A2.1.1 Rotational Motion

Taking the derivative of Equations (A2.18) – (A2.20) and subbing in for H_G Equation (A2.12) can now be expressed in terms of the angular velocity in the x, y and z directions.

$$\sum M_x = \bar{I}_x \dot{p} + qr(I_z - I_y) \quad \text{(A2.22)}$$

$$\sum M_y = \bar{I}_y \dot{q} + pr(I_x - I_z) \quad \text{(A2.23)}$$

$$\sum M_z = \bar{I}_z \dot{r} + pq(I_y - I_x) \quad \text{(A2.24)}$$

The sum of moments in the x, y and z directions can now be expressed as a function of aerodynamics, tethers and buoyancy and are defined as follows

$$M^{aero} = \begin{bmatrix} M_x^{aero} \\ M_y^{aero} \\ M_z^{aero} \end{bmatrix} \tag{A2.25}$$

$$M^{tether} = \begin{bmatrix} M_x^{tether} \\ M_y^{tether} \\ M_z^{tether} \end{bmatrix} \tag{A2.26}$$

$$M^{b} = \begin{bmatrix} M_x^{b} \\ M_y^{b} \\ M_z^{b} \end{bmatrix} \tag{A2.27}$$

Rewriting Equations (A2.22) – (A2.24) in terms of the moments derived in Equations (A2.25) – (A2.27), we obtain expressions for the angular velocity in terms of the moments on the shroud and inertia. This defines the equation of motions in the *rotational direction*

$$\dot{p} = \frac{1}{\overline{I_x}}\left(M_x^{aero} + M_x^{tether} + M_x^{b} - qr\left(I_z - I_y\right)\right) \tag{A2.28}$$

$$\dot{q} = \frac{1}{\overline{I_y}}\left(M_y^{aero} + M_y^{tether} + M_y^{b} - pr(I_x - I_z)\right) \tag{A2.29}$$

$$\dot{r} = \frac{1}{\overline{I_z}}\left(M_z^{aero} + M_z^{tether} + M_z^{b} - pq\left(I_y - I_x\right)\right) \tag{A2.30}$$

A2.1.2 Translational Motion

To describe the motion of the rigid body in the translational direction, velocities are defined in the x, y and z directions as follows

$$\Omega_{tran} = [u\ v\ w] \tag{A2.31}$$

The linear momentum in the x, y and z direction are then defined following standard Newtonian dynamics

$$L_x = mu \tag{A2.32}$$

$$L_y = mv \tag{A2.33}$$

$$L_z = mw \tag{A2.34}$$

Where, m is the mass of the rigid body. The forces summed in the x, y and z direction are then calculated from the rate of change of linear momentum L

$$\sum F = \dot{L} \tag{A2.35}$$

$$\dot{L} = \dot{L}(xyz) + \Omega \times L \tag{A2.36}$$

Evaluating in the x, y and z direction where $F = [F_x\ F_y\ F_z]$ the forces are related to the translational velocities

$$\sum F_x = m\dot{u} - m(vr - wq) \tag{A2.37}$$

$$\sum F_y = m\dot{v} - m(wp - ur) \tag{A2.38}$$

$$\sum F_z = m\dot{w} - m(uq - vp) \tag{A2.39}$$

As with the rotational equations of motion, the translational forces can be broken up into constituent parts consisting of an aerodynamic, tether and buoyancy contributions

$$F^{aero} = \begin{bmatrix} F_x^{aero} \\ F_y^{aero} \\ F_z^{aero} \end{bmatrix} \tag{A2.40}$$

$$F^{tether} = \begin{bmatrix} F_x^{tether} \\ F_y^{tether} \\ F_z^{tether} \end{bmatrix} \tag{A2.41}$$

$$F^{net} = \begin{bmatrix} F_x^{net} \\ F_y^{net} \\ F_z^{net} \end{bmatrix} \tag{A2.42}$$

Equations (A2.37) – (A2.39) can be rewritten to include the terms provided in (A2.40) – (A2.42)resulting in the overall equations of motion in the *translational direction*

$$\dot{u} = \frac{1}{m}\left(F_x^{aero} + F_x^{tether} + F_x^{net}\right) + (vr - wq) \tag{A2.43}$$

$$\dot{v} = \frac{1}{m}\left(F_y^{aero} + F_y^{tether} + F_y^{net}\right) + (wp - ur) \tag{A2.44}$$

$$\dot{w} = \frac{1}{m}\left(F_z^{aero} + F_z^{tether} + F_z^{net}\right) + (uq - vp) \tag{A2.45}$$

Equations (A2.43) – (A2.45) and (A2.28) – (A2.30), describe the motion of the shroud in six degrees of freedom and form the basis of the model.

Appendix A3

Bode Plots for different operating conditions

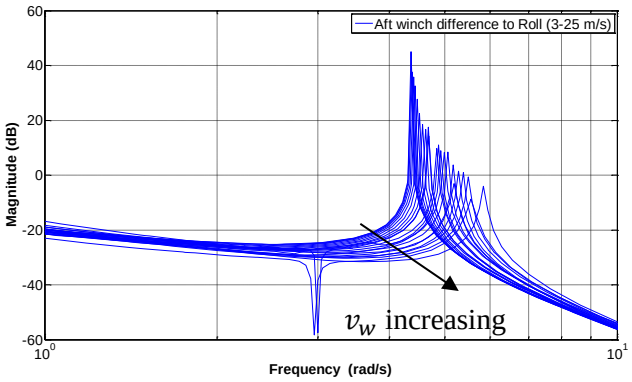

Figure A3-1 - Open loop Roll Dynamics

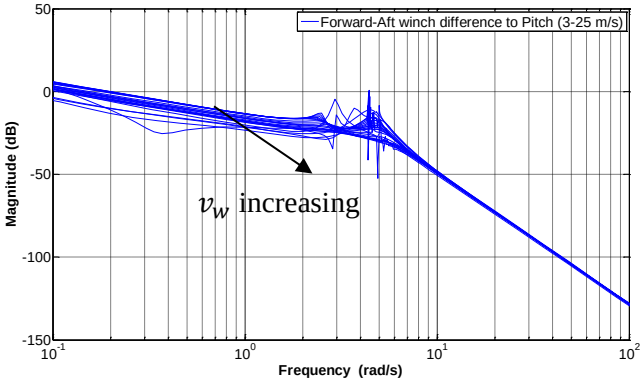

Figure A3-2 - Open loop Pitch Dynamics

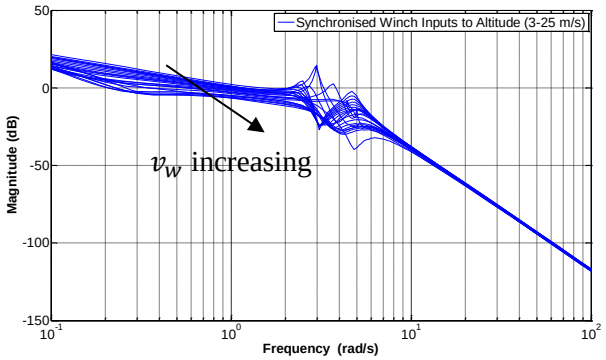

Figure A3-3 - Open loop Altitude Dynamics

Appendix A4

Align Algorithm

The idea of a commutative compensator was developed in Chapter 4. That is, some matrices $A(s)$ and $B(s)$ are chosen to be realizable forms of $W^{-1}(s)$ and $W(s)$ respectively. The commutative compensator is shown in Figure A4.1:

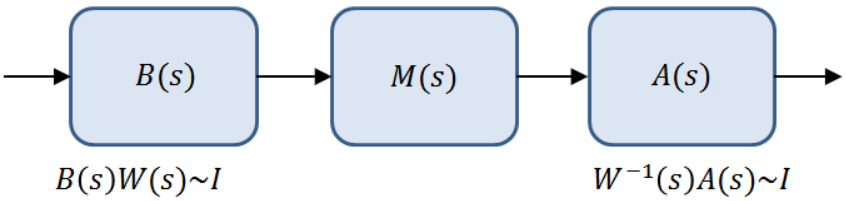

Figure A4.1 - The commutative compensator

In order to determine a realizable suitable solution for $A(s)$ and $B(s)$, a frequency s_0 is chosen around which each matrix is evaluated. That is, at points $A(s_0)$ and $B(s_0)$. To do this, the ALIGN algorithm is employed. This algorithm was first given by Kouvaritkas in [76].The algorithm is based on the observation that a commutative compensator is obtained at point s_0 regardless of whether A is not equal to $W(s_0)$. The columns of A only have to be scalar multiples of $W(s_0)$, that is the columns share the same 'directions'. We can write:

$$A = (a_1, a_2, \ldots\ldots, a_m) \tag{A4.1}$$

And

$$W(s_0) = (w_1, w_2, \ldots\ldots, w_m) \tag{A4.2}$$

A commutative compensator is obtained at s_0 if

$$a_i = w_i z_i, \qquad i = 1,2, \ldots\ldots, m \tag{A4.3}$$

For some scalar complex numbers z_i and

$$B = A^{-1} \tag{A4.4}$$

If we define

$$V(s) = W^{-1}(s) \tag{A4.5}$$

And say

$$V^T(s_0) = (v_1, v_2, \ldots\ldots, v_m) \tag{A4.6}$$

Then

$$v_j^H a_i = 0, \qquad i \neq j \tag{A4.7}$$

The maximization problem can be solved as a least-squares problem (A4.7). If we impose the constraint

$$|a_i| = |w_i| \tag{A4.8}$$

without, loss of any generality we see we must have

$$|z_i| = e^{j\delta_i} \tag{A4.9}$$

For some real δ_i. If (A4.8) holds we can write

$$A = W(s_0)diag\{e^{j\delta_i}\} \tag{A4.10}$$

which implies,

$$V(s_0)A = diag\{e^{j\delta_i}\} \tag{A4.11}$$

The ALIGN algorithm applied in MATLAB therefore chooses a_i

$$a_i = \arg\min_{a_i,\delta_i} \|V(s_0)a_i - e^{j\delta_i}e_i\| \tag{A4.12}$$

Where e_i denotes the ith standard basis vector and the norm defined as

$$\|x\|^2 = x^H x \tag{A4.13}$$

Appendix A5

Nonlinear Simulink Model